

# **AN INTEGRATED EARLY WARNING FORECAST SYSTEM FOR WET SEASONS AND THEIR RELATIONSHIP TO FLOODING EVENTS: A PREDICTABILITY STUDY IN SUPPORT OF HYDROLOGICAL APPLICATIONS**

Report to the

**Water Research Commission**

by

**LE Mpheshea; FA Engelbrecht; AF Beraki; R Maisha; R Nkoana and J van der Merwe**

Council for Scientific and Industrial Research (CSIR)

**WRC Report No. 2522/1/18**

**ISBN 978-0-6392-0044-6**

**September 2018**

**Obtainable from:**

**Water Research Commission  
Private Bag X03  
Gezina, 0031**

[orders@wrc.org.za](mailto:orders@wrc.org.za) or download from [www.wrc.org.za](http://www.wrc.org.za)

**DISCLAIMER**

This report has been reviewed by the Water Research Commission (WRC) and approved for publication. Approval does not signify that the contents necessarily reflect the views and policies of the WRC, nor does mention of trade names or commercial products constitute endorsement or recommendation for use.

**Printed in the Republic of South Africa**

**© WATER RESEARCH COMMISSION**

## EXECUTIVE SUMMARY

Southern Africa, defined here as the landmass area enclosed between 22–35° S and 12–36° E, receives the bulk of its rainfall during the austral summer. Moreover, the region exhibits pronounced interannual rainfall variability linked to the teleconnected influence of sea surface temperature (SST) anomalies in the tropical Pacific Ocean. In events where anomalously positive (negative) SSTs are observed over the domain between 5° N and 5° S and between 120° W and 170° W, which is commonly referred to as the Niño 3.4 region, there tends to be higher (lower) than normal rainfall conditions over southern Africa.

For the purpose of this project, the sub-region located in north-eastern South Africa [2–28° S; 24–33° E] is considered as the main focus area. The north-eastern part of South Africa is characterised by a vast network of rivers that include the trans-country boundary formed by the Limpopo River. The region is also highly susceptible to the impact of tropical lows and cyclones. For instance, the landfall of tropical cyclone Eline in February 2000 caused severe flooding in the Limpopo River system, which led to devastating socio-economic impacts.

Seasons associated with flooding in north-eastern South Africa tend to be strongly associated with La Niña events. The seasonal predictive skill in giving early warning of such events is high. This predictability, in combination with the high vulnerability of the region to flood events, gave rise to this project with its focus of a *ready-set-go* strategy to manage flood events in north-eastern South Africa. The basic idea is that seasonal forecasts can provide early warning of potentially wetter than normal seasons, which may imply the occurrence of flood events (*ready* mode). Those who are likely to be affected by floods as well as risk managers can then begin to monitor the medium-range forecast (up to 14 days) (*set* mode) to ensure that contingency plans in risk-prone areas are updated. The *go* part includes short-range weather forecasting for the next 48-hour period, which is the action step. Risk managers can then start to evacuate people to lessen the societal impacts of floods.

Against this background, the project used the weather prediction system of the Council for Scientific and Industrial Research (CSIR) to explore the skill of forecasting rainfall and streamflow for north-eastern South Africa at seasonal to short-range timescales. More specifically, the project aimed to:

- Expand on the Conformal Cubic Atmospheric Model (CCAM) seasonal forecasting capability of the CSIR by combining it with the Coupled Atmosphere Biosphere Land Exchange (CABLE) dynamic land-surface model and using its river routing scheme.
- Expand the CCAM short-range forecast system to medium-range (forecasts up to 14 days ahead).
- Explore the impacts of very high spatial resolution on short-range and seasonal forecasts over the north-eastern interior of South Africa and adjacent countries.
- Develop statistical downscaling schemes for seasonal, medium-range and 48-hour forecasts of river flows over the north-eastern interior of South Africa by using the daily flow data hosted by the Department of Water and Sanitation.

In order to address the aims of the project, the CCAM was used to generate short-range through to seasonal timescale forecasts over north-eastern South Africa. These forecasts were statistically downscaled to streamflows in quaternary catchment areas. The study also explored the use of a dynamical river routing scheme within the CABLE dynamic land-surface model to simulate river states at daily and seasonal timescales. This work represents the first application of a dynamic river routing scheme in South Africa.

A key project finding is that the seasonal forecast skill used to predict wet conditions over north-eastern South Africa during La Niña years does translate into a skill for forecasting anomalously high values of streamflow (as obtained through statistical downscaling). This implies that numerical seasonal forecast systems can provide the ready stage of a ready-set-go early warning approach to manage floods over this region. These forecasts have been found to be skilful at lead times of one to three months.

Short-range weather forecasting in combination with statistical downscaling can indeed also function as the go component in a ready-set-go early warning flood management tool for north-eastern South Africa, with medium-range forecasts that can be used for the set stage of such a system. In particular, the research demonstrates that such forecasts can provide accurate guidance on the spatial occurrence and timing of occurrence of major flood events induced by landfalling tropical cyclones.

The findings of this study shows that the spin-up time period required by the CCAM CABLE with the dynamic river routing scheme, as well as the initialisation of streamflow within the river routing scheme, can be a limiting factor for the practical application of this system as an early flood warning management tool. However, at a high spatial resolution, many of the key South African river systems are resolved realistically, which indicates the potential of applying the system to seasonal forecast systems and climate change projections.

## ACKNOWLEDGEMENTS AND REFERENCE GROUP

The authors would like to thank the following persons and institutions:

- The Water Research Commission for funding and managing the project.
- Prof. Willem Landman for his valuable contribution during the proposal writing and continuous support to the lead author.
- The Centre for High Performance Computing of the Meraka Institute of the Council for Scientific and Industrial Research for providing computational resources.
- The Limpopo Department of Economic Development, Environment and Tourism for providing a platform to engage with potential users of 'ready-set-go' flood warning system.
- Ms MC Mothapo from the Department of Geography and Environmental Studies at the University of Limpopo for generating updated maps showing river networks in the Limpopo Province.

The following members of the reference group are also thanked for their valuable contributions:

- Dr Brilliant Petja                      Water Research Commission (Chairman)
- Mr Chris Moseki                      Department of Water and Sanitation
- Dr Juliet Hermes                      South African Environmental Observation Network
- Mr Matiga Motsepe                    Department of Agriculture, Forestry and Fisheries
- Mr Pieter Visser                      Aon Benfield

*Page left blank intentionally*

## TABLE OF CONTENTS

<b>EXECUTIVE SUMMARY</b> .....	<b>III</b>
<b>ACKNOWLEDGEMENTS</b> .....	<b>V</b>
<b>TABLE OF CONTENTS</b> .....	<b>VII</b>
<b>LIST OF FIGURES</b> .....	<b>VIII</b>
<b>LIST OF TABLES</b> .....	<b>X</b>
<b>ABBREVIATIONS</b> .....	<b>XI</b>
<b>1 INTRODUCTION</b> .....	<b>1</b>
1.1 Background .....	1
1.2 Project Aims .....	5
1.3 Capacity and Competency Development.....	5
1.4 Structure of the Report .....	6
<b>2 DYNAMICAL SIMULATION OF STREAMFLOWS OVER SOUTH AFRICA</b> .....	<b>7</b>
2.1 Introduction.....	7
2.2 Data and Methodology .....	7
2.3 Results.....	9
2.3.1 Experiment 1 .....	9
2.3.2 Experiment 2.....	14
2.4 Synopsis .....	29
<b>3 STATISTICAL DOWNSCALING OF CCAM SIMULATIONS TO STREAMFLOW</b> .....	<b>30</b>
3.1 Introduction.....	30
3.2 Data and Methodology .....	30
3.2.1 Modelling technique .....	30
3.2.2 Verification data .....	34
3.3 Results.....	35
3.3.1 Statistical Hydrologic Model: Seasonal analysis and forecast products.....	35
3.3.2 A link between daily rainfall and river flows .....	37
3.3.3 Predicting the impact of tropical depressions and cyclones on river flows in Limpopo .....	39
3.4 Synopsis .....	42
<b>4 FORECAST PRODUCTS: DISPLAYS AND TAILOR MADE OUTPUTS</b> .....	<b>43</b>
4.1 Introduction.....	43
4.2 Forecast Displays .....	43
4.2.1 Seasonal outlook .....	43
4.2.2 Medium- to short-range forecast products.....	50
4.3 Community Engagement.....	57
4.4 Synopsis .....	57
<b>5 CONCLUSION AND RECOMMENDATIONS</b> .....	<b>58</b>
<b>LIST OF REFERENCES</b> .....	<b>60</b>
<b>APPENDIX</b> .....	<b>69</b>

## LIST OF FIGURES

Figure 1: The location of the study area .....	1
Figure 2: Climatological annual cycle of the Climate Research Unit's (CRU) TS4.01 precipitation and WR2012 naturalised streamflow for the period 1921–2009.....	2
Figure 3: Network of primary rivers across the Limpopo Province .....	2
Figure 4: C192 quasi-uniform conformal cubic grid .....	8
Figure 5: CRU (observed) annual rainfall climatology (top left) and corresponding CCAM-simulated climatology (top right) for the period 1979–2010 .....	10
Figure 6: Spinning-up the dynamic river routing scheme over southern Africa .....	11
Figure 7: Simulated dynamic river routing surface water climatology over South Africa.....	12
Figure 8: DJF anomalies from 2002 to 2014 in the Limpopo River at the Beitbridge station .....	13
Figure 9: CCAM 8 km ERA Interim data simulated averaged 24-hour accumulated rainfall (mm) over South Africa for January to June 2013.....	15
Figure 10: CCAM 8 km ERA Interim data simulated averaged 24-hour accumulated rainfall (mm) over South Africa for July to December 2013 .....	16
Figure 11: CCAM 8 km ERA Interim data simulated average river water depth (mm) over South Africa for the period January to June 2013 .....	18
Figure 12: CCAM 8 km ERA Interim data simulated average river water depth (mm) over South Africa for the period July to December 2013.....	19
Figure 13: CCAM 8 km ERA Interim data simulated average river run-off (mm/day) over South Africa for the period January to June 2013 .....	20
Figure 14: CCAM 8 km ERA Interim data simulated average river run-off (mm/day) over South Africa for the period July to December 2013.....	21
Figure 15: CCAM 8 km ERA Interim data simulated average 24-hour accumulated rainfall (mm) over South Africa for January 2006–2011 .....	23
Figure 16: CCAM 8 km ERA Interim data simulated average 24-hour accumulated rainfall (mm) over South Africa for January 2012–2016 .....	24
Figure 17: CCAM 8 km ERA Interim data simulated average river water depth (mm) over South Africa for January 2006–2011 .....	25
Figure 18: CCAM 8 km ERA Interim data simulated average river water depth (mm) over South Africa for January 2012–2016.....	26
Figure 19: CCAM 8 km ERA Interim data simulated average river run-off (mm/day) over South Africa for January 2006–2011 .....	27
Figure 20: CCAM 8 km ERA Interim data simulated average river run-off (mm/day) over South Africa for January 2012–2016 .....	28
Figure 21: Drainage regions of South Africa.....	34
Figure 22: Spearman correlation values .....	35
Figure 23: Hit scores .....	36
Figure 24: Probabilistic forecasts of downscaled flows .....	37
Figure 25: Mean monthly hydrographs of the observed flow rates.....	38
Figure 26: A lagged correlation coefficient between rainfall and observed streamflow anomalies .....	38



Figure 27: Synoptic chart showing tropical depression Dando .....	39
Figure 28: Forecast of sea level pressure in the south-west Indian Ocean .....	40
Figure 29: Observed streamflow for the days between 16 and 28 January 2012 .....	41
Figure 30: CCAM-simulated rainfall (top row) and predicted streamflow of 16 January 2012 .....	41
Figure 31: CCAM-simulated rainfall (top row) and predicted streamflow of 25 January 2012 .....	42
Figure 32: Time series of SST anomalies in the Niño 3.4 region .....	44
Figure 33: Probabilistic seasonal rainfall forecast release of the CCAM CABLE operation ensemble prediction system .....	44
Figure 34: Probabilistic forecast of precipitation for Dec 2009–Feb 2010 .....	45
Figure 35: Probabilities of above-normal accumulated streamflow statistically downscaled in the quaternary catchment areas over the north-eastern region of South Africa for the 2009/2010 summer (Dec–Feb) season.....	46
Figure 36: Probabilities of below-normal accumulated streamflow statistically downscaled in the quaternary catchment areas over the north-eastern region of South Africa for the 2009/2010 summer (Dec– Feb) season.....	46
Figure 37: Probabilistic forecast of precipitation for Dec 2010–Feb 2011 .....	47
Figure 38: Probabilities of above-normal accumulated streamflow statistically downscaled in the quaternary catchment areas over the north-eastern region of South Africa for the 2010/2011 summer (Dec–Feb) season.....	48
Figure 39: Probabilities of below-normal accumulated streamflow statistically downscaled in the quaternary catchment areas over the north-eastern region of South Africa for the 2010/2011 summer (Dec–Feb) season.....	48
Figure 40: Probabilistic forecast of precipitation for Dec 2014–Feb 2015 .....	49
Figure 41: Probabilities of above-normal accumulated streamflow statistically downscaled in the quaternary catchment areas over the north-eastern region of South Africa for the 2014/2015 summer (Dec–Feb) season.....	50
Figure 42: Probabilities of above-normal accumulated streamflow statistically downscaled in the quaternary catchment areas over the north-eastern region of South Africa for the 2014/2015 summer (Dec–Feb) season.....	50
Figure 43: CCAM rainfall (accumulated over 24 hours) four-day forecast .....	51
Figure 44: Fourteen-day forecast produced on 5 February 2018, 12 February 2018 and 19 February 2018 at Great Letaba River .....	52
Figure 45: Fourteen-day forecast produced on 5 February 2018, 12 February 2018 and 19 February 2018 at Luvuvhu River .....	53
Figure 46: Fourteen-day forecast produced on 5 February 2018, 12 February 2018 and 19 February 2018 at Mokolo River .....	54
Figure 47: Fourteen-day forecast produced on 5 February 2018, 12 February 2018 and 19 February 2018 at Komati River.....	55
Figure 48: Fourteen-day forecast produced on 5 February 2018, 12 February 2018 and 19 February 2018 at Tshinane River .....	56

## LIST OF TABLES

Table 1: Correlation coefficients between surface water level observed at Beitbridge and CCAM-simulated river water level, surface run-off and rainfall for the period 2002 to 2014 .....	14
Table 2: Location/description of selected river stations in the north-eastern region as defined by the DWS .....	33
Table 3: Location and description of the five selected river stations in the north-eastern region as defined by the DWS .....	52

## ABBREVIATIONS

AGCM	Atmospheric General Circulation Model
AMIP	Atmospheric Model Intercomparison Project
CABLE	Coupled Atmosphere Biosphere Land Exchange
CCAM	Conformal Cubic Atmospheric Model
CGCM	Coupled Global Circulation Model
CHPC	Centre for High Performance Computing
CMIP5	Coupled Model Intercomparison Project Phase Five
CPT	Climate Prediction Tool
CRU	Climate Research Unit
CSIR	Council for Scientific and Industrial Research
CSIRO	Commonwealth Scientific and Industrial Research Organisation
DJF	December–January–February
DoE	Department of Energy
DWS	Department of Water and Sanitation
ENSO	El Niño Southern Oscillation
ERA	European Centre for Medium Range Weather Forecasting Reanalysis
GCM	Global Climate Model
GFDL	Geophysical Fluid Dynamics Laboratory
GFS	Global Forecasting System
IRI	International Research Institute for Climate and Society
LEDET	Limpopo Department of Economic Development, Environment and Tourism
NCEP	National Centers for Environmental Prediction
NEMO	Nucleus for European Modelling of the Ocean
NOAA	National Oceanic and Atmospheric Administration
OASIS	Ocean Atmosphere Sea Ice Soil
ONI	Ocean Niño Index
ROC	Relative Operating Characteristics
SIC	Sea Ice Concentration
SST	Sea Surface Temperature
TTT	Tropical Temperate Trough
WRC	Water Research Commission

*Page left blank intentionally*

# 1 INTRODUCTION

## 1.1 Background

Southern Africa, defined here as a landmass area enclosed between 22–35° S and 12–36° E, exhibits pronounced climate variability on a range of timescales. The interannual climate variability in the region is mostly driven by the fluctuations of positive and negative sea surface temperature (SST) anomalies in the tropical Pacific Ocean, which are commonly known as El Niño and La Niña events, respectively (Lindesay, 1988; Mpheshea & Landman, 2015; Ropelewski & Halpert, 1989; Rouault & Richard, 2003). The SST anomalies in the adjacent Indian Ocean domain were found to modulate the impact of the El Niño/La Niña events on southern Africa (Behera et al., 2001; Mpheshea, 2014; Reason, 2000).

With the exception of the south-western Cape region, maximum rainfall totals over southern Africa typically occur during summer. The greater percentage of summer rainfall in the country can largely be accounted for by tropical temperate troughs (TTTs) (Harrison, 1984; Hart et al., 2010; Pohl et al., 2008; Reason et al., 2006). These rain-bearing systems manifest as cloud bands with a north-west to south-east alignment stretching over the tropical landmass to a mid-latitude disturbance passing south of South Africa. Thus, TTTs also act as channels for the large-scale transfer of heat and moisture fluxes from the tropics to the extra-tropical regions to the south.

The red box in Figure 1 indicates the location of the north-eastern region of South Africa [22–28 ° S; 24–33 ° E], which is the main focus area of this project. The onset of rainfall in this region tends to occur around October and the rainfall peaks in January (Figure 2). The region is characterised by a vast network of rivers (Figure 3), which include the second-largest river in Africa, namely, the Limpopo River.

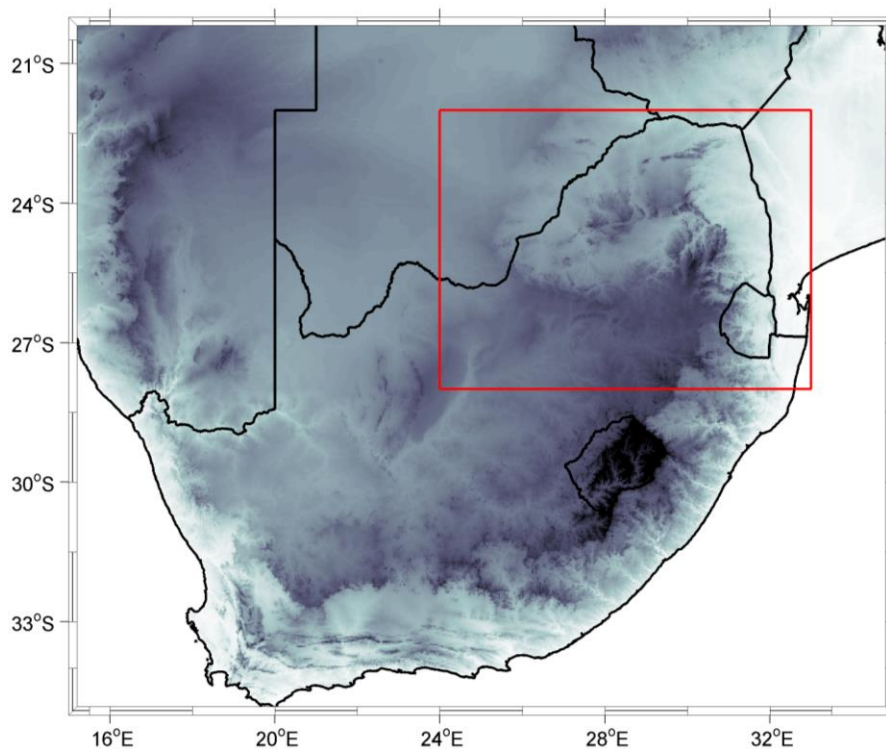


Figure 1: The location of the study area is demarcated in red

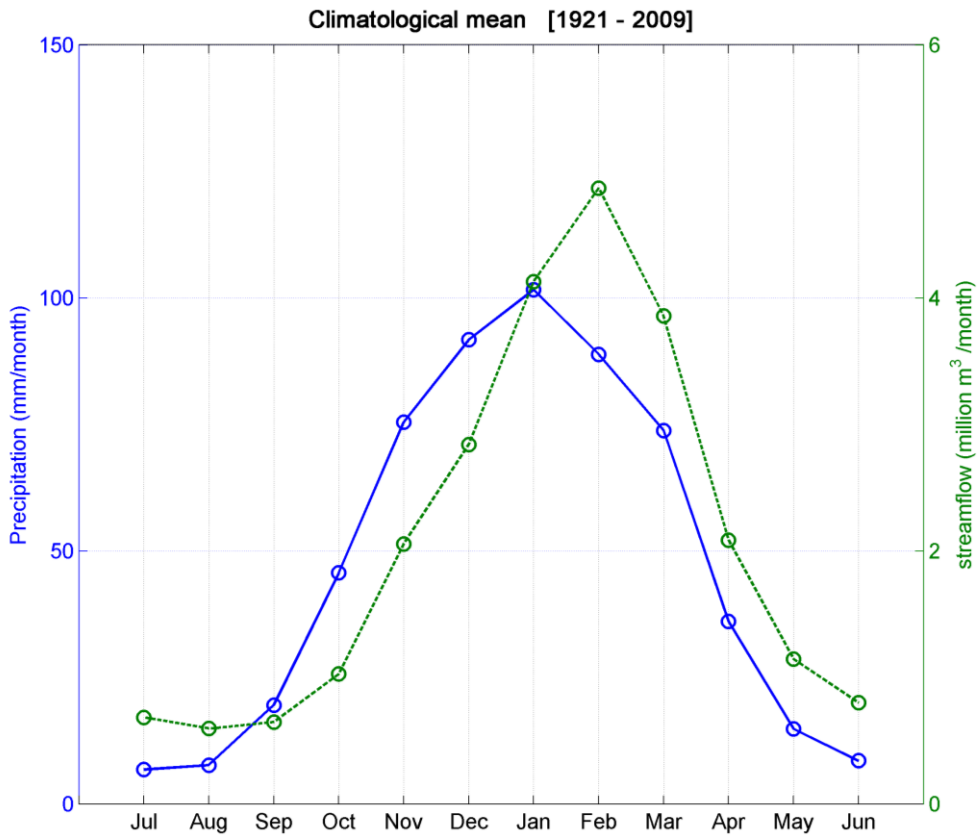


Figure 2: Climatological annual cycle of the Climate Research Unit's (CRU) TS4.01 precipitation and WR2012 naturalised streamflow for the period 1921–2009 over the north-eastern region of South Africa, which is defined as the domain [24–33° E; 22–28° S]. The blue line represents precipitation; the green line represents streamflow

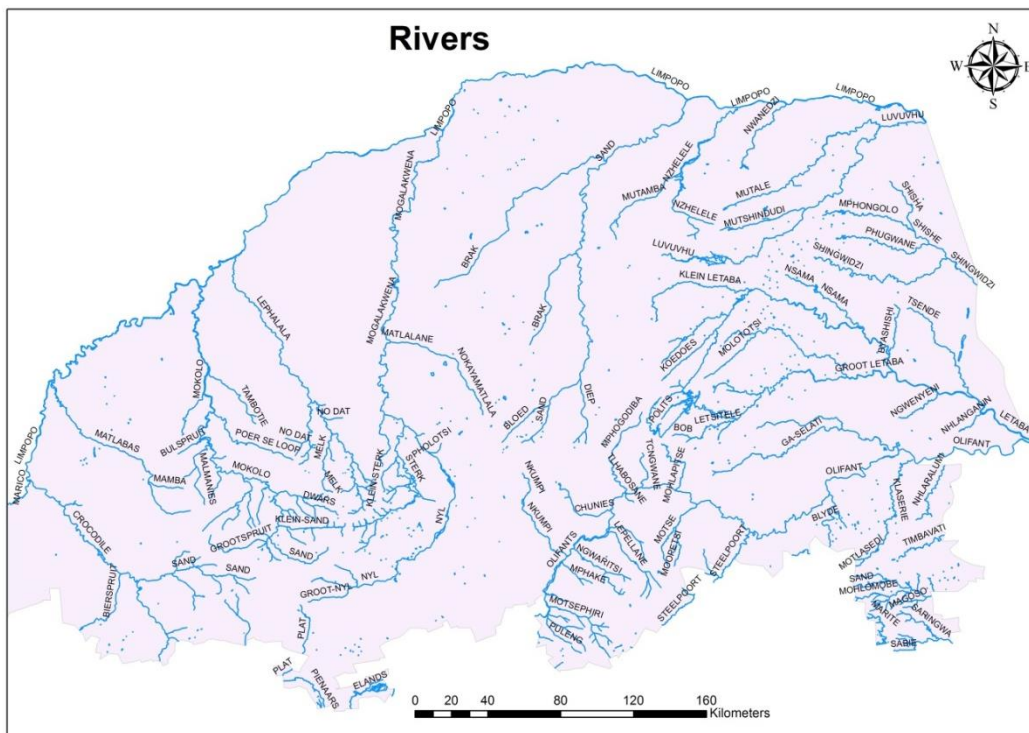


Figure 3: Network of primary rivers across the Limpopo Province (map courtesy of the University of Limpopo, Department of Geography and Environmental Studies)

The annual cycle analysis of naturalised streamflow for the 89-year climatological period shows that the peak flow in the region tends to occur in February (Figure 2). Furthermore, the region is susceptible to the effect of tropical cyclones. For instance, the landfall of tropical cyclone Eline in February 2000 caused severe flooding in the Limpopo River system (Asante et al., 2007). This flooding led to devastating socio-economic impacts (Du Plessis, 2002). Therefore, an efficient flood risk management and early warning system for north-eastern South Africa will benefit from accurate predictability of rain-bearing weather systems that could potentially lead to flooding.

The accuracy of forecasting such rain-bearing systems at a short- to medium-time range (1–14 days) depends on the accurate description of the state of the atmosphere at the start of the forecast, which is also referred to as the initial conditions. This dependency on initial conditions emanate from the chaotic nature of the atmosphere (Leutbecher & Palmer, 2008; Palmer, 1999). In an effort to reduce the uncertainties associated with the initial condition and model formulation, various ensemble forecasting techniques are employed. For example, Landman et al. (2012) took a multi-model ensemble approach using the Unified Model and the Conformal Cubic Atmospheric model (CCAM), which are used at the South African Weather Service as well as the Council for Scientific and Industrial Research (CSIR), respectively, to improve short-range forecasting in South Africa. A project completed for the Water Research Commission (WRC) in 2016 (WRC 2345) used a time-lagged ensemble approach, which increased the horizontal resolution as a method of reducing uncertainties associated with weather forecasting and initial states. In both studies, the results showed that an ensemble forecast system tends to be more skilful than a single deterministic forecast system. The one limiting factor to adopting ensemble systems operationally is the availability of computer resources.

In South Africa, operational seasonal forecasting activities commenced in the early 1990s (Landman, 2014). Such activities are still being maintained owing to the strong evidence that seasonal rainfall and temperatures over South Africa are predictable at lead times of a few months (e.g. Landman & Beraki, 2012; Landman et al., 2014a; 2014b; Lazenby et al., 2014; Yuan et al., 2014). Furthermore, a variety of users utilise these types of forecast (Johnston et al., 2004). Moreover, through concerted modelling efforts, forecast skills have improved locally over the years ever since such forecasts have been issued operationally (Landman, 2014). These modelling efforts have also led to new initiatives. For example, coupled model development has taken off (Beraki et al., 2014; Landman et al., 2014a) and application models have been developed (Malherbe et al., 2014; Muchuru et al., 2015).

Verification of forecasts for the southern African mid-summer rainfall from the Demeter project (Palmer et al., 2004) shows that seasonal predictions of both above- and below-normal rainfall tend to be overconfident, that is, the probabilities of these forecasts are most often higher than the frequencies at which they occur. Verification of more recent model runs shows an improvement in forecast skill to the extent that the reliability of predicting extremely wet mid-summer seasons over South Africa (wetter than the 75<sup>th</sup> percentile of the climatological record) has improved over that of extremely dry seasons: from being overconfident to close to perfect reliability (Landman et al., 2014a). The same was found for central southern Africa where almost perfectly reliable wet mid-summer seasonal forecasts have been demonstrated (Muchuru et al., 2014). For both regions, the relative operating characteristics (ROC) scores are higher than 0.7 when predicting wet mid-summer seasons. This demonstrates that current forecast models have the capability to effectively discriminate wet seasons from the rest of the seasons.

The discussion above has provided evidence from previous work that wet summer seasons are not only predictable, but they are also more predictable than droughts. Moreover, such a skill level can be achieved at a lead time of several months. Wet seasons are often associated with tropical systems making landfall over eastern-southern Africa; for example, tropical cyclone Bonita in January 1996 and tropical cyclone Eline in February 2000 (Reason & Keibel, 2004). In fact, the tropical cyclone season over the southern Indian Ocean for the year 2000 was exceptional in terms of tropical cyclone landfall

over eastern-southern Africa. Such landfalling systems have often been recorded during La Niña seasons (Vitart et al., 2003). Severe flooding seasons over the north-eastern parts of South Africa have been associated with such events and have been demonstrated to be predictable (Landman et al., 2012).

The 2010/2011 La Niña season was also exceptionally wet over the study region. This was predicted skilfully, including the high flows in the Zambezi River (Muchuru et al., 2015). Cai et al. (2015) showed that the frequency of extreme La Niña events may increase under climate change – typically, a large fraction of extreme La Niña events tend to occur after an extreme El Niño event. An example of this phenomenon is the extreme 1998/1999 La Niña event in which large parts of southern Africa were inundated with rainfall; this event followed the extreme 1997/1998 El Niño event. Therefore, one may be able to conclude that it may be possible due to climate change that extreme flood seasons may continue to occur over parts of our region.

Since we have demonstrated our ability to predict severe flooding seasons (and some of these happen to have occurred during La Niña seasons), we can thus put those affected by floods as well as managers of impending flood situations in a *ready* mode when a coming summer season is expected to be excessively wet. Such users can then begin to monitor medium-range forecasts (up to 14 days), update contingency plans, make the community under threat sensitive to flooding aware of the situation, and consider training volunteers. Medium-range forecast production has been shown to be of value in South Africa (Tennant et al., 2007), especially if such forecasts can be improved further through statistical post-processing (Hamill et al., 2004; 2014). In fact, medium-range forecasts have found application in ensemble flood forecasting (Cloke & Pappenberger, 2009). However, atmospheric modelling for this timescale needs further work to demonstrate the level of predictability more comprehensively (the ability of models to provide guidance that a user will judge as valuable) (Hamill & Kiladis, 2014). However, given predictability at this timescale will enable reliable alerts to flood-threatened communities so that they can start preparation activities including mobilising response teams as the time of a potential impact comes closer. Local actors therefore *set* themselves up to begin initial preparations. Near the time of the potential flooding impact, typically a day or two ahead of the predicted event, appropriate actions (*go*), for example evacuations, can be taken directly to lessen societal impact and the cost of recovery (Goddard et al., 2014). The *go* part includes short-range weather forecasting for the next 48-hour period. This *ready-set-go* approach has in fact been put into action during flooding events in West Africa (Braman et al., 2013).

Flood events may also occur during seasons of relatively low rainfall totals. When this phenomenon happens, the ready part of the *ready-set-go* approach may fail since the seasonal forecast may have been skilful in predicting an increased likelihood of drought conditions for a season that is also associated with flood cases. An example of a summer season with generally low rainfall totals but with flood events is 2007 (El Niño year). During 2007, tropical systems caused floods over Mozambique and adjacent areas. Another example is the floods caused by tropical cyclone Domoina in 1984. Notwithstanding, the probabilistic way in which seasonal forecasts are presented will, at least over southern Africa, allow for a chance of above-(below-)normal rainfall to occur when the most likely outcome is predicted to be for below-(above-)rainfall totals to occur. At the CSIR, more in-depth verification work on the CCAM's existing seasonal hindcasts will investigate what the chances of flood events are within a season when below-normal rainfall totals are predicted to be most likely.

This modelling framework involves three time range tiers: The first deals with seasonal forecasts with lead times spanning a number of months. The second tier predicts the likelihood of specific weather extremes occurring over the next two weeks. The third involves detailed weather forecasting over the next 48 hours. The CSIR has a developed capacity to deal with these tiers through a recently completed



WRC project that employed the variable-resolution CCAM in a so-called seamless configuration (Engelbrecht et al., 2011; Landman et al., 2015).

Regarding seasonal timescales: a comprehensive set of CCAM hindcasts have been developed for model testing and calibration. Hindcasts demonstrate predictability – including predicting extreme seasons – and can be used to downscale river flows as has recently been done for southern Africa (Muchuru et al., 2015). On the medium-range timescale, forecastability of the CCAM has also been demonstrated but only up to seven days ahead.

One of the aims of the current project is for the CCAM forecast system to be extended to a medium-range timescale of 14 days. The 48-hour CCAM forecasts of weather extremes have been demonstrated to be skilful for extremes events that occurred over a number of wet seasons. Moreover, a previous WRC project (K5/2325) involved modelling work to expand on the number of weather forecast ensemble members and to produce forecasts at horizontal resolutions from 1 km to 4 km.

The current project commenced by detailing how the CSIR expanded and improved various CCAM configurations and couplings (e.g. with the land surface) over all time ranges. Moreover, the project developed a methodology of how CCAM forecasts can be used further to predict daily, monthly and seasonal flows in major river systems over the north-eastern interior to develop a hydrological forecasting capability. To this end, the project focused on statistical predictions of flows, but also incorporated a dynamic river routing scheme developed to use with climate models (Miller et al., 1994).

## **1.2 Project Aims**

The aims of this project included:

- To expand on the CCAM seasonal forecasting capability of the CSIR by combining it with the Coupled Atmosphere Biosphere Land Exchange (CABLE) dynamic land-surface model and using its river routing scheme. The horizontal resolution of the CCAM in seasonal forecasting mode was targeted at 200 km.
- To expand the 15 km resolution seven-day forecasts of CCAM to the medium range (14 days). CABLE coupling and river routing for four-day forecasts were to be implemented in this framework.
- To further enhance the high-resolution (4 km) weather forecasting capability of the CCAM by producing flow forecasts through the river routing scheme of CABLE. The area of interest was set to be the north-eastern interior of South Africa and adjacent countries.
- To develop statistical downscaling schemes for seasonal, medium-range and 48-hour forecasts of river flows over the north-eastern interior of South Africa by using the daily flow data hosted by the Department of Water and Sanitation (DWS).

## **1.3 Capacity and Competency Development**

The project leader and a lead author of this report is a doctorate candidate at the University of Pretoria. This current project was designed such that it would form an applications chapter in her PhD dissertation to be submitted for review in 2019.

## 1.4 Structure of the Report

The project was designed around the following scientific questions:

- How can CSIR's current weather and seasonal forecast model configurations be further utilised for hydrological applications?
- How skilful are CCAM weather and hydrological forecasts over four-day lead times?
- How well is the river routing system of the CABLE land-surface model able to represent real flows over the north-eastern interior of South Africa?
- Can the CCAM output be successfully downscaled to daily river flows over the north-eastern interior?
- How much benefit does the envisaged ready-set-go approach hold for society and disaster management?

In terms of results, the report is organised such that Chapter 2 presents a new dynamical river routing scheme. Chapter 2 examines the scheme's ability to simulate streamflow over the north-eastern region of South Africa. Chapter 3 examines the application of statistical downscaling methods to simulate streamflow over the focus area. Chapter 4 presents the forecast products and dissemination strategies of these products to benefit end users. Chapter 5 discusses the conclusions and recommendations.

## 2 DYNAMICAL SIMULATION OF STREAMFLOWS OVER SOUTH AFRICA

### 2.1 Introduction

Southern Africa's climate exhibits a great deal of natural variability. The region is prone to frequent droughts and floods. Also, the region is thought to be highly vulnerable to anthropogenically-induced climate change. Temperatures are projected to rise rapidly over southern Africa under the enhanced greenhouse effect – at about twice the global rate of temperature increase (Engelbrecht et al., 2015), while the region is also likely to become generally drier (e.g. Niang et al., 2014). Furthermore, the frequency of extreme weather events, such as droughts, dry spells, heatwaves and high fire danger days, is projected to increase in association with rapidly rising surface temperatures (e.g. Christensen et al., 2007; Engelbrecht et al., 2015). There is evidence that the frequency of heavy rainfall events may increase despite the general decreases in rainfall projected for southern Africa (e.g. Engelbrecht et al., 2013). Such events may lead to flash floods and high flow volumes in the region's major river systems.

The skilful prediction of weather and, in particular, extreme weather events over southern Africa, from short-range (days ahead) to seasonal timescales (months ahead), is therefore of the utmost importance as an adaptation tool within a changing climate (e.g. Winsemius et al., 2014). It is also important that the accuracy and skill that exist in short-range and seasonal weather prediction (Landman et al., 2011; Landman & Beraki, 2012; Winsemius et al., 2013) are translated into the operational prediction of streamflow at short-range and seasonal forecasts.

This project explores the extent to which skilful early warning of flood events can be provided in South Africa across short-range, medium-range and seasonal timescales. This chapter, in particular, reports on the development of a new type of streamflow forecast model in South Africa with the immediate application being at the seasonal timescale.

### 2.2 Data and Methodology

The regional climate model used in the project, namely, CCAM, is a variable-resolution global climate model (GCM) developed by the Commonwealth Scientific and Industrial Research Organisation (CSIRO) (McGregor, 2005; McGregor & Dix, 2001; 2008). The CCAM solves hydrostatic primitive equations using a semi-implicit semi-Lagrangian solution procedure, which includes a comprehensive set of physical parameterisations. It employs the Geophysical Fluid Dynamics Laboratory's (GFDL) parameterisation for long-wave and shortwave radiation (Schwarzkopf & Fels, 1991) with interactive cloud distributions determined by the liquid and ice water scheme of Rotstajn (1997). The model employs a stability-dependent boundary layer scheme based on the Monin–Obukhov similarity theory (McGregor et al., 1993). The CCAM runs in combination with the CABLE dynamic land-surface model. The cumulus convection scheme uses mass-flux closure, as described by McGregor (2003), and includes both downdrafts and detrainment.

The CCAM may be employed in a quasi-uniform or stretched mode by using Schmidt's (1977) transformation to obtain a high resolution over the area of interest. Figure 4 shows the model grid that was used for the quasi-uniform simulations analysed in this deliverable (every 4<sup>th</sup> grid point is shown), of C192 resolution (about 50 km in the horizontal).

Simulations of hydrology in this chapter are based on the simulations of a state-of-the-art dynamic hydrological model (river routing model) that runs fully coupled to the CCAM CABLE modelling system. This system has recently been developed further to include the river run-off scheme previously used within the CSIRO Mk3.5-coupled GCM. The river run-off is directed down to coastal points using the local topography for river direction. A time delay method is applied to transfer water to the oceans, with

river flow being processed via river reservoirs per model land point using the flow velocities to adjacent grid points (CSIRO, 2013).

Due to the complexity of river systems in reality, with the actual terrain not being adequately resolved by typical climate model simulations, there is an option of a pre-computation stage using a high-resolution surface topography data set, together with manual intervention, to help define realistic surface flow directions for the river run-off on the model grid. The river routing scheme is fairly simple with no meandering term, although there are options for allowing moisture to seep into the surrounding soil. The local slope is used to estimate the water flux leaving the four sides of each model grid. More advanced river models allow water to leave in eight directions.

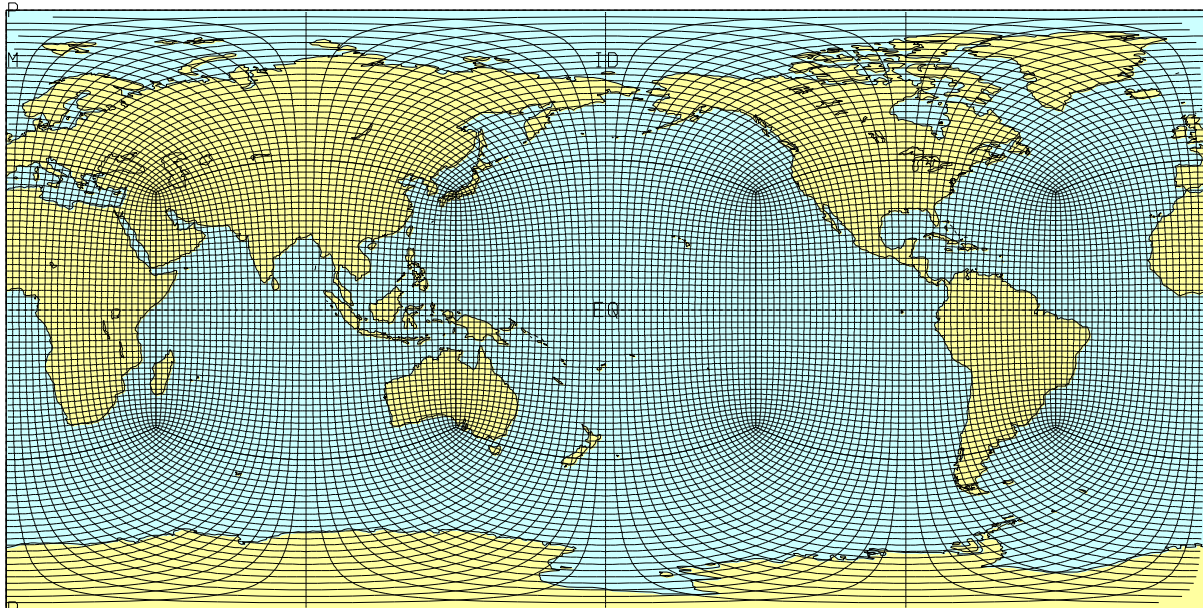


**Figure 4: C192 quasi-uniform conformal cubic grid (every 4<sup>th</sup> grid point is shown), providing a horizontal resolution of about 50 km globally**

#### *Experiment 1*

The CCAM hindcasts were generated for the period 1979–2015 by downscaling the European Centre for Medium-range Weather Forecasting Reanalysis (ERA) data to a resolution of 50 km globally. The model was forced at its lower boundary with observed SSTs and sea ice (Engelbrecht et al., 2009) with data input at six-hour intervals. Only weak atmospheric forcing from the ERA reanalysis data was used. Therefore, the skill of these simulations to represent rainfall patterns provided an upper boundary to the skill of a seasonal forecast system. Twenty-seven levels were used in the vertical.

#### *Experiment 2*

The second set of CCAM simulations for the period 2006–2016 was set up at an 8 km resolution in the horizontal and nudged within the quasi-uniform horizontal resolution downscaling of the ERA reanalysis data. Other variables provided as lower boundary forcing to the 8 km resolution simulations included urban fraction, soil type, vegetation type, vegetation fraction, surface roughness and leaf area index. Updated South African land cover at a resolution of 300 m was acquired from the MODIS satellite. The river routing algorithm was activated during the model set-up to simulate both river water depth and water run-off. The CCAM CABLE modelling system was thus applied in combination with a dynamic river routing scheme.

## **2.3 Results**

### **2.3.1 Experiment 1**

The results in this sections are for the CCAM CABLE model set-up of Experiment 1 as described in Section 2.2.

#### **2.3.1.1 Rainfall simulations**

The CCAM CABLE dynamic regional climate model with dynamic river routing provides a system that simulates the complete hydro-climatic system using the principles of physics (see Section 2.2). Towards obtaining reliable simulations and skilful seasonal forecasts of streamflow using dynamic river routing, it is therefore essential that the model simulates rainfall skilfully. Feedback from the hydrological system to the atmosphere is probably of less importance for the seasonal forecasting problem, although the freshwater flux of the world's major river systems is important in terms of the global ocean circulation (and therefore climate).

As a first step in evaluating the simulations obtained using the CCAM CABLE system coupled with dynamic river routing, the simulated annual rainfall climatology was compared with the CRU-observed rainfall (Figure 5). The model exhibited a generally positive rainfall bias with the largest overestimations east of the Lesotho–Drakensberg escarpment. Rainfall was underestimated over the winter rainfall region of the south-western Cape and also over the north-eastern parts of the country. These underestimations could be attributed to the topography of the eastern escarpment in the north-east as well as the Cape South Coast mountains not being sufficiently resolved in the 50 km resolution simulations.

The over- and underestimations of rainfall could affect the simulations of streamflow in the dynamic river routing system directly coupled to CCAM. In an off-line hydrological system, or in the case of the statistical downscaling of streamflow (as reported in Chapter 3), it would have been possible to first bias-correct the rainfall simulations before the model was applied to drive the hydrological forecast.

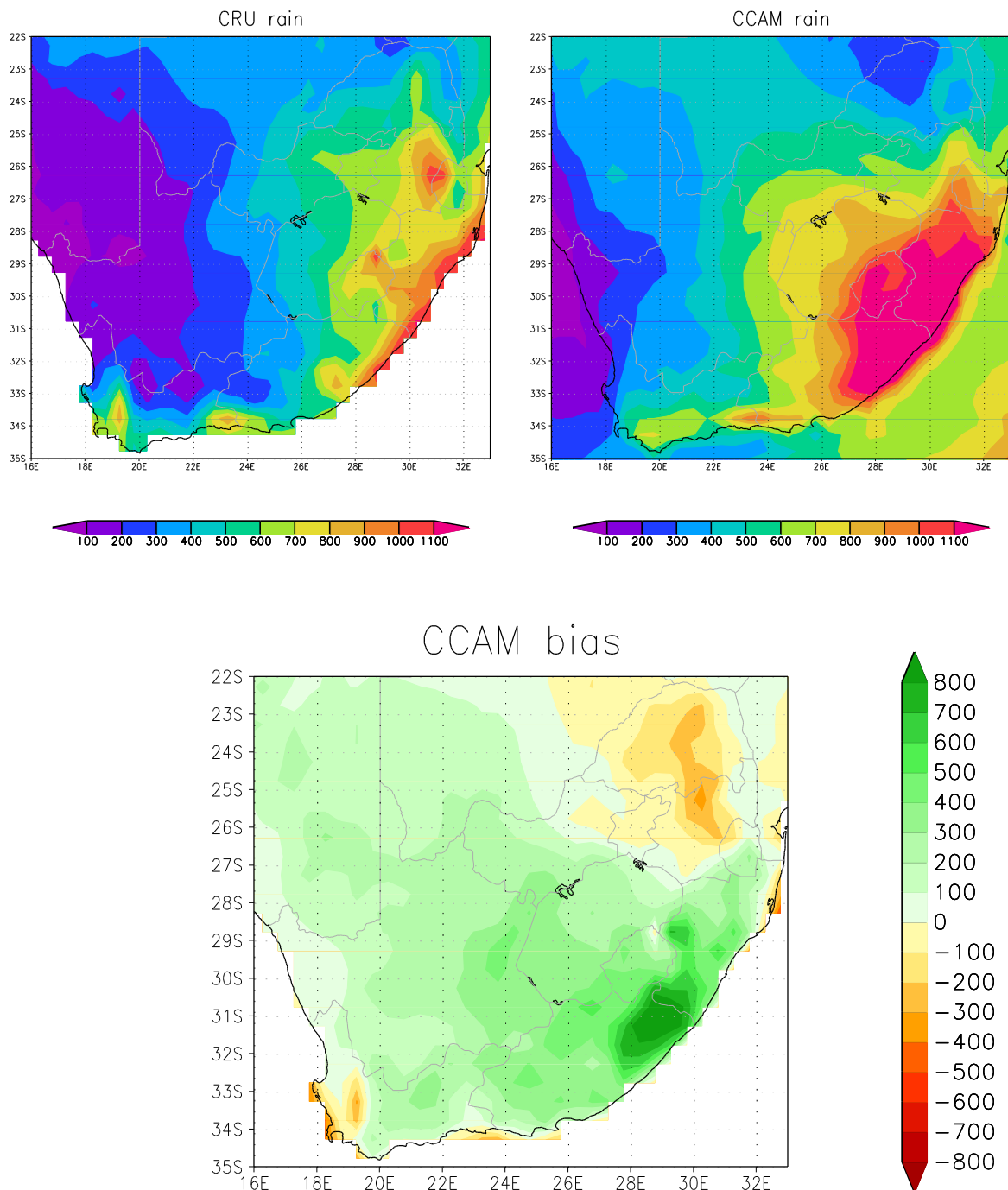


**Figure 5: CRU (observed) annual rainfall climatology (top left) and corresponding CCAM-simulated climatology (top right) for the period 1979–2010. The CCAM annual rainfall bias (bottom) is indicative of general rainfall overestimations, except over the north-eastern and south-western parts of South Africa**

### 2.3.1.2 Dynamic river routing simulations

At the start of model simulations, the model needs to be spun up from a dry state – that is, none of the river basins contain any surface water. Figure 6 shows the state of the surface height after a single month (January 1979), 13 months (January 1980), 25 months (January 1981) and 37 months (January 1982). The convergence of the surface water state, prone only to changes in interannual variability, seems to be well established after three years of integration.

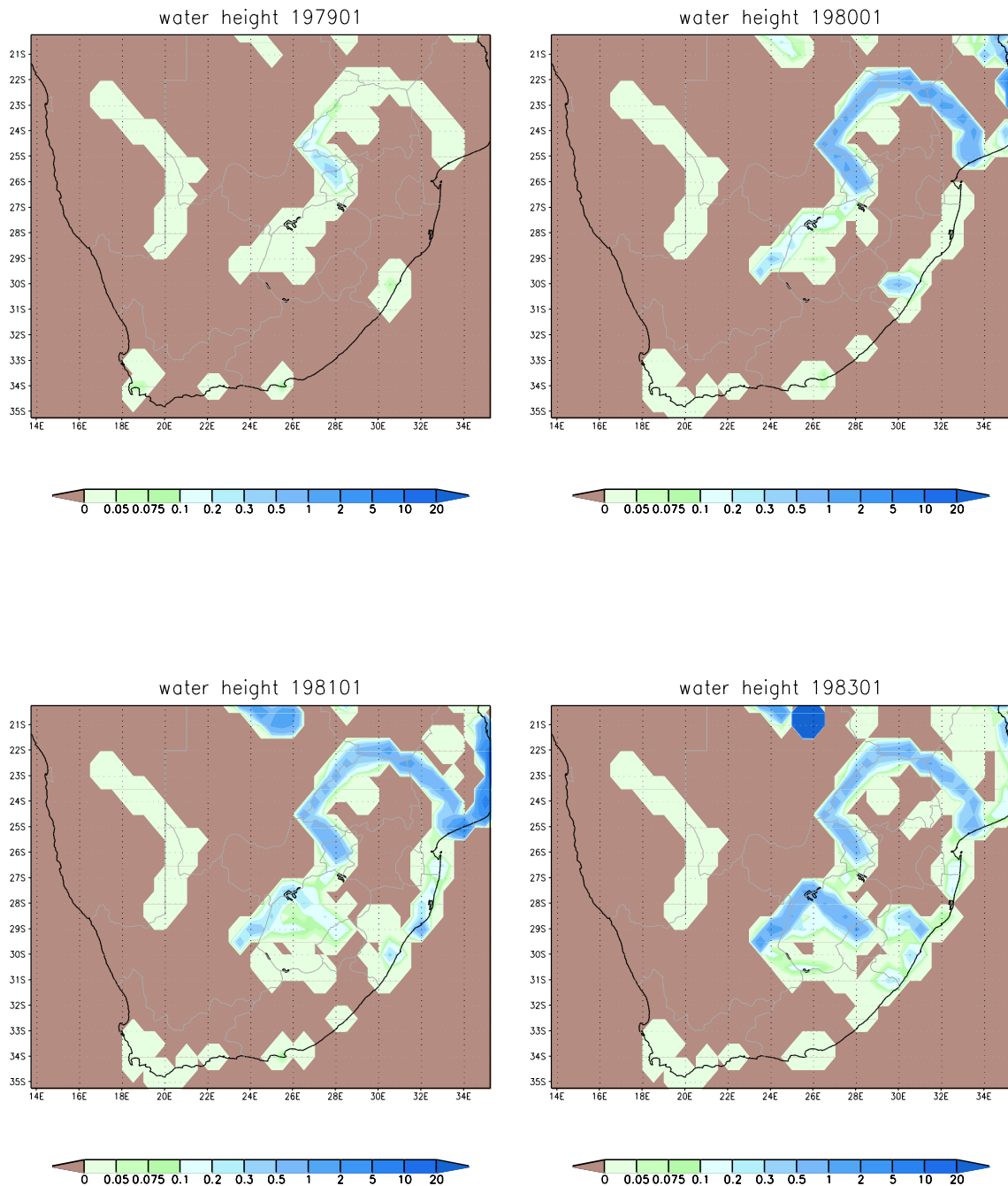


**Figure 6: Spinning-up the dynamic river routing scheme over southern Africa. A balanced state is reached after about **three years** of model integration**

The simulated dynamic river routing climatology is displayed in Figure 7. At a 50 km resolution, using only the principles of river routing physics as outlined in Section 2.2, the dynamic river routing produced a well-resolved Limpopo River. The Vaal and Tugela rivers can also be discerned. More of South Africa's river systems can be resolved at a higher spatial resolution (see next section).

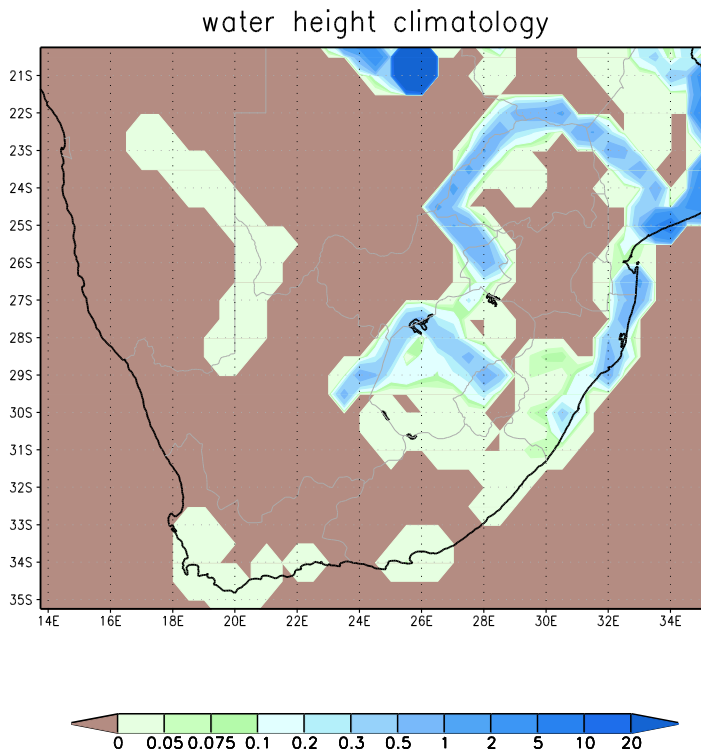


**Figure 7: Simulated dynamic river routing surface water climatology over South Africa**

### 2.3.1.3 Interannual variability simulations

The previous section showed that the dynamic river routing of CCAM tended to resolve the Limpopo River well. In order to examine the performance of the river routing scheme to simulate interannual variability in the Limpopo Basin, the seasonal (December–February) anomalies of the CCAM-simulated variables were correlated to the observed flow anomalies at the station in the main stem of the Limpopo River, which is located at Beitbridge [29°59'25" E; 22°13'37" S].

The analysis was performed for the period from 2002 to 2014 as a complete observational data set was available. Figure 8 shows a time series of normalised anomalies of the observed flow and simulated CCAM variables. During the December–January–February (DJF) summer season of 2005/2006, observations revealed that the recorded flow was over two standard deviations above the climatological mean at Beitbridge station (Figure 8a). The CCAM-simulated river water level, surface run-off and rainfall anomalies presented in Figure 8b, Figure 8c and Figure 8d respectively also show the occurrence of an anomalously positive event in the 2005/2006 season. However, the model simulations that coincide with the observed river flows do not show a consistent pattern throughout the simulations. It could be that the 2005/2006 flows at the Beitbridge station were highly influenced by rainfall events at that particular area as opposed to the influx of water from the tributaries; hence, the model was able to resolve this event.



Limpopo River @ Beit Bridge

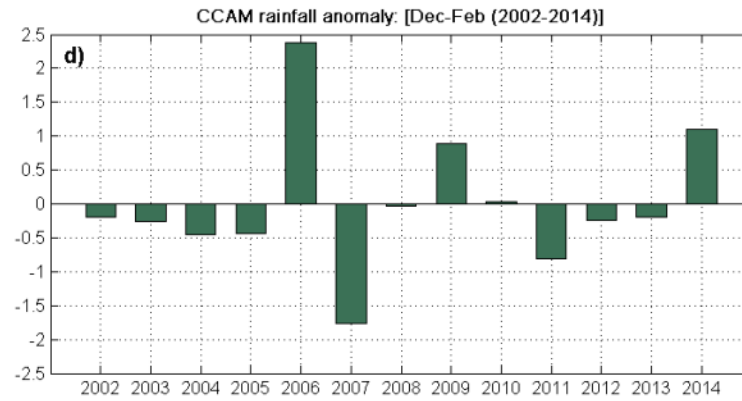
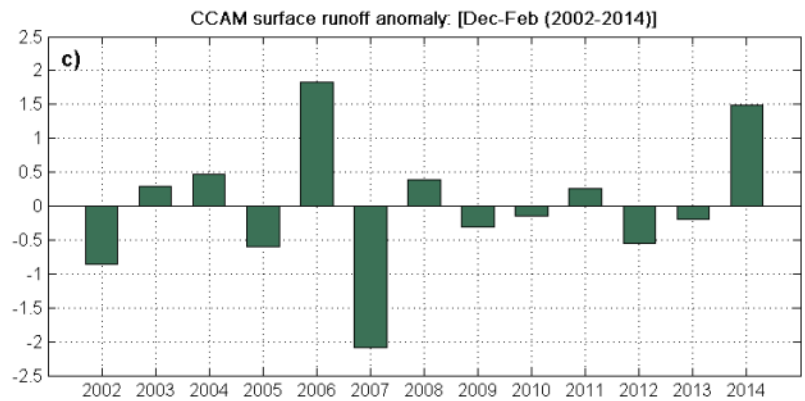
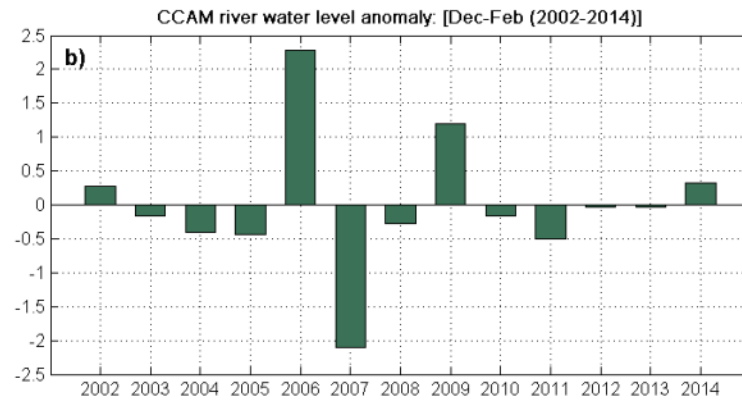
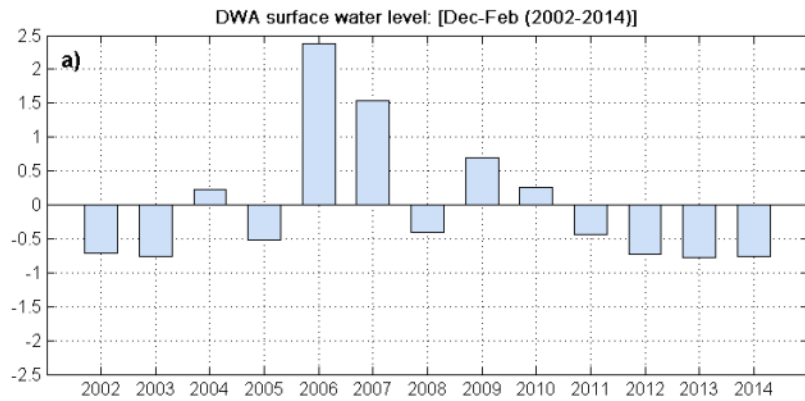


Figure 8: DJF anomalies from 2002 to 2014 in the Limpopo River at the Beitbridge station of a) observed surface water level and CCAM's; b) river water level; c) surface run-off; and d) rainfall

Table 1 presents the correlation coefficients between the observed surface water level and simulated river water level, surface run-off and rainfall at Beitbridge. Overall, the results reveal that there is a direct although weak relationship between observations and model-simulated variables. The CCAM's dynamic routing scheme was run at a relatively low resolution in these simulations. With further improvements of the horizontal resolution, the model might resolve the Limpopo River and its tributaries well, thereby providing insight into to the dynamics of interbasin flow transfers.

**Table 1: Correlation coefficients between surface water level observed at Beitbridge and CCAM-simulated river water level, surface run-off and rainfall for the period 2002 to 2014**

	River water level (CCAM)	Surface run-off (CCAM)	Rainfall (CCAM)
Surface water level	0.2662	0.0728	0.3231

### 2.3.2 Experiment 2

The results in this sections are for the CCAM CABLE model set-up of Experiment 2 as described in Section 2.2

#### 2.3.2.1 Analysis of rainfall, streamflow or river routing and water depth over South Africa during 2013

In this simulation, the CCAM CABLE model was configured to produce outputs with a horizontal grid resolution of 8 km centred over South Africa. The model simulations were performed with the river routing scheme switched on. The CCAM 8 km simulation of 24-hourly rainfall for the period January to December 2013 is depicted in Figure 9 and Figure 10. The purpose of this analysis was to determine how realistic the annual cycle was represented in the simulations. Firstly, it could be seen that during January, February and December (Figure 9a, Figure 9b and Figure 10f), most of the rainfall was simulated over the northern and north-eastern parts of South Africa, which are regions classified as summer rainfall regions (e.g. Rouault & Richard, 2003).

An average rainfall of up to 10 mm/day was simulated over the steep eastern escarpment regions during this season. There tended to be a reduction in rainfall intensity and a southwards shift from March to April 2013 (see Figure 9c and Figure 9d), with more rain simulated over the south-east coast of South Africa and over the all-year rainfall region (Rouault & Richard, 2003).

For the period between May and September (as shown in Figure 9e, Figure 9f, Figure 10a, Figure 10b and Figure 10c), rainfall occurrence and intensity tends shifted towards the south-western Cape. These results were similar to those presented in previous studies (e.g. Rouault & Richard, 2003; Philippon et al., 2012). During October and November (Figure 10d and Figure 10e), rainfall occurrence tended to shift more towards the south and east coast as well as the south-eastern interior of South Africa with the highest average values up to 10 mm/day.

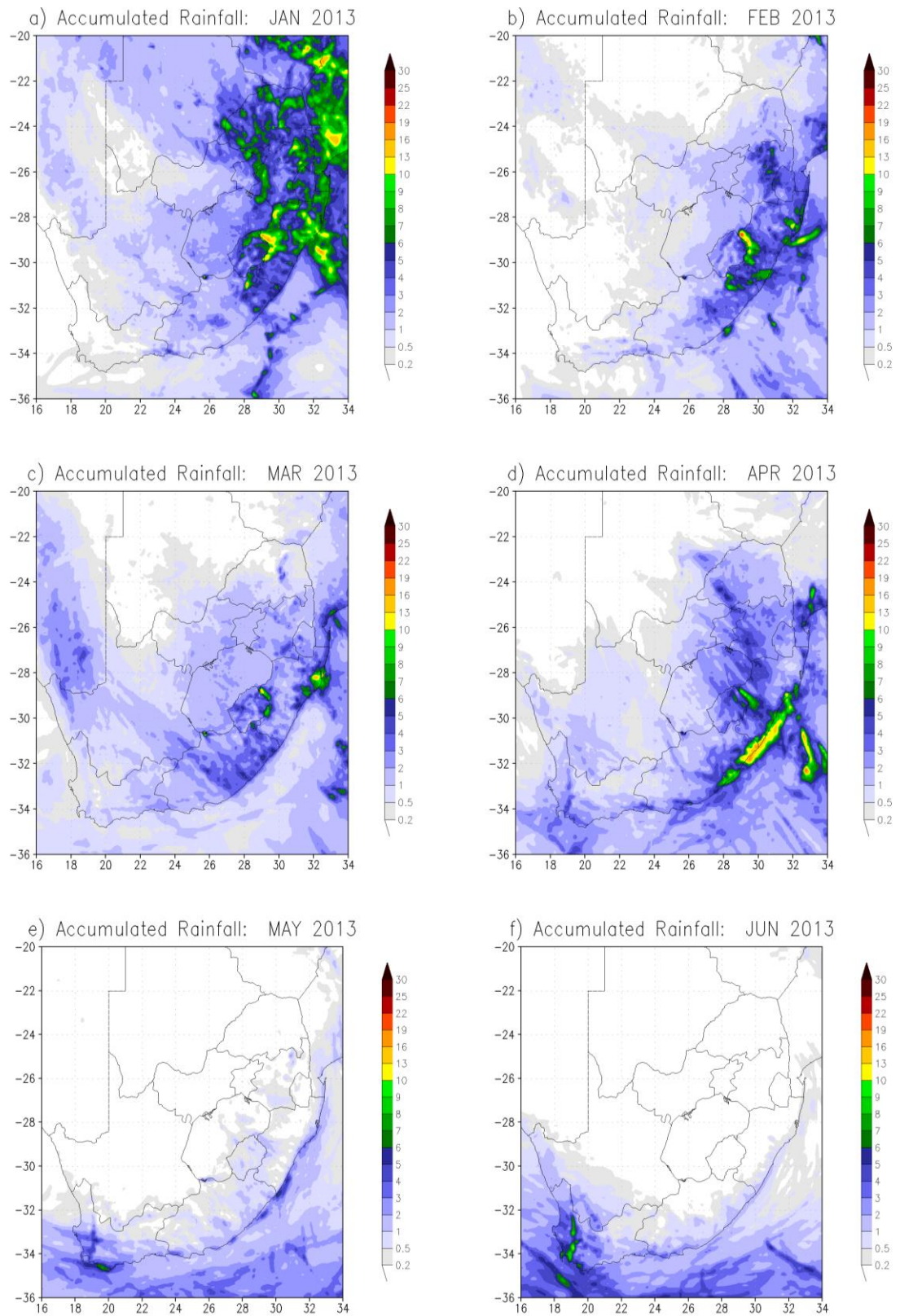


**Figure 9: CCAM 8 km ERA Interim data simulated averaged 24-hour accumulated rainfall (mm) over South Africa for January to June 2013**

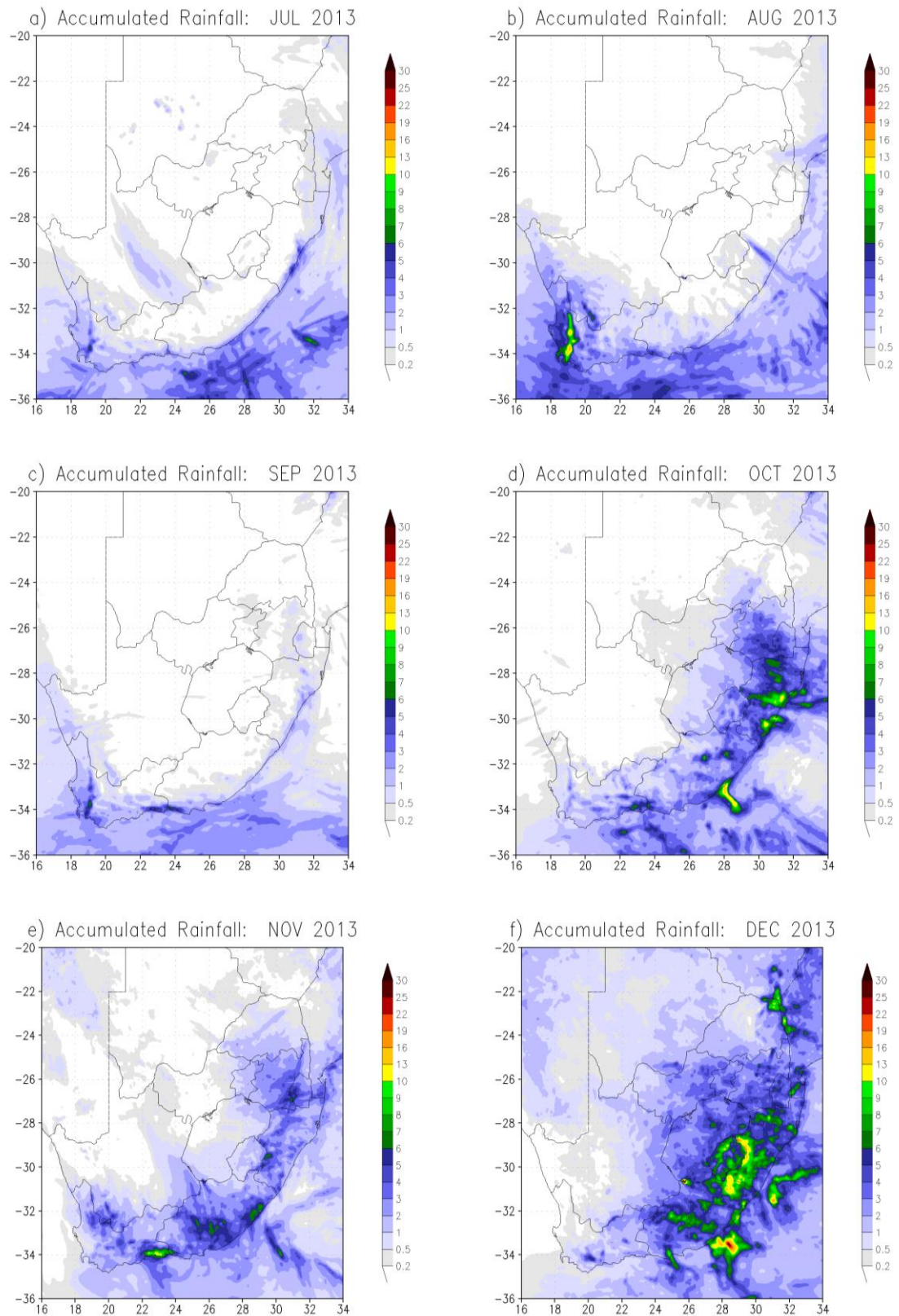


**Figure 10: CCAM 8 km ERA Interim data simulated averaged 24-hour accumulated rainfall (mm) over South Africa for July to December 2013**

Figure 11 and Figure 12 show the CCAM 8 km simulation of water depth for the period January to December 2013 over South Africa. The Orange, Vaal, Limpopo and Tugela rivers show a higher water depth of up to 10 mm during most of the months including December, and from January until April (Figure 11a, Figure 11b, Figure 11c, Figure 11d and Figure 12f). These depths correspond to the higher average rainfall simulated presented in Figure 9 and Figure 10.

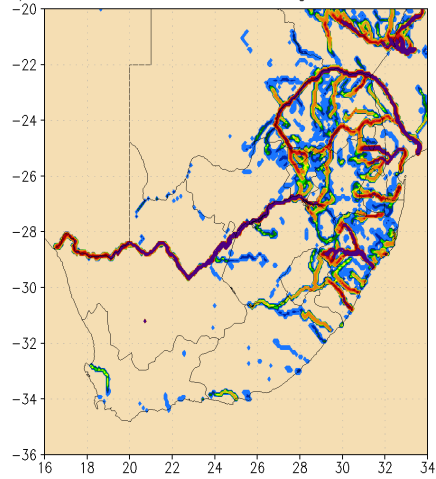
The Orange, Vaal, Limpopo and Tugela rivers are mostly perennial rivers. From May to July 2013 (Figure 11e, Figure 11f and Figure 12a), the water depth reduced over the Limpopo and Orange rivers. The Orange River had higher depth towards the river mouth over the Atlantic Ocean whereas the Limpopo River had more water towards the river mouth in Mozambique into the Indian Ocean (Figure 11e and Figure 11f). During this time period, South African rainfall was mostly distributed to the south and the interior of the country.

From August to September 2013 (Figure 12b and Figure 12c), the water depth over Limpopo reduced considerably, and reduced slightly over the Orange River. During these months, a higher water depth up to 10 mm was simulated over the Western Cape Province (Figure 12b and Figure 12c). This corresponds with the rainfall simulations presented in Figure 10.

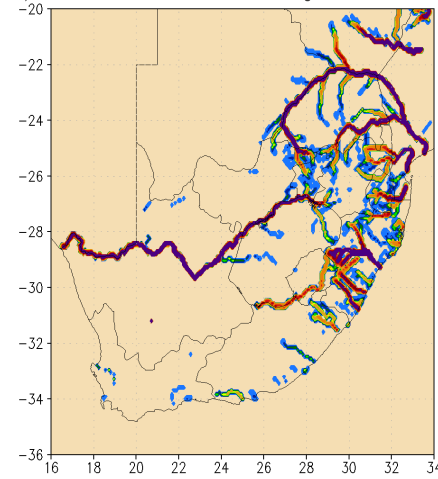
For the period between October and December 2013 (Figure 12d–Figure 12f), there is a northwards shift of the water level, which is consistent with the rainfall spatial pattern simulated over the eastern and north-eastern parts of South Africa (Figure 10d–Figure 10f).

Overall, the results presented in this section indicate that the simulated water depth is related to the amount of rainfall that fell over a given time period.

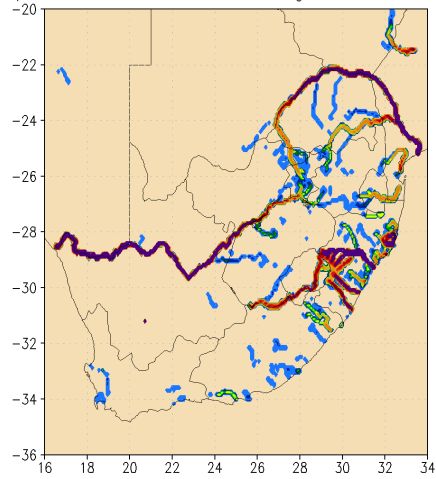
a) Accumulated Water Height: JAN 2013



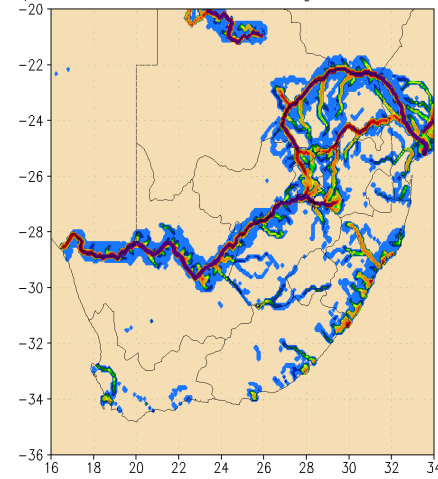
b) Accumulated Water Height: FEB 2013



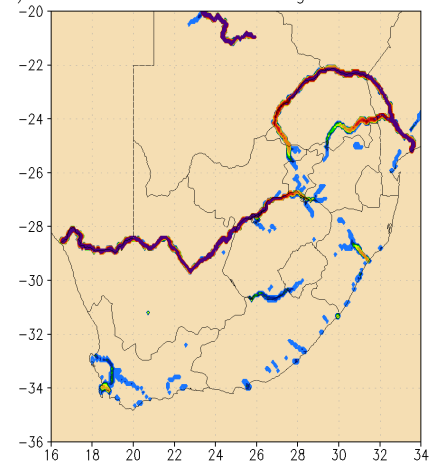
c) Accumulated Water Height: MAR 2013



d) Accumulated Water Height: APR 2013



e) Accumulated Water Height: MAY 2013



f) Accumulated Water Height: JUN 2013

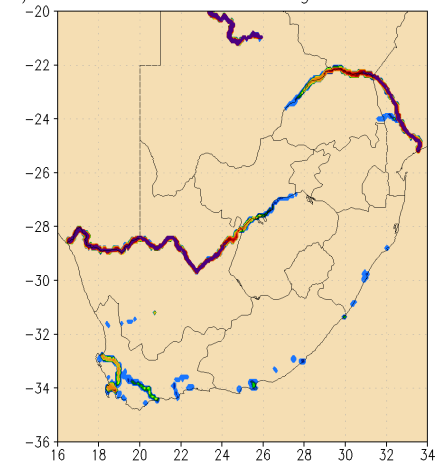
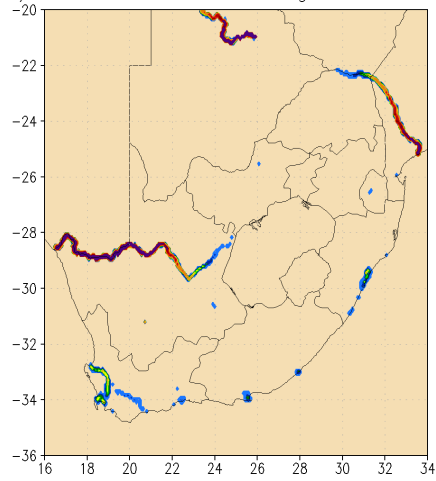
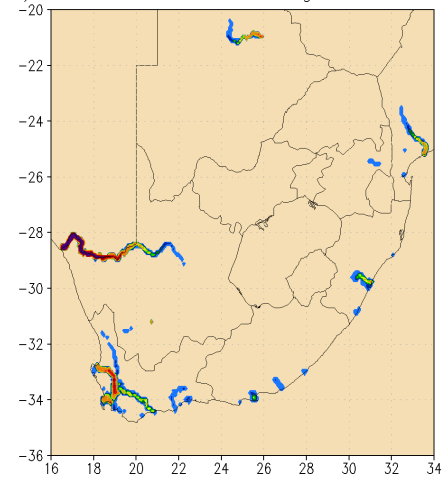


**Figure 11: CCAM 8 km ERA Interim data simulated average river water depth (mm) over South Africa for the period January to June 2013**

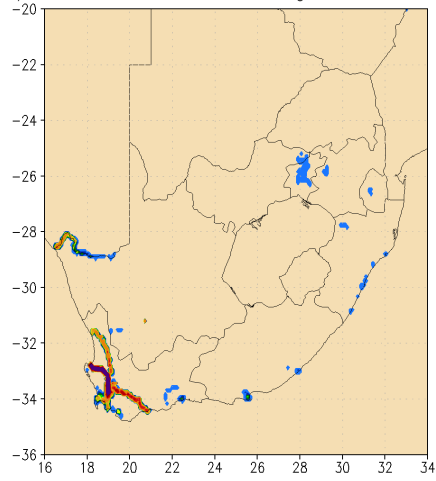
a) Accumulated Water Height: JUL 2013



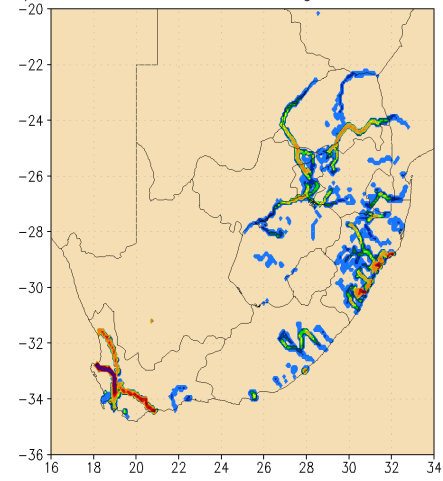
b) Accumulated Water Height: AUG 2013



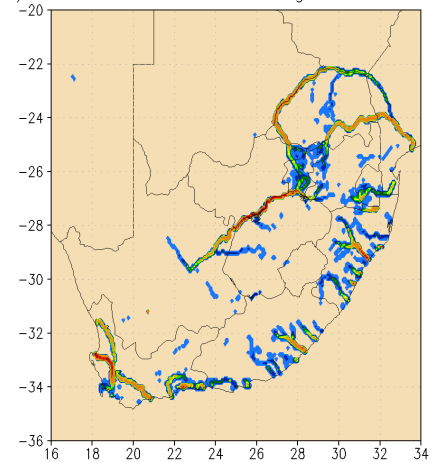
c) Accumulated Water Height: SEP 2013



d) Accumulated Water Height: OCT 2013



e) Accumulated Water Height: NOV 2013



f) Accumulated Water Height: DEC 2013

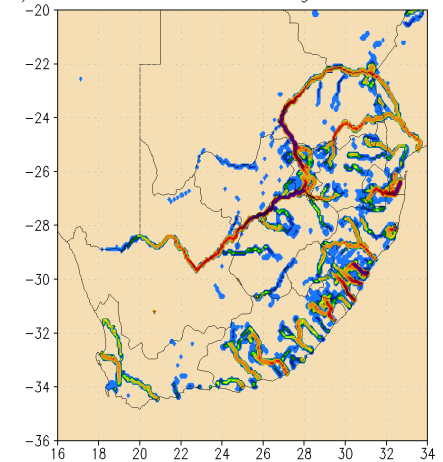


**Figure 12: CCAM 8 km ERA Interim data simulated average river water depth (mm) over South Africa for the period July to December 2013**

The CCAM CABLE river run-off simulations are depicted in Figure 13 and Figure 14. Run-off is a variable that describes the amount of rainfall that is transferred to streamflow (as opposed to the components of rainfall that evaporate or become soil moisture). During most of the summer months including January, February, March and December 2013 (Figure 13a, Figure 13b, Figure 13c and Figure 14f), there tended to be more run-off in areas that corresponded to the regions where more rainfall was received (see Figure 9a, Figure 9b, Figure 9c, Figure 10f).

For the period between May and November 2013 (Figure 13e, Figure 13f and Figure 14a–Figure 14e), run-off weakened and disappeared in the east, leaving only the Western Cape as a region that experienced some run-off. This result is consistent with the simulated rainfall (see Figure 9 and Figure 10) and water depth (as shown in Figure 11 and Figure 12).

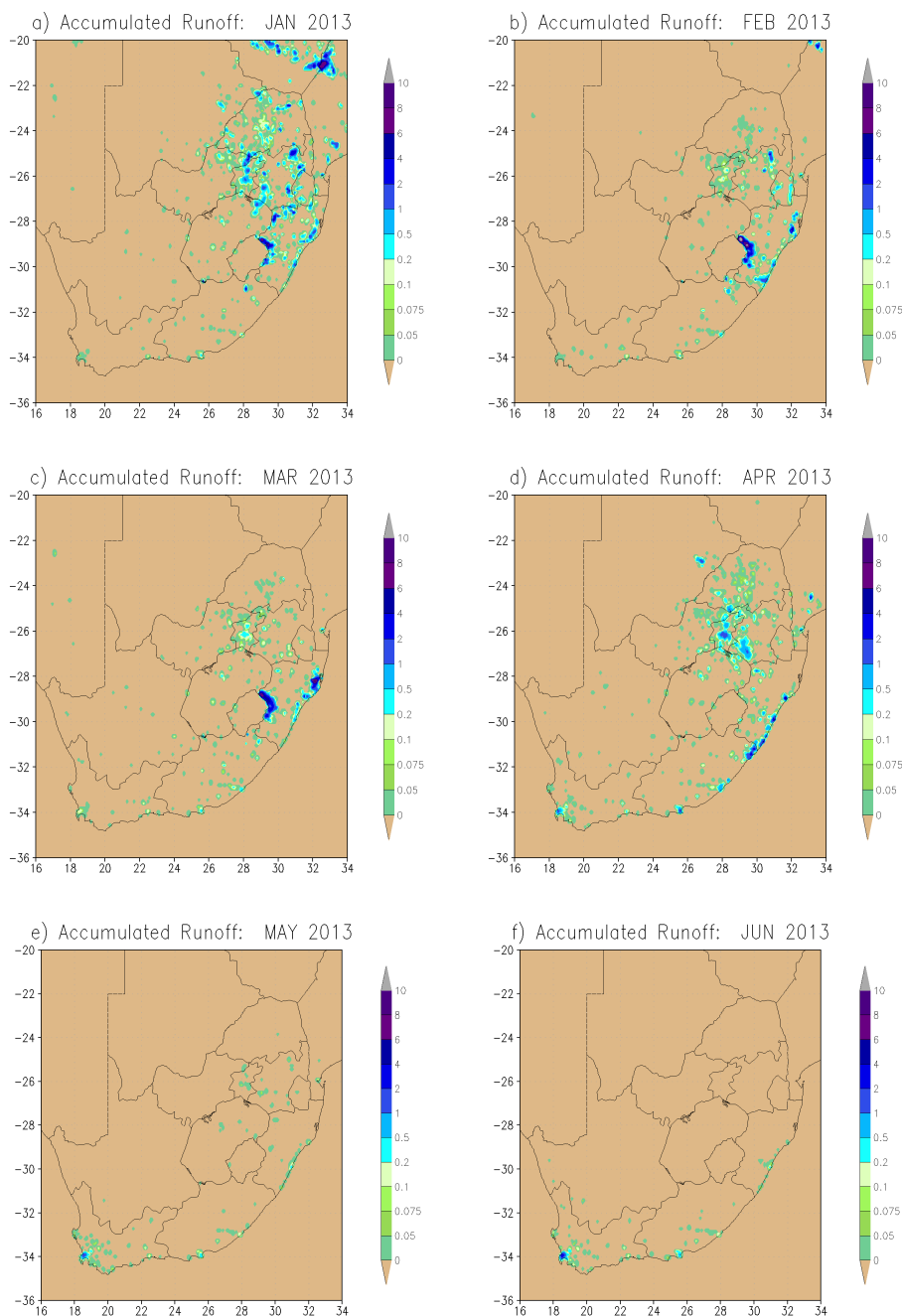


**Figure 13: CCAM 8 km ERA Interim data simulated average river run-off (mm/day) over South Africa for the period January to June 2013**



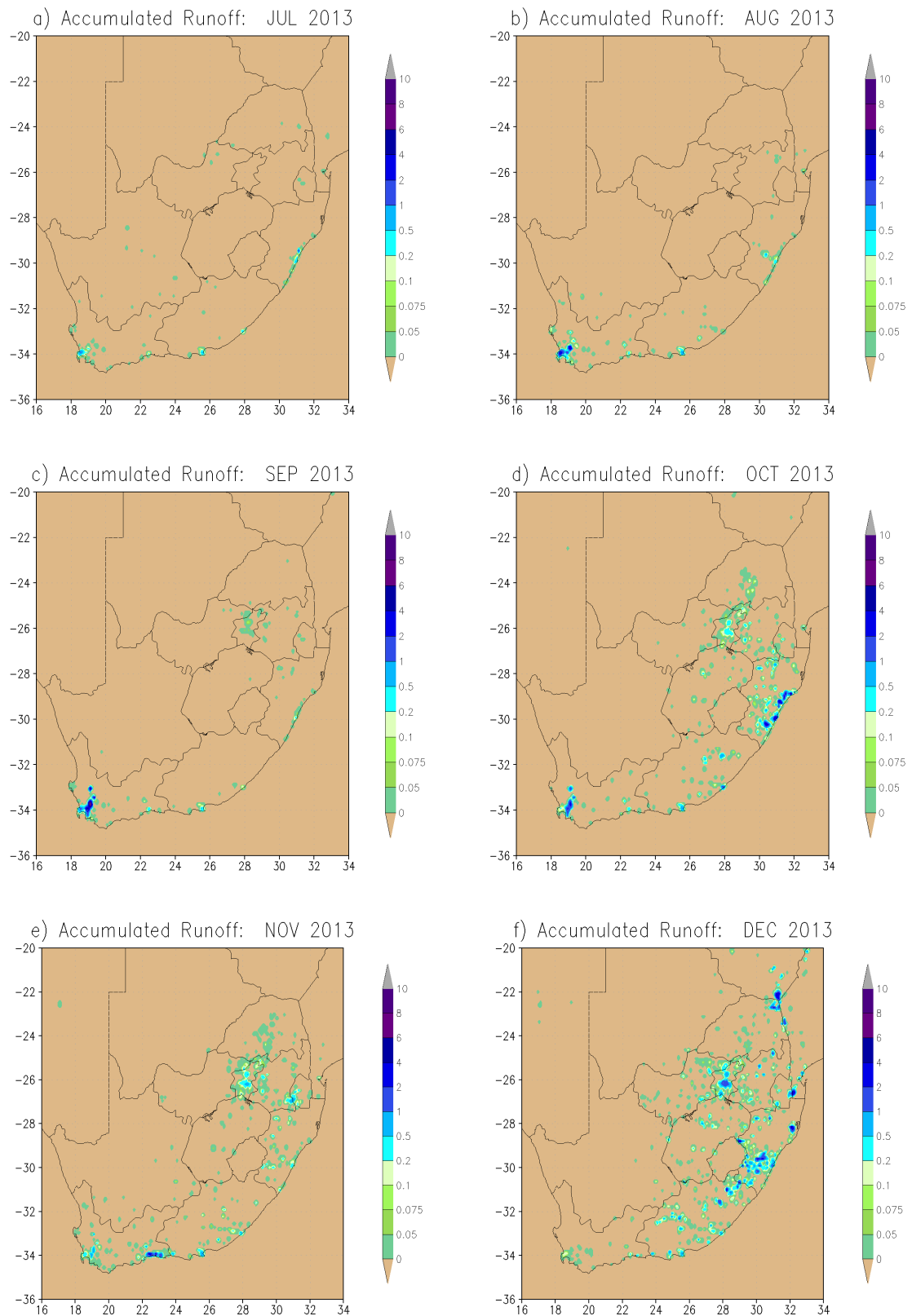


**Figure 14: CCAM 8 km ERA Interim data simulated average river run-off (mm/day) over South Africa for the period July to December 2013**

### **2.3.2.2 Analysis of rainfall, streamflow or river routing and water depth over South Africa for the period 2006–2016**

The annual cycle analysis of rainfall, river routing and river depths presented in the previous subsection showed that the domain covering the central interior and north-eastern region of South Africa tends to receive more rainfall during the austral summer period with maximum totals occurring in January. During winter, the highest totals were seen in August over the south-western Cape region of South Africa. Based on these results that are indicative of a realistic representation of the seasonal cycle, an extended analysis was done for the period between 2006 and 2016 to examine the interannual variation of these variables.

Simulations of rainfall for January 2006 to 2016 (Figure 15 and Figure 16) showed that over South Africa, the central parts of the country received more rainfall on average than any other regions, with the highest rainfall of 20 mm/day occurring over the Drakensberg mountains in KwaZulu-Natal. However, in the years 2011 and 2013, the maximum rainfall occurred over the eastern summer rainfall region of South Africa with simulated values of 10 mm/day on average. By August, rainfall shifted to the winter rainfall regions of the Western Cape and also to the south coastal areas. During August 2006, 2012, 2013 and 2016, the South Coast and Western Cape received relatively high rainfall with a margin of up to 20 mm (not shown).

Figure 17 and Figure 18 indicate the water depth over South African rivers for the period 2006 to 2016. A simulation of water depth indicated that there tended to be more water over the eastern part rather than the western part of the country, with only the Orange River flowing to the western parts with its river mouth on the Atlantic Ocean. This simulation showed relatively less interannual variability.

Over the entire 10-year period from 2007 to 2016 (considering January 2006 a model spin-off month), the Limpopo River (flowing over the north of South Africa, connecting Botswana, Zimbabwe and Mozambique), the Orange River (flowing towards the Atlantic Ocean) and the Tugela River (flowing over KwaZulu-Natal) had water depths spanning more than 10 mm. Only during January 2011 did the Orange River show signals of drying when the water depth was less than 1 mm (Figure 17f). On average, all three above major river basins showed depths of more than 10 mm (Figure 17 and Figure 18). During August, the water depth reduced significantly over the eastern half of the country in comparison to the western part of the country, with Limpopo water slightly reduced to values less than 2 mm. During August 2009, 2010, 2012, 2012, 2014 and 2015, the entire Gauteng and Limpopo provinces were dry (not shown).

Figure 19 and Figure 20 depict the water run-off in rivers across South Africa during January for the period 2006 to 2016. Simulations over a 10-year period (considering 2006 a model spin-off period) showed more run-off over the eastern parts of South Africa, which correlates with the rainfall pattern (Figure 15 and Figure 16) as well as river water depth (Figure 17 and Figure 18). The most run-off was simulated over the high topography area over the Drakensberg Mountains of KwaZulu-Natal over the entire period, with an average more than 10 mm. There were also higher values of run-off over the northern border of South Africa and Zimbabwe, with values more than 8 mm. These simulations showed evidence of interannual variation of river flows over South Africa, with the model simulation showing less run-off during 2010 and 2012 with values less than 3 mm.

During August for the period 2006 to 2016, simulations showed run-off values of less than 0.6 mm over the eastern half of the country, but with most run-off over the Western Cape and the coastal areas with values up to 1 mm. When compared with the rainfall simulations, the Western Cape had less or no rivers depicted at this resolution, but some visible values of run-off (not shown).

All these results give a clear indication that river water depth and run-off depend on the amount of rainfall that is experienced over specific areas. Likewise, since most parts of South Africa receive rainfall in summer, the water depth is higher during such periods whereas the depth and river run-off get higher during winter (August) in Western Cape.

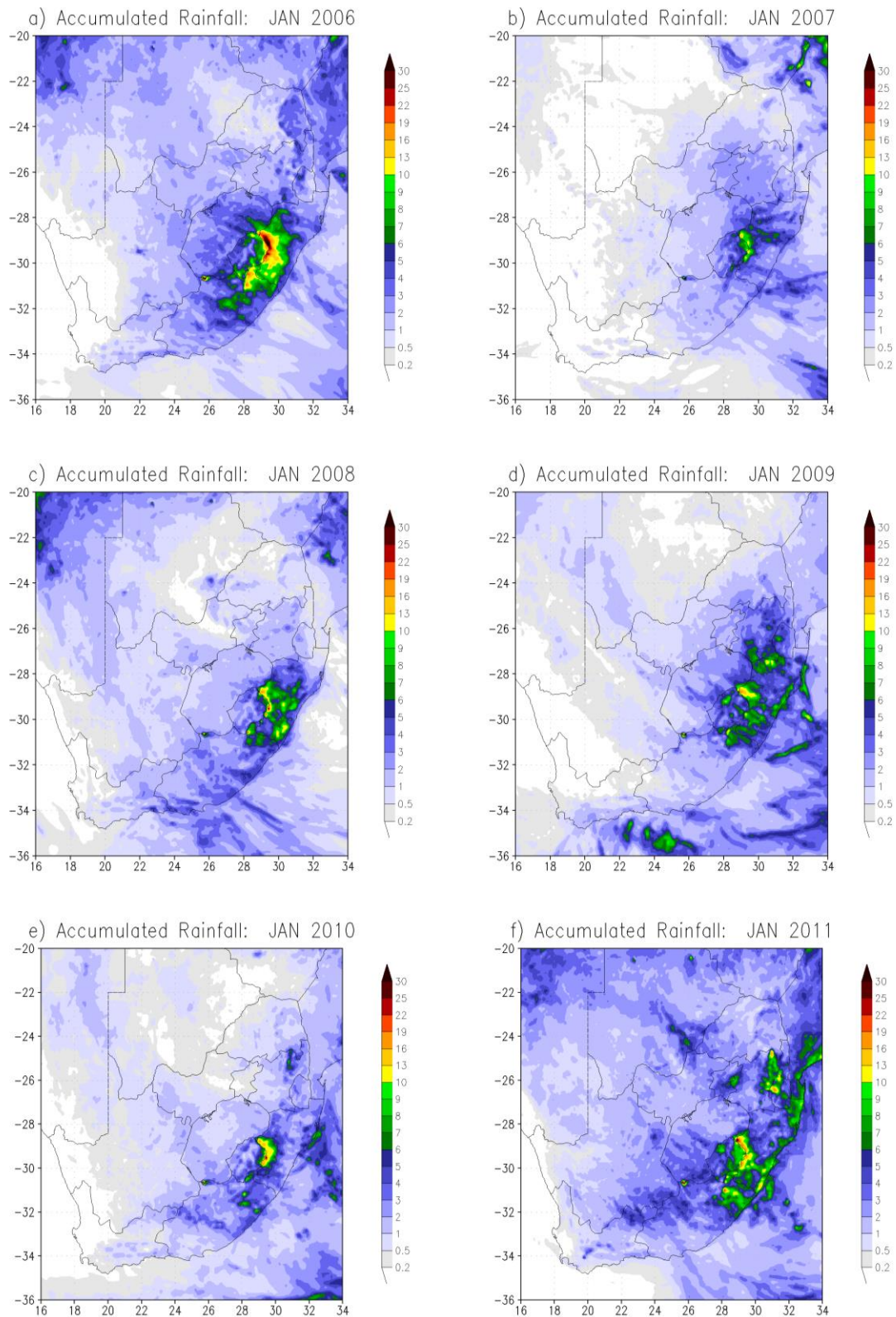


**Figure 15: CCAM 8 km ERA Interim data simulated average 24-hour accumulated rainfall (mm) over South Africa for January 2006–2011**

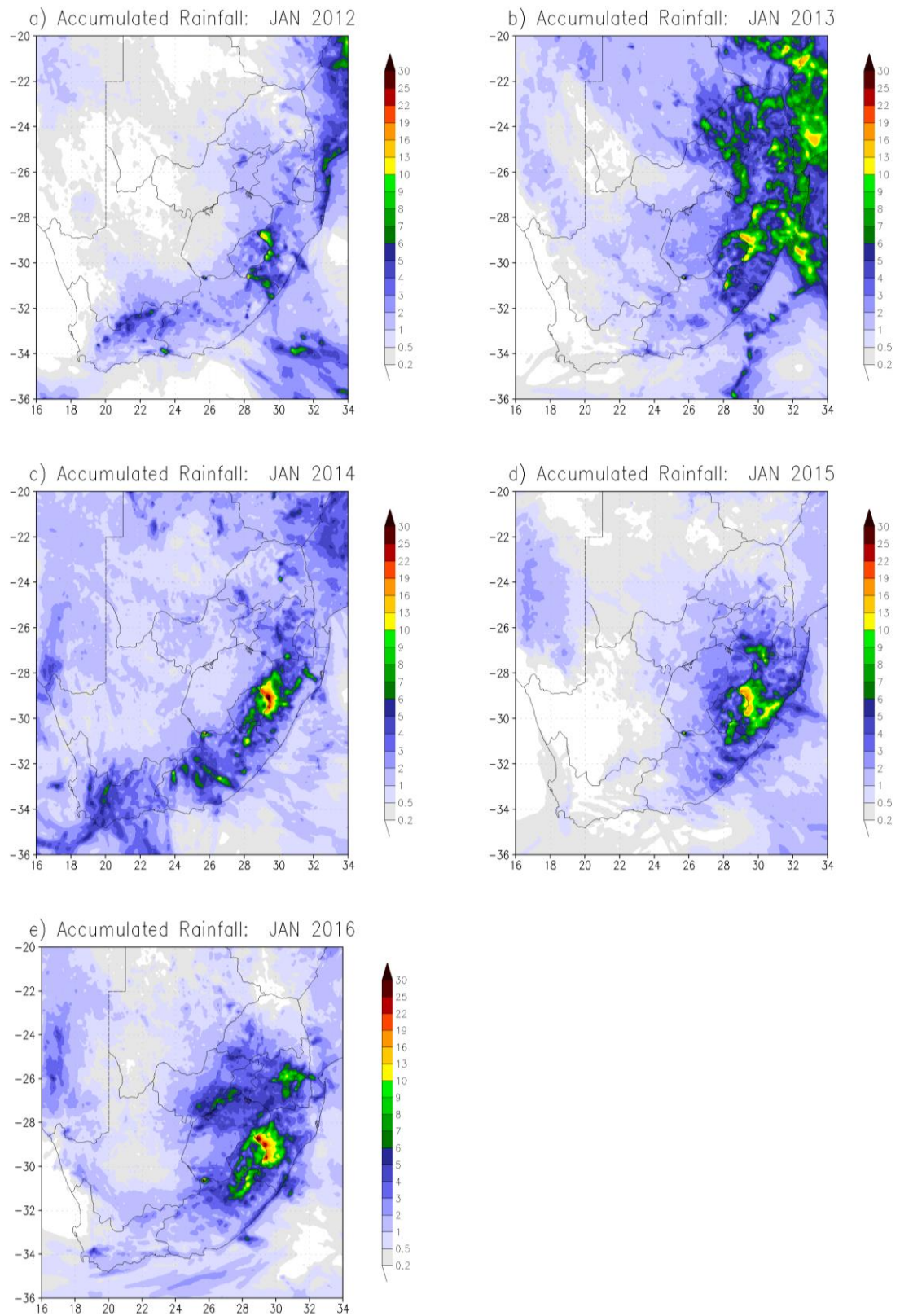
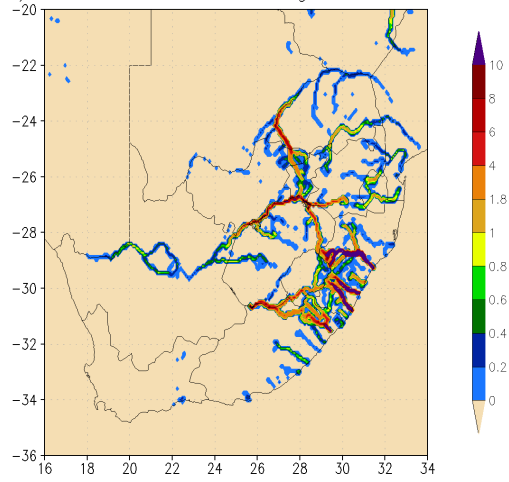
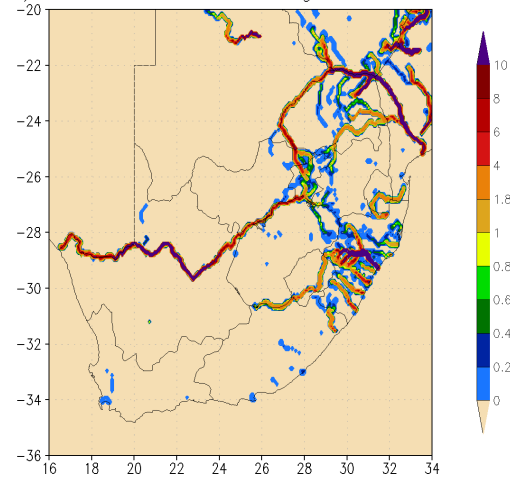


**Figure 16: CCAM 8 km ERA Interim data simulated average 24-hour accumulated rainfall (mm) over South Africa for January 2012–2016**

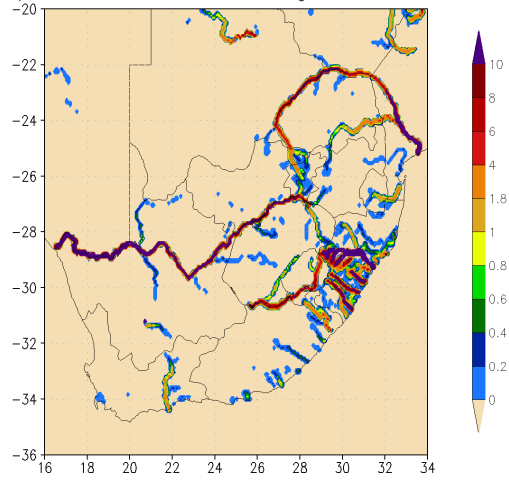
a) Accumulated Water Height: JAN 2006



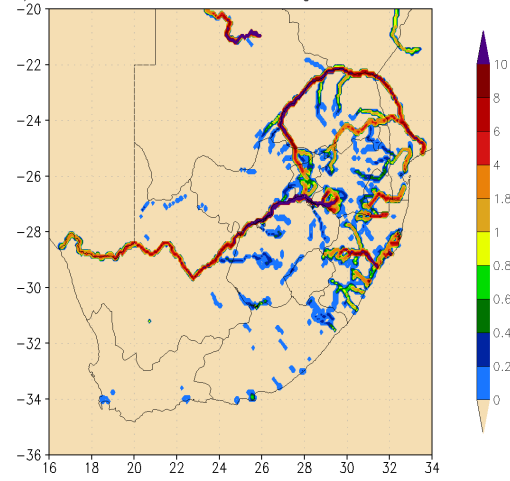
b) Accumulated Water Height: JAN 2007



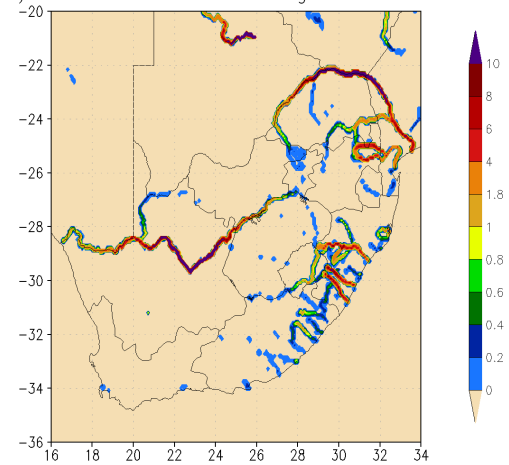
c) Accumulated Water Height: JAN 2008



d) Accumulated Water Height: JAN 2009



e) Accumulated Water Height: JAN 2010



f) Accumulated Water Height: JAN 2011

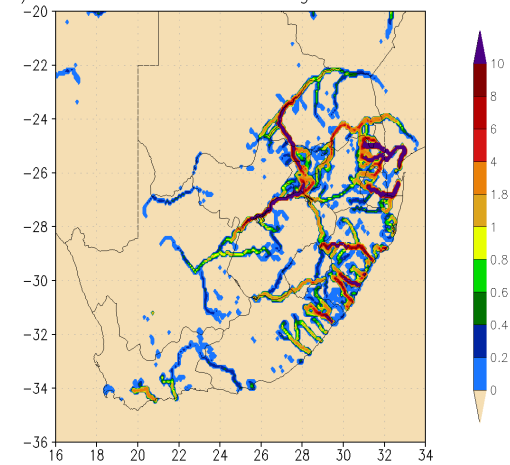


**Figure 17: CCAM 8 km ERA Interim data simulated average river water depth (mm) over South Africa for January 2006–2011**

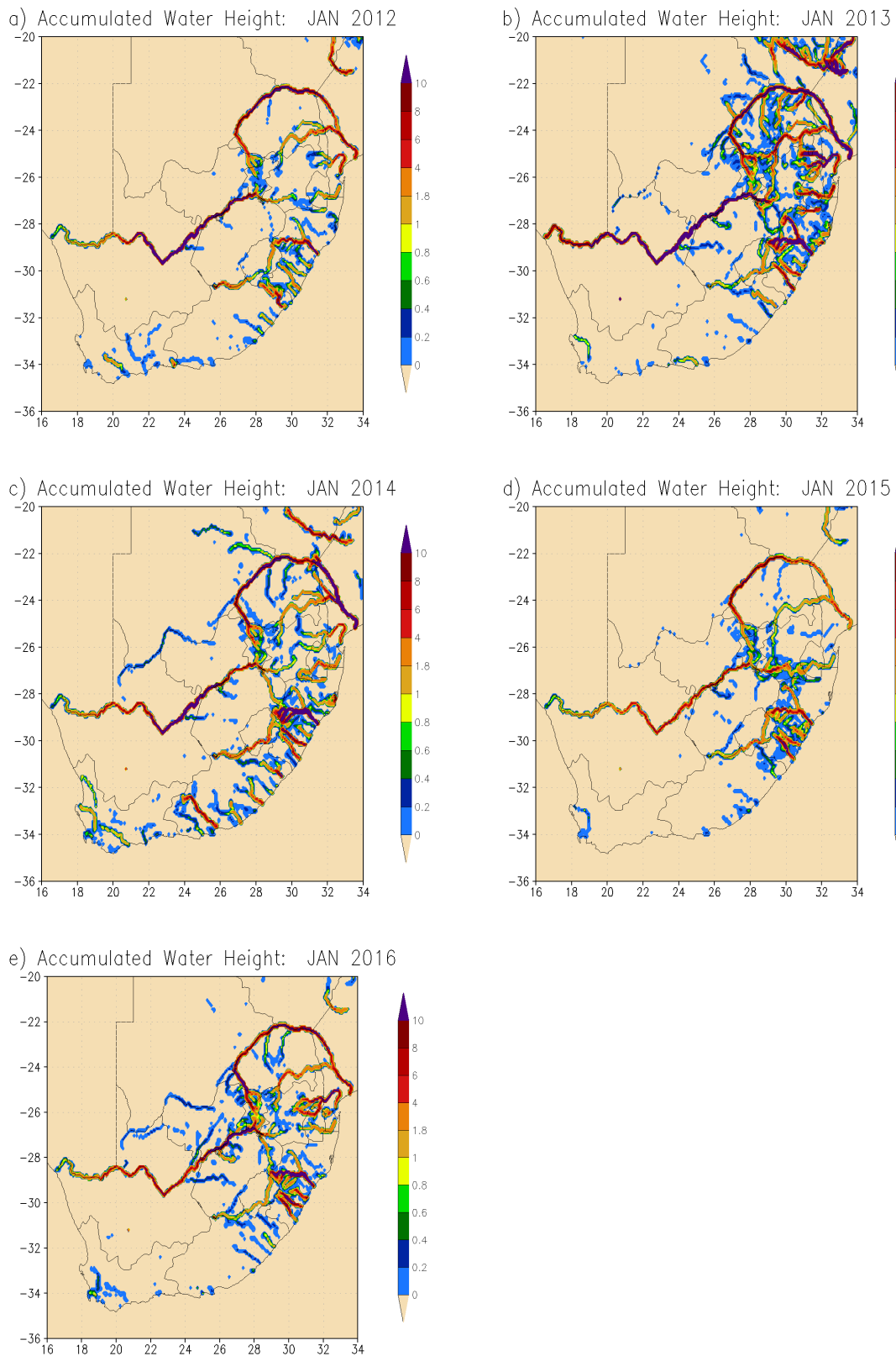


**Figure 18: CCAM 8 km ERA Interim data simulated average river water depth (mm) over South Africa for January 2012-2016**

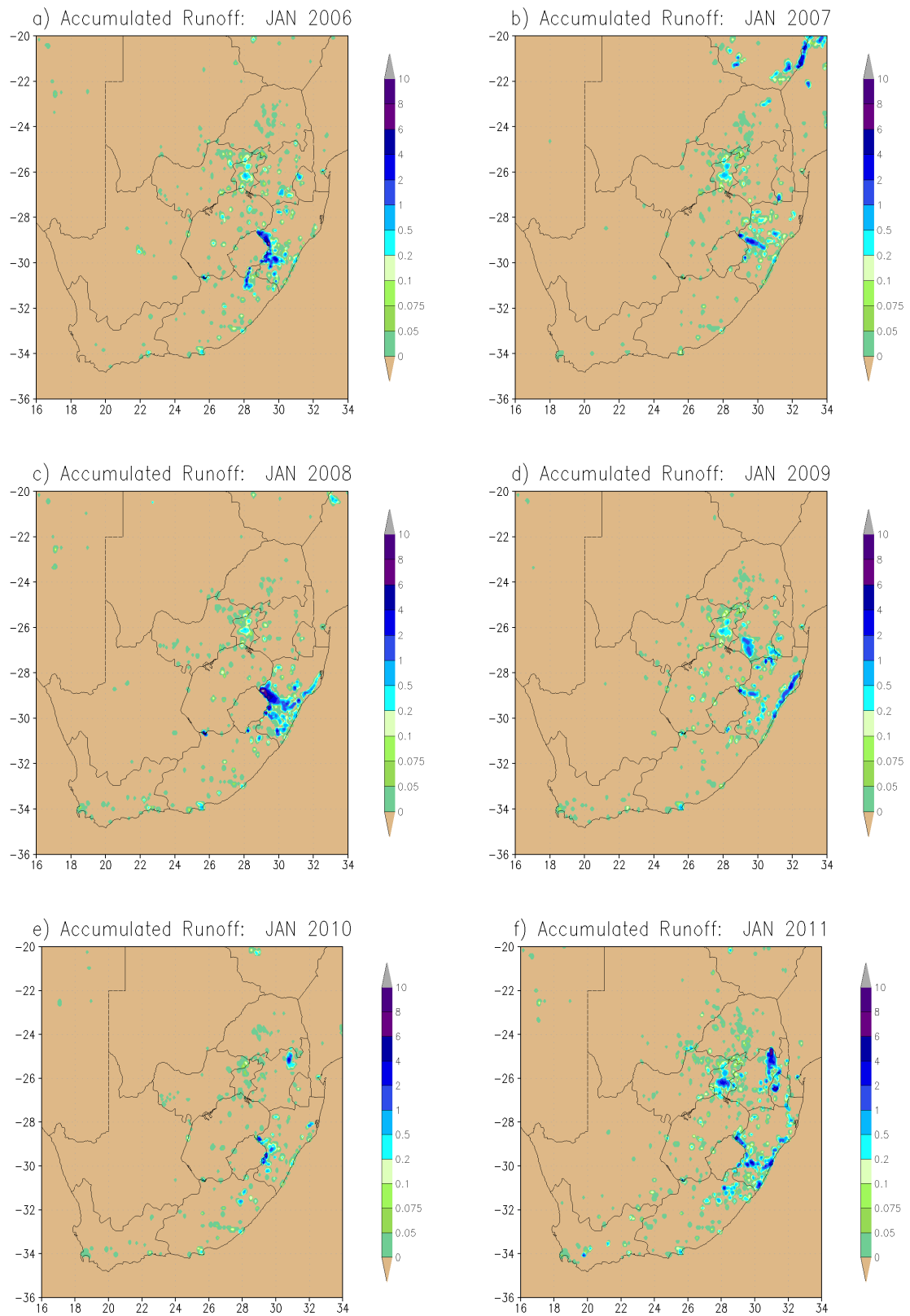


**Figure 19: CCAM 8 km ERA Interim data simulated average river run-off (mm/day) over South Africa for January 2006–2011**

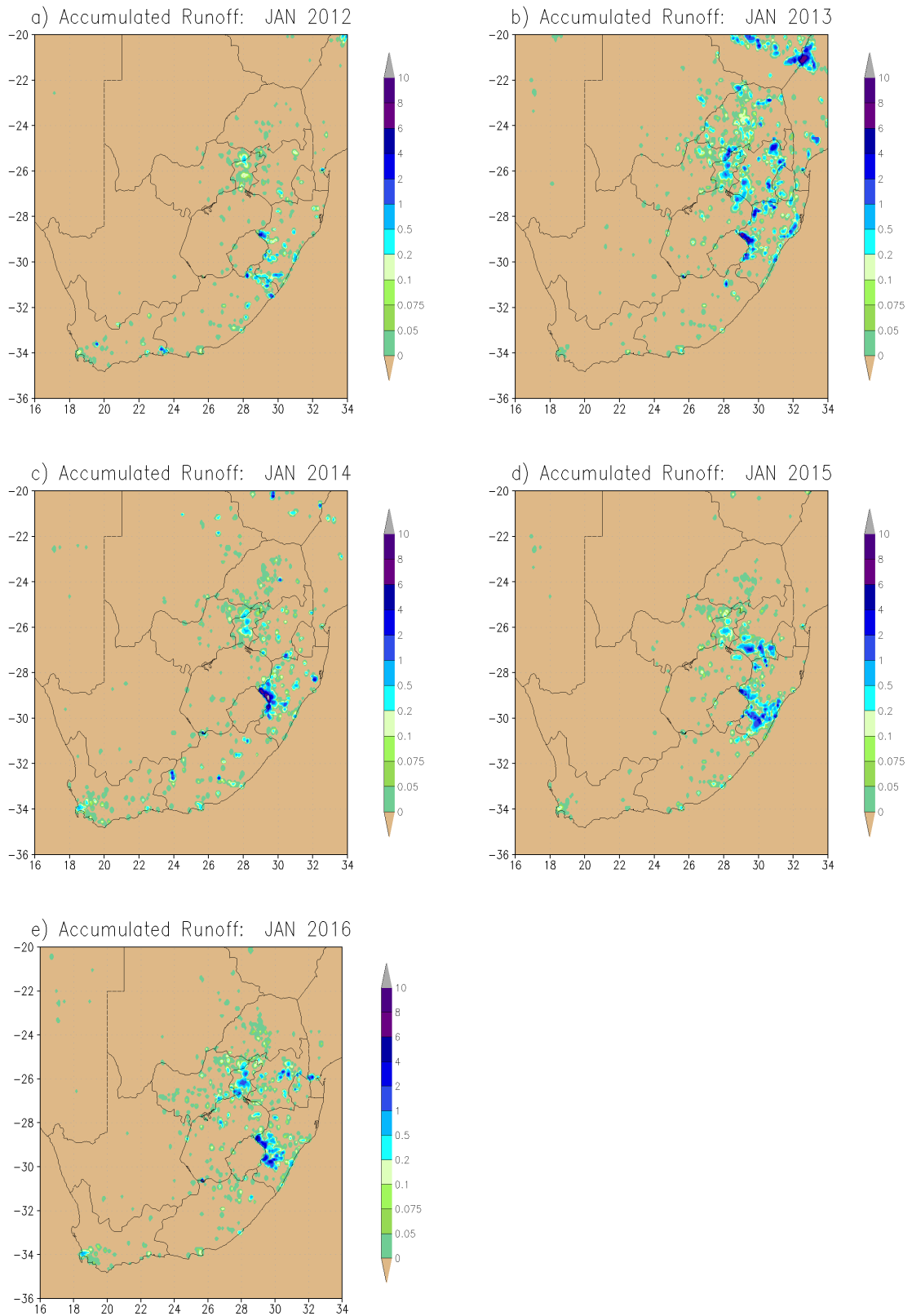


**Figure 20: CCAM 8 km ERA Interim data simulated average river run-off (mm/day) over South Africa for January 2012–2016**



## 2.4 Synopsis

This chapter investigated whether the CCAM and CABLE dynamic land-surface model combination was able to simulate river flows in the north-east region of South Africa when coupled to a dynamic river routing scheme. During the project, two model experiments were performed to demonstrate and improve the capability of the CCAM CABLE model to dynamically downscale rainfall to streamflow over the north-eastern region of South Africa at seasonal and monthly timescales, using river routing based on the physics of streamflow.

Considering rainfall as prime factor that determines streamflow, it should be noted that the CCAM-simulated rainfall exhibited a notable positive rainfall bias over most of South Africa. The results presented in Section 2.3.1 of the CCAM CABLE model's first experimental set-up show that at a 50 km resolution, the Limpopo River was well resolved, and that the Vaal and Tugela rivers were present although they were resolved less realistically. In the well-resolved Limpopo system, interannual variability in streamflow was skilfully represented by the modelling system as indicated by the positive correlations between simulated water surface height and observed streamflow.

At an 8 km horizontal resolution (Experiment 2 set-up, presented in Section 2.3.2), there was evidence of a considerable degree of improvement in the capability of the CCAM CABLE model to simulate major rivers across South Africa (such as Orange River, Vaal River, Tugela River, Limpopo River etc., see Figure 13).

The results presented here represent, as far as the authors know, the first application of a dynamic river routing scheme over southern Africa. The river routing scheme essentially computes all flow-related variables based purely on a rainfall-flow relationship; however, it does not include factors such as inter-basin transfers, and dynamic and physical attributes of catchment areas. The new technology presented here, namely, dynamic river routing simulations of naturalised streamflow, may be of value in operational seasonal forecasts of streamflow in South Africa.

### 3 STATISTICAL DOWNSCALING OF CCAM SIMULATIONS TO STREAMFLOW

#### 3.1 Introduction

The south-western Cape region of South Africa is currently facing one of the most devastating hydrological droughts to date. This highlights the role that hydrological forecasts can potentially play in assisting with emergency management, routine operations and long-term strategic planning. There is a wealth of research conducted globally to showcase a broad application of hydrological forecasts in areas such as flood warning, drought forecasting, irrigation scheduling and river basin management (e.g. Anghileri et al., 2016; Gibbs et al., 2018; Muchuru et al., 2014; 2015; Pappenberger et al., 2015a; 2015b; Schwanenberg et al., 2015).

In hydrological modelling, rainfall data is one of the most important inputs required by all run-off models (Devia et al., 2015). In order to extend the lead time of flow forecasts, quantitative rainfall forecasts are typically used as external inputs to run-off models (Collischonn et al., 2005; Sene, 2010). Thus, the accuracy of rainfall forecasts tends to have a significant impact on the reliability of streamflow forecasts (Ran et al., 2018).

Numerical weather forecasting has improved significantly in recent years. Bauer et al. (2015) showed that the current six-day forecast is as accurate as the five-day forecast issued a decade ago. These improvements can be attributed to the increase in observational data globally as derived from both weather stations and meteorological satellites; a more comprehensive understanding of physical processes in the atmosphere; and the ability to represent them in global weather models (Simmons & Hollingsworth, 2002). In addition, the advancement of computational structure over the years has also played a role in improving forecasts. Lately, numerical models have been able to simulate the future state of the atmosphere at a relatively high spatial resolution (e.g. Schwartz et al., 2017). At these high spatial resolutions, models are able to simulate meso-scale features realistically, which improves the quality of forecasts. However, high-resolution numerical weather prediction models are usually applied over relatively small domains and/or short lead times as the simulations tend to be computationally expensive.

The main focus of this chapter is to investigate whether the CCAM forecasts can successfully downscale river flows of the north-eastern interior of South Africa statistically at timescales from seasonal to short-range. The data and methodology applied to achieve this aim are presented in Section 3.2. The overall results are discussed in Section 3.3. The synopsis follows in Section 3.4.

#### 3.2 Data and Methodology

##### 3.2.1 Modelling technique

###### 3.2.1.1 Model description and experimental design: Seasonal timescale

###### *Atmospheric general circulation model description*

This study used the CSIRO CCAM in Australia as climate model (McGregor, 2005a). This stretched-grid atmospheric climate model was combined with the CSIRO dynamic land-surface model, namely, CABLE. The CCAM Atmospheric General Circulation Model (AGCM), a  $\sigma$ -coordinate model, employed a semi-implicit semi-Lagrangian method to solve hydrostatic primitive equations (a non-hydrostatic version also exists). It used an R-grid (reversible staggering for the wind components) for good gravity wave dispersion behaviour (McGregor, 2005b). The GFDL parameterisations for long-wave and shortwave radiation were used with interactive cloud distributions determined by the liquid and ice water

scheme of Rotstayn (1997). A stability-dependent boundary layer scheme based on the Monin–Obukhov similarity theory was used (McGregor et al., 1993) together with the non-local treatment of Holtslag and Boville (1993). The cumulus convection scheme used a mass-flux closure, as described by McGregor (2003), which included downdrafts, entrainment and detrainment. The CCAM included a prognostic aerosol scheme, which could be applied consistently with the emission inventories and radiative forcing specifications of the Coupled Model Intercomparison Project Phase Five (CMIP5). CABLE included a dynamic river routing scheme adapted from the CSIRO Mk3.5 Ocean Atmosphere Coupled Global Circulation Model (CGCM).

#### *Lower boundary forcing*

The CCAM CABLE model was forced with predicted sea ice concentrations (SICs) and SSTs as acquired from the outputs of the SINTEX-F2v ensemble seasonal prediction system (Doi et al., 2014; 2016). It was based on SINTEX-F2 CGCM (Sasaki et al., 2013; 2014; 2015). The atmospheric component was ECHAM5 (Roeckner et al., 2003). The oceanic component was the Nucleus for European Modelling of the Ocean (NEMO) system (Madec, 2006).

The atmospheric component had a T106 horizontal resolution (approximately horizontal resolution of 125 km at equator) with 31 vertical levels. The oceanic component employed the ORCA05 grid, which used a tripolar grid with 0.58 zonal resolution and 0.58 cosine (latitude) meridional resolution with 31 vertical levels. The atmospheric and oceanic components were coupled with the data being exchanged every two hours, including SST, sea ice fraction, fresh water, surface heat, surface current and momentum fluxes, by means of the Ocean Atmosphere Sea Ice Soil, version 3 (OASIS3) coupler (Valcke et al., 2004). Doi et al. (2016) provide a complete description of the CGCM experimental design.

#### *Retroactive forecasts design*

The AGCM retroactive experiment consisted of 18 ensemble members, each six months in length, which were built as a function of both atmospheric states (initial conditions) and boundary forcing (boundary conditions) (Beraki et al., 2016). This model configuration offered a better description of uncertainties that could arise from the initial and boundary forcings. The uncertainties that arose from the initial conditions were accounted for by taking six consecutive daily realistic atmospheric states as atmospheric initial conditions. For example, for hindcasts initialised in November, the observed atmospheric states for the period 1–6 November were used as six initial conditions to launch model runs on 1 November.

The hindcasts were performed for a period of 15 years – spanning the period 2000 to 2014. To minimise the potential climate drift, the CCAM CABLE was nudged at its surface to the SINTEX-F2 CGCM SSTs, using the spectral nudging method of Thatcher and McGregor (2009; 2010). Furthermore, all climate simulations were forced by time-varying CO<sub>2</sub> and ozone fields provided through the CMIP5 archive for the period 1870–2100. The atmospheric initial conditions were acquired from the National Centers for Environmental Prediction (NCEP)/Department of Energy (DoE) Atmospheric Model Intercomparison Project (AMIP) II Reanalysis (R2) data set (Kanamitsu et al., 2002). The NCEP/DoE atmospheric states were transformed to the CCAM CABLE quasi-uniform (C96) horizontal resolution (approximately 105 km<sup>2</sup> in the horizontal) and 27 vertical sigma layers, which was similar to the experimental design of Beraki et al. (2014).

Forcing the AGCM with all ensemble realisations of the SINTEX-F2 CGCM was computationally inhibiting. This was due to a double-fold increase in the AGCM integrations by the size of atmospheric initial conditions as it was also important to account for uncertainties arising from the atmospheric

states. Hence, the prescription of the SST scenarios followed a manner that optimised the representation of the uncertainty envelope and that also considered the computational constraints.

The background error was estimated from the standard deviation of the six CGCM ensemble integrations and subsequently added/subtracted to the ensemble mean anomalies. It is also worth noting that the SIC and SST anomalies were superimposed to the AMIP-observed climatology to minimise the biases in the boundary forcings (Beraki et al., 2016; Ratnam et al., 2017). In the CGCM experiment, as noted in Doi et al. (2016), uncertainties in ocean vertical mixing estimations and ocean physics were perturbed in two different ways by considering or neglecting the ocean vertical mixing induced by small vertical-scale structures within and above the equatorial thermocline (Sasaki et al., 2012). This similar paradigm also ensured the quantification of uncertainties of both initial conditions and model physics for forecasts.

For the purpose of this deliverable, the geopotential heights at 850 hPa level for all 18 ensemble members of CCAM AGCM were extracted and used to construct an ensemble mean, which was subsequently used to build a statistical model to produce streamflow forecast products. More details of statistical model are provided in the subsection that follows.

### **3.2.1.2 Model description and experimental design: Weather timescale**

At the CSIR, CCAM is used operationally as a weather prediction model. The data set from the Global Forecasting System (GFS) weather model of the NCEP was acquired and subsequently transformed to C48 quasi-uniform conformal cubic grid of about 200 km resolution in the horizontal. Thereafter, the transformed GFS data was used to initialise the CCAM to produce global forecasts at a 200 km resolution. A two-step nudging process was applied to get a high-resolution forecast over South Africa and its neighbouring countries.

First, the CCAM global output was spectrally nudged over the African continent so that the resultant forecasts had a horizontal resolution of about 50 km resolution. These were nudged further to produce a 15 km resolution of South Africa. This two-step nudging process was done to ensure efficient use of the in-house computer resources and to reduce the runtime as the forecasts were generated six-hourly.

For the purpose of this study, a set of daily hindcasts were produced for the December to February months of 2013/2014; 2014/2015; 2015/2016 and 2016/2017. The hindcasts were generated using the Centre for High Performance Computing's (CHPC) computational resources, which allowed for the CCAM to be initialised with transformed GFS atmospheric conditions and integrated temporally for up to 14 days into the future to produce global simulations at a 50 km spatial resolution. The high-resolution simulations were obtained by dynamically downscaling the 50 km global forecast output to an 8 km horizontal resolution over southern Africa.

### **3.2.1.3 Statistical model**

#### *Seasonal timescales*

The Climate Prediction Tool (CPT) statistical software of the International Research Institute for Climate and Society (IRI) was used to construct and validate a statistical model. The geopotential height forecast at 850 hPa level generated by CCAM was used as a predictor variable. The naturalised streamflow data set was used as predictand variable. The domain for the predictor variable on CPT was set as [0–40° S; 0–50° E] to only consider the regional forcing when building the statistical model. The predictor variable was then executed through canonical correlation analysis of CPT. To assess the model skill, a cross-validated forecast procedure was employed to obtain a realistic estimation of its prediction skill.

### Weather timescales

A random sampling method was applied to extract 100 days between 1 January 2000 and 31 December 2012 to minimise errors in data sets associated with serial correlation in the subsequent verifications. The rainfall and streamflow data corresponding to the random cases were extracted and correlated against each other to examine their relationship. A linear regression technique was used to find the best estimate of streamflow at a station point given the corresponding rainfall measure. A nearest neighbour technique was applied to identify grid points that were close to the location of the river stations considered (see Table 2). The analysis between rainfall and river flow was computed at point to point.

**Table 2: Location/description of selected river stations in the north-eastern region as defined by the DWS**

Station		Longitude (° E)	Latitude (° S)
A4H005	Mokolo River @ Dwaalhoek	27.77267	-24.08066
A4H007	Tambotie River @ Blakeney	27.90899	-23.76388
A6H029	Mogalakwena River @ Glen Alpine	28.69959	-23.18419
A8H010	Nwanedzi River @ Nwanedzi Nat. Res.	30.39868	-22.63424
B4H005	Waterval River @ Modderspruit	30.21941	-25.03594
X1H001	Komati River @ Hooggenoeg	30.99761	-26.03616
X1H005	Mlumati River @ Lomati	31.97694	-24.44972
A9H003	Tshinane River @ Chibase	30.52378	-22.89814
A9H012	Luvuvhu River @ Mhinga	30.88925	-22.76851
A9H013	Mutale River @ Kruger National Park	31.07783	-22.43773
B8H018	Letaba River @ Engelhardt dam Kruger National Park	31.63744	-23.83532
A6H035	Mogalakwena River @ Leniesrus	28.8974	-22.55021
A7H007	Sand River @ Pietersburg	29.43149	-23.88294
A7H008	Limpopo River @ Beitbridge	29.99035	-22.22718
A7H010	Sand River @ Waterpoort	29.61103	-22.91019
B9H003	Shingwidzi River @ Kanniedood Kruger National Park	31.46262	-23.14326
B8H017	Great Letaba River @ Prieska	30.71844	-23.64701
X2H097	Crocodile River @ Esselen	31.47608	-25.49786
A9H028	Luvuvhu @ Nooitgedacht	30.17487	-23.08645

### 3.2.2 Verification data

#### 3.2.2.1 Naturalised stream flow

Naturalised streamflow data used in this present study was constructed by Royal HaskoningDHV for the WRC project of 2012 (WR2012), which is available online ([www.waterresourceswr2012.co.za](http://www.waterresourceswr2012.co.za)). Naturalised flow was obtained by removing man-made influences such as dams, irrigation schemes, abstractions for mines, industry and towns, and the return flows from treatment works.

The WR2012 streamflow data consists of monthly flows in million cubic metres per month. The data spans the period from 1920 to 2009. For the purpose of this report, data for the months from November to April for the years between 2000 and 2009 was used. From this subset data, the three-month accumulated streamflows were computed in all quaternary catchment areas for the months: November–January; December–February; January–March and February–April. To ensure efficient computation, station points were constructed and placed at the centre of each quaternary catchment area to represent its geographical position.

#### 3.2.2.2 Observed daily average flows

The DWS (through its Hydrological Information System) allowed free access to data in all drainage regions across South Africa (accessible online at [www.dwa.gov.za/Hydrology/](http://www.dwa.gov.za/Hydrology/)). For the purpose of this chapter, 19 stations spread across drainage regions A, B and X (Limpopo, Olifants and Sabie–Krokodil–Komati) were selected (see Figure 21). These drainage regions cover the north-east domain of South Africa. The observed daily flow rate data spanning from 2000 to 2014 was extracted for each of the 19 river stations. Table 3 displays the station numbers and location details of the selected river station as defined by the DWS.

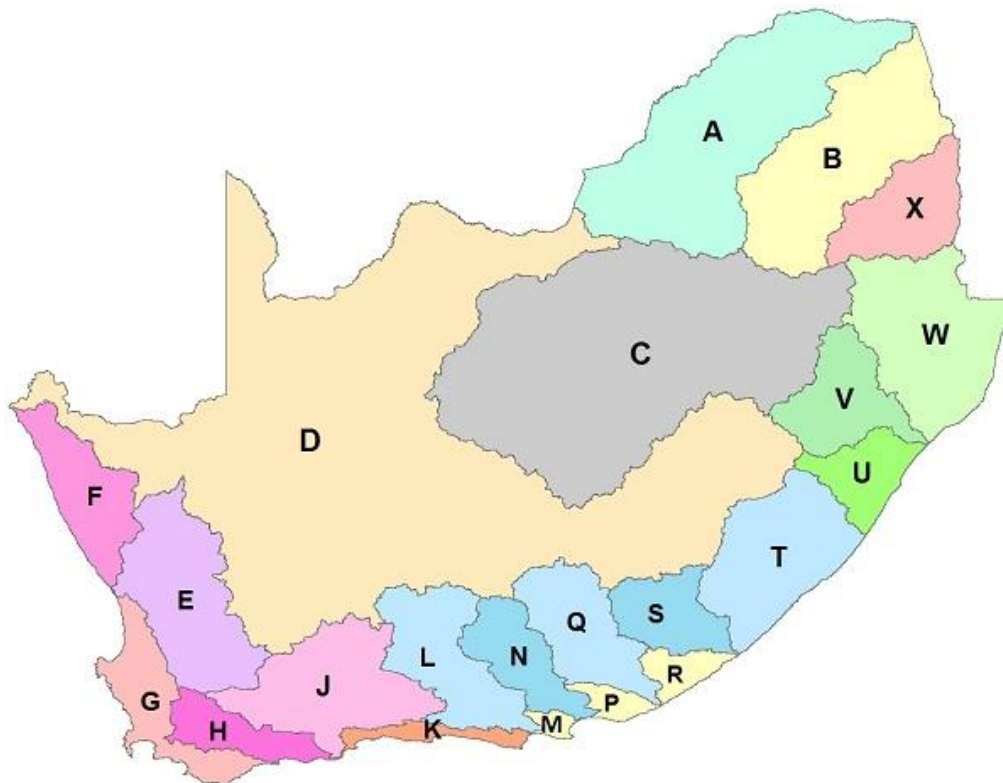
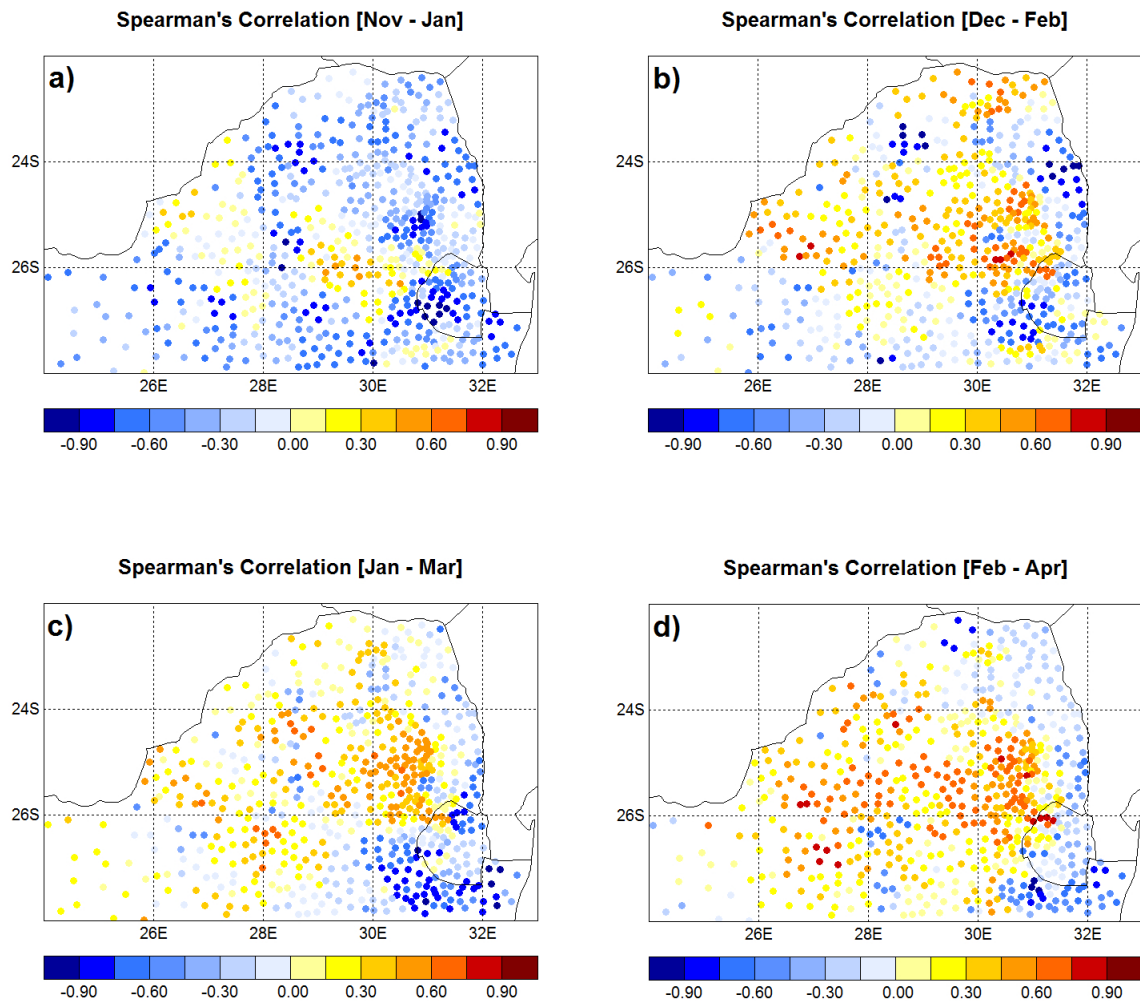


Figure 21: Drainage regions of South Africa (<http://www.dwa.gov.za/Hydrology/Weekly/Drainage.aspx>)

### 3.3 Results

#### 3.3.1 Statistical Hydrologic Model: Seasonal analysis and forecast products

This section presents the results of a statistical model built to downscale the CCAM's outlook of geopotential heights at an 850 hPa level to streamflow in the quaternary catchment areas throughout South Africa. In order to investigate the degree at which the cross-validated forecasts corresponded with the naturalised flows, the spearman correlation analysis was computed for all quaternary catchments over South Africa. The analysis was performed for four three-month periods (November–January; December–February; January–March and February–April) starting from November 2000 to April 2009. The results are shown in Figure 22.



**Figure 22: Spearman correlation values between cross-validated streamflow forecast and naturalised streamflow over quaternary catchment areas in the north-eastern region of South Africa for a) Nov–Jan; b) Dec–Feb; c) Jan–Mar; and d) Feb–Apr period**

Even though the analysis covers the entire country, this section only discusses the results obtained in key study area of this current WRC project, namely, the north-eastern part of South Africa. Streamflow forecasts produced at a 0-month lead time (i.e. November–January, see Figure 22a) tend to be negatively correlated to naturalised streamflow; however, there are catchment areas around the southern border of Limpopo Province that show a positive correlation.

As the lead time increases to one month (i.e. December–February); two months (i.e. January–March) and three months (i.e. February–April) as respectively shown in Figure 22b–Figure 22d, the degree of association between predicted and naturalised streamflow tends to be mostly positive over the extended spatial area in the north-eastern region of South Africa. During the period between December and February, relatively strong relationships tend to be localised in the catchment areas at the centre of the study region, and there seems to be a strong indirect relationship between predicted and naturalised streamflow towards the east. A similar pattern persists for January–March and February–April as depicted in Figure 22c and Figure 22d respectively. For the months January to March, the positive correlation pattern extends down to catchment areas in the south-western part to the north-eastern region. Moving to the February–April period, the relationship between downscaled and naturalised streamflow tends to strengthen more in the central interior of the focus area.

Hit scores were computed to further quantify the accuracy of the downscaled streamflow. The scores shown in Figure 23 represent the percentage at which the forecast system predicted the streamflow in quaternary catchment areas with success over the north-eastern region of South Africa. In Figure 23a, the overall success rates of statistically downscaled forecasts range mostly between 10% and 50%. However, there are sparsely scattered catchment areas where the success rate exceeds 50%. The spatial spread of the > 50–80% success bracket seems to grow as the lead time increases. The larger spread is seen during the February–April period (shown in Figure 23d).

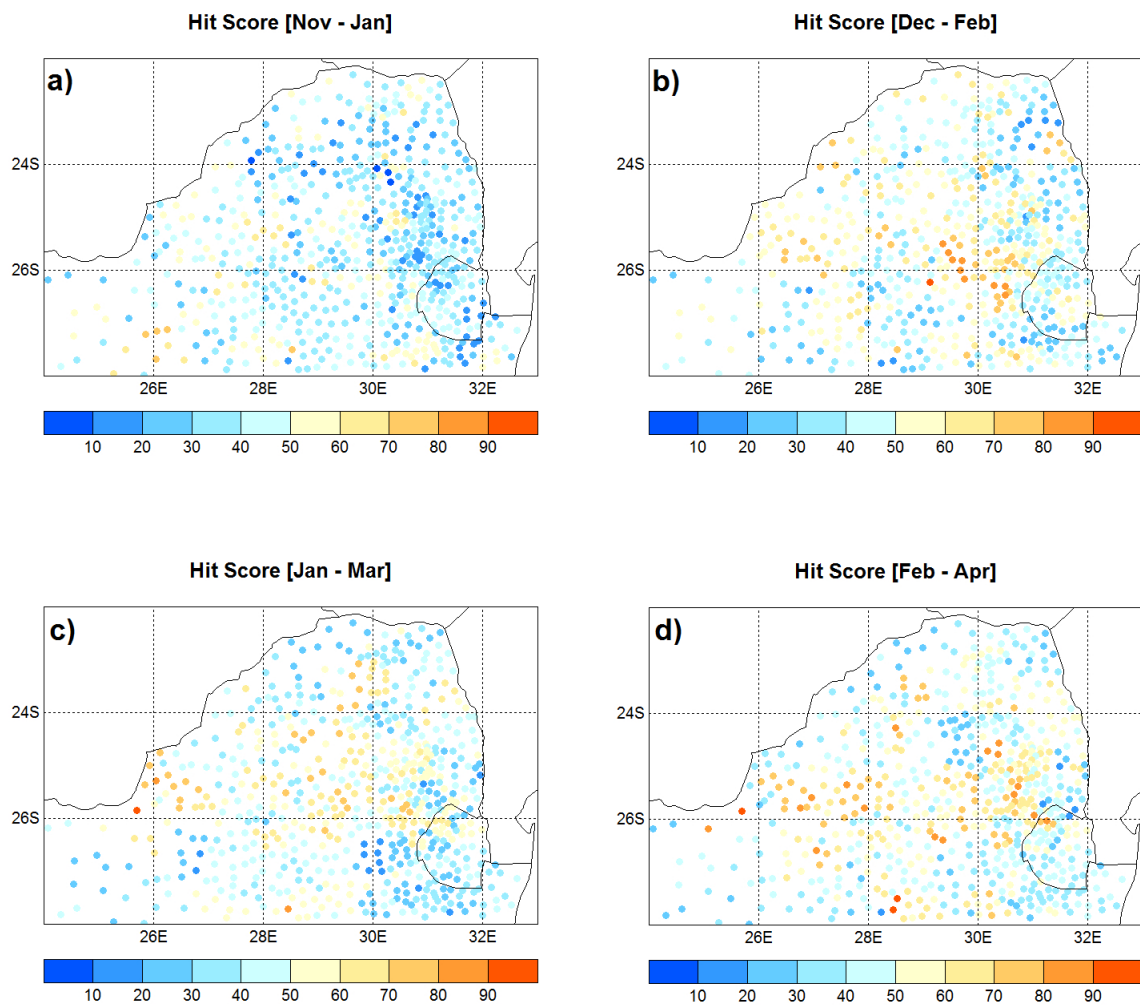


**Figure 23: Hit scores – the percentage at which the statistical forecast system successfully predicts the streamflow in quaternary catchments areas over north-eastern region of South Africa for a) Nov–Jan; b) Dec–Feb; c) Jan–Mar; and d) Feb–Apr period**



Thus, the results presented here suggest that downscaled streamflow forecasts – particularly in the north-eastern region of South Africa – compare well with naturalised streamflow. Figure 24 shows the probabilistic streamflow forecasts for the four three-month periods between November 2014 and April 2015. These maps represent the primary streamflow forecast products generated through the project, which are designated for operational dissemination. These probabilistic streamflow forecasts, along with rainfall forecasts at medium and short timescales, can be used to guide disaster managers in sectors such as agriculture, transport, water management to prepare for flood events.

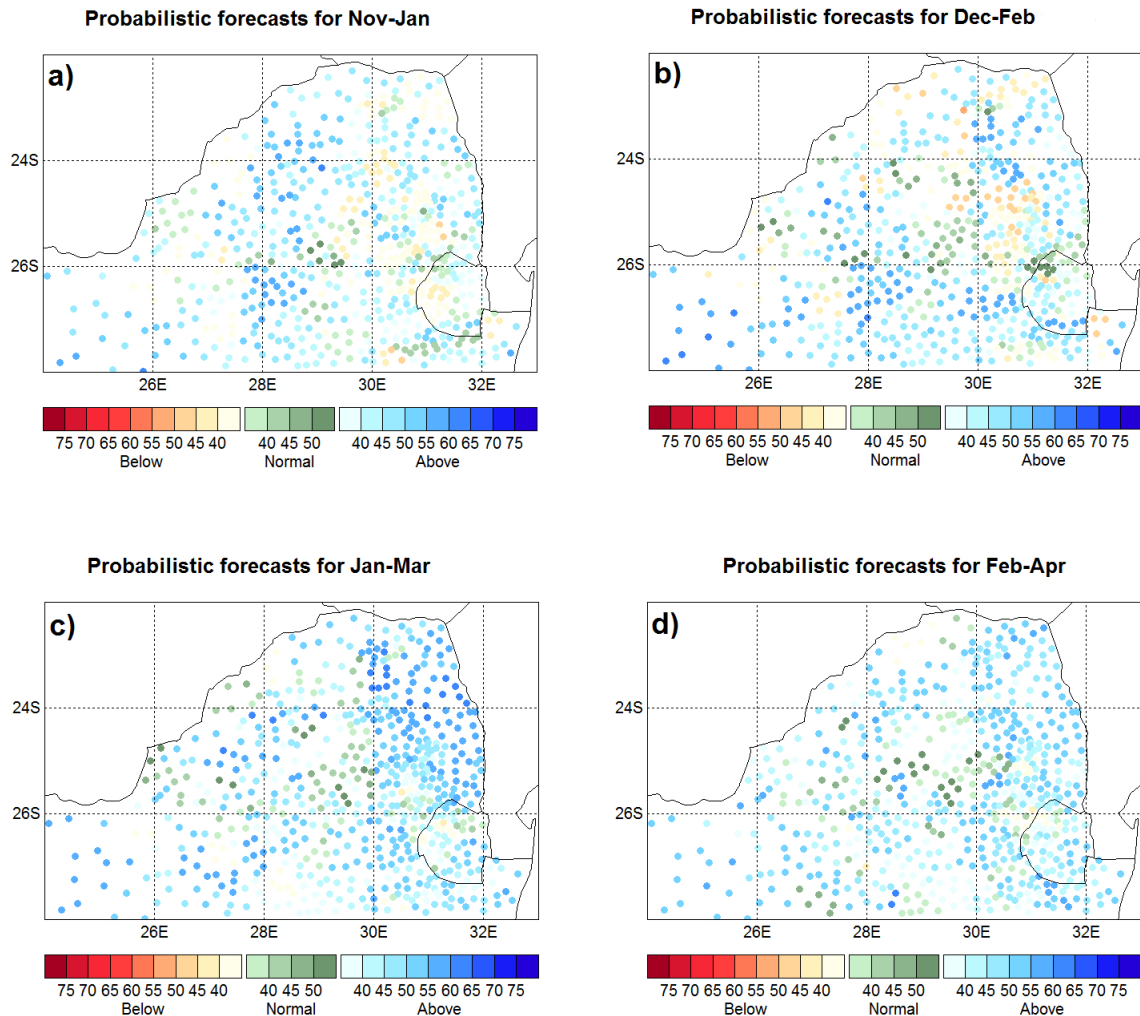


**Figure 24: Probabilistic forecasts of downscaled flows in quaternary catchments areas over north-eastern region of South Africa for a) Nov–Jan; b) Dec–Feb; c) Jan–Mar; and d) Feb–Apr periods of 2015**

### 3.3.2 A link between daily rainfall and river flows

Figure 25 shows the monthly hydrographs of the 19 stations computed from the daily observed data. The station in the Limpopo River located at Beitbridge (A7H008) has the highest climatological flow rate compared with other stations. Generally, all stations exhibit a similar seasonal cycle – lowest flow rates occur in October and the highest peaks in January.

Standardised anomalies of simulated rainfall and observed streamflow for 100 cases randomly extracted during the period from 1 January 2000 to 31 December 2012 were correlated to examine the statistical relationship between both variables. For the days where there were no observed records, rainfall simulations were not considered. Figure 26 shows the lagged correlation coefficients at each of the stations computed for 100 cases. The correlation values within the dashed line bounds are

statistically insignificant. Overall, the results suggest that a significant positive relationship exists between rainfall and river flows. The degree of association varies between stations. This could be because of factors such as the character of rainfall varying in space and time coupled with the dynamical and physical variation between catchments.

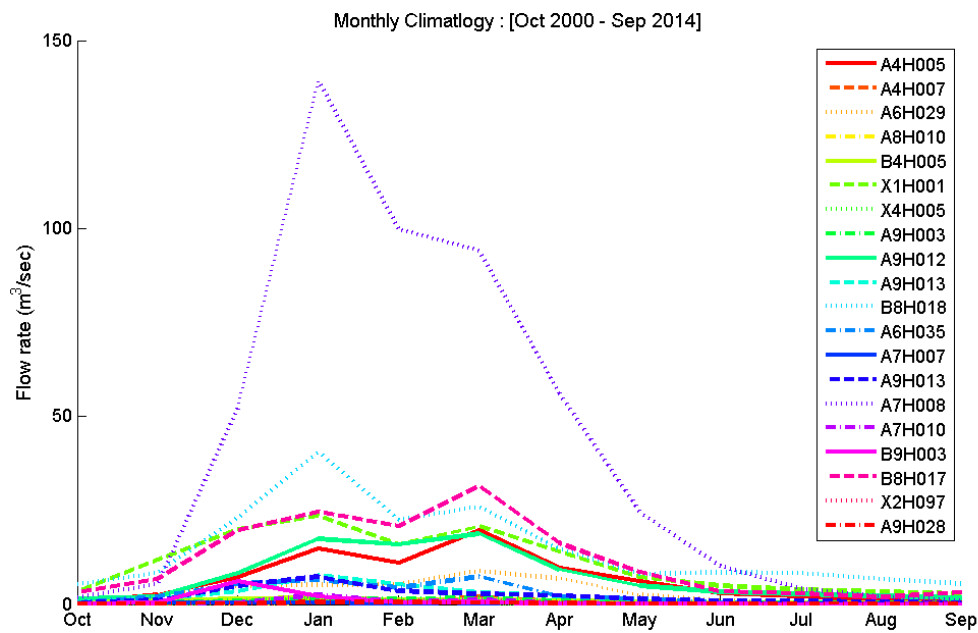


Figure 25: Mean monthly hydrographs of the observed flow rates at 19 stations spread across the north-eastern region of South Africa for the period between October 2000 and September 2014

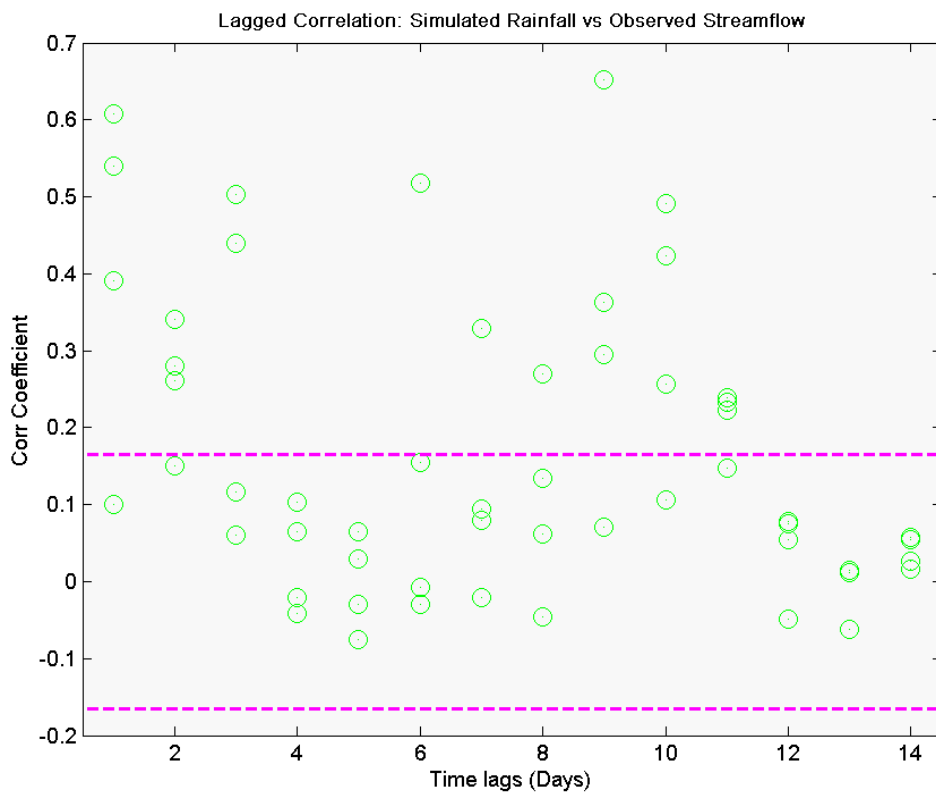


Figure 26: A lagged correlation coefficient between rainfall and observed streamflow anomalies at 19 selected stations spread across north-east region of South Africa. Correlation was computed for a 100 randomly selected cases between 1 January 2000 and 31 December 2012. The dashed lines represent the 95% significance level bounds

### 3.3.3 Predicting the impact of tropical depressions and cyclones on river flows in Limpopo

The flood event of February 2000 was one of the most devastating floods in Mozambique, Zimbabwe and South Africa (Reason & Keibel, 2004). This flood event was a result of landfall of the tropical cyclone Eline late February 2000 and a tropical depression that occurred early in the month. A similar event occurred in January 2012 when tropical depression Dando preceded tropical cyclone Funso, which led to flooding in some parts of Mozambique. Heavy rains triggered by Dando reached the north-east parts of South Africa (see Figure 27).

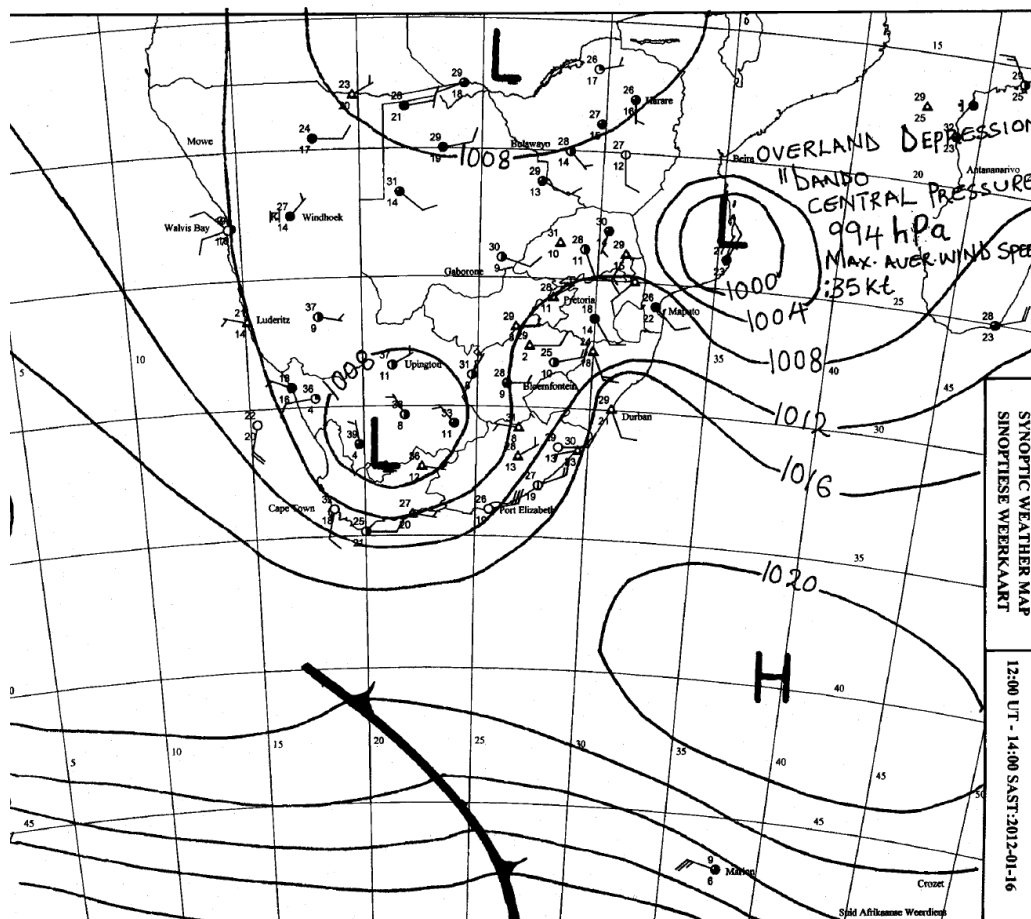
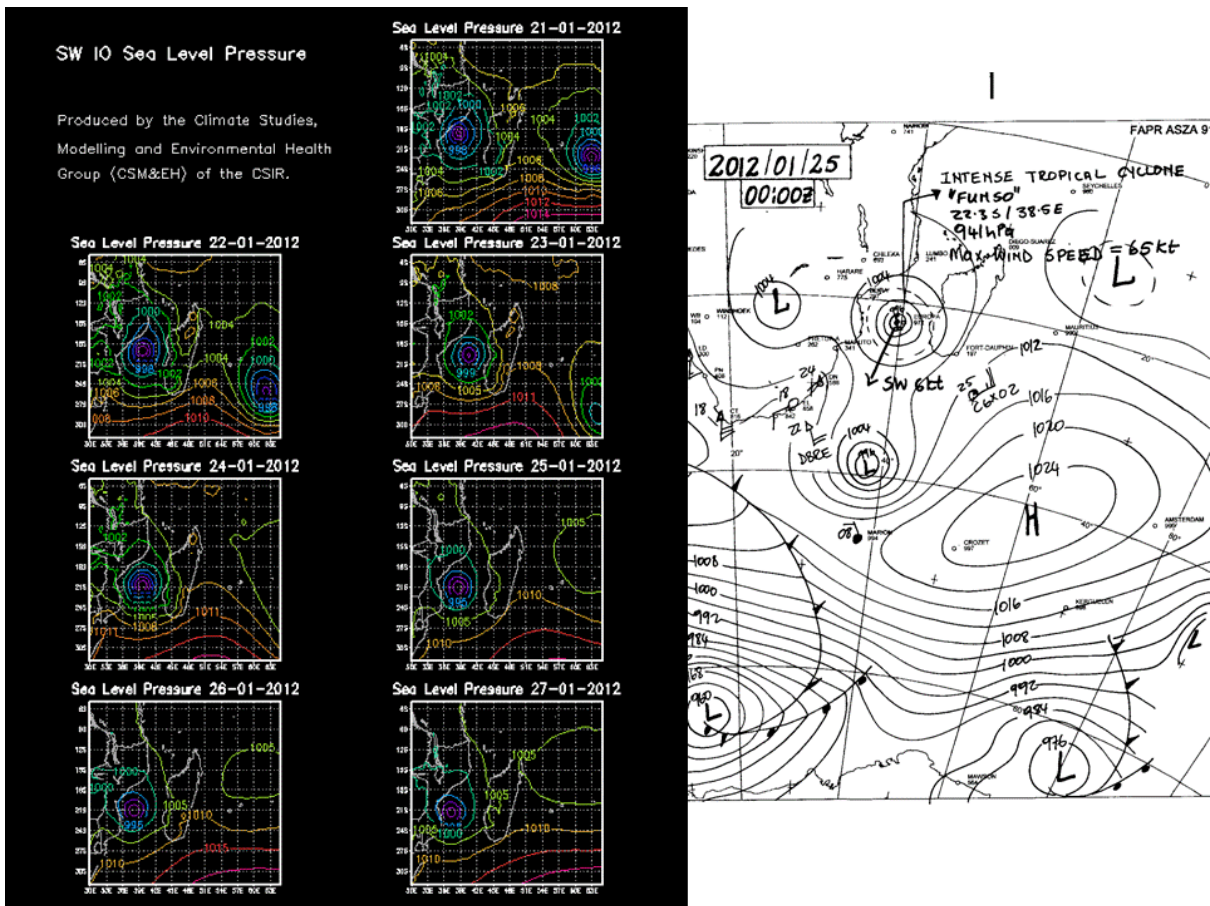


Figure 27: Synoptic chart showing tropical depression Dando

Figure 28 shows the CCAM's forecast of sea level pressure from 21 to 27 January 2012 (left) indicating the evolution of tropical cyclone Funso and the synoptic map of the 25 January 2012 (right).



**Figure 28: Forecast of sea level pressure in the south-west Indian Ocean to track the development of tropical cyclone Funso between 21 and 27 January 2012 (left) and a synoptic weather map indicating the landfall of Funso (right)**

Figure 29 shows the observed rainfall during the event of Funso. Rainfall measured ranged between 5 mm and 15 mm over the central interior of Mpumalanga and the south-eastern parts of Limpopo. Figure 29 shows the observed river discharge over Limpopo for the days between 16 January and 27 January 2012. Only four out of 19 stations had missing values during the analysis period. Linear regression coefficients were computed based on the randomly selected 100 cases between 1 January 2000 and 31 December 2014.

By substituting the CCAM-simulated rainfall in the linear model as a predictor variable, the flow at each station point could be predicted (as seen in Figure 30 and Figure 31). Figure 30 and Figure 31 present the streamflow forecasts associated with the impact of tropical depression Dando and tropical cyclone Funso respectively. Forecasts were computed for the day of the event (0-day); a week prior to the event (seven-day) and two weeks ahead of the event. The analyses only show forecasts at the stations where rainfall-streamflow relationships were statistically significant as described in the previous section. The magnitude of predicted flows is relatively small compared with the actual observed flows. Given that conditions such as infiltration, surface storage, evapotranspiration, inception and channel losses that have to be satisfied before streamflow occurs and that the interbasin transfers were not accounted for in the linear model, the results obtained here cannot be regarded as insignificant.

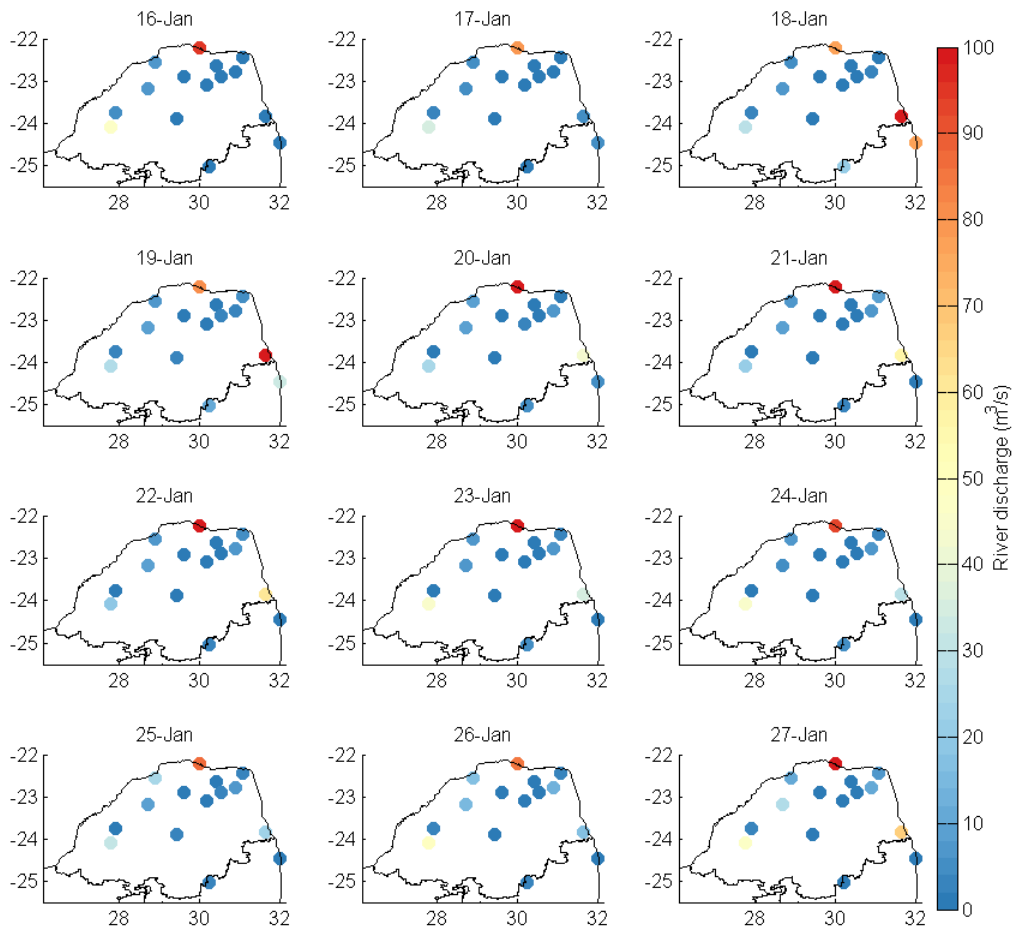
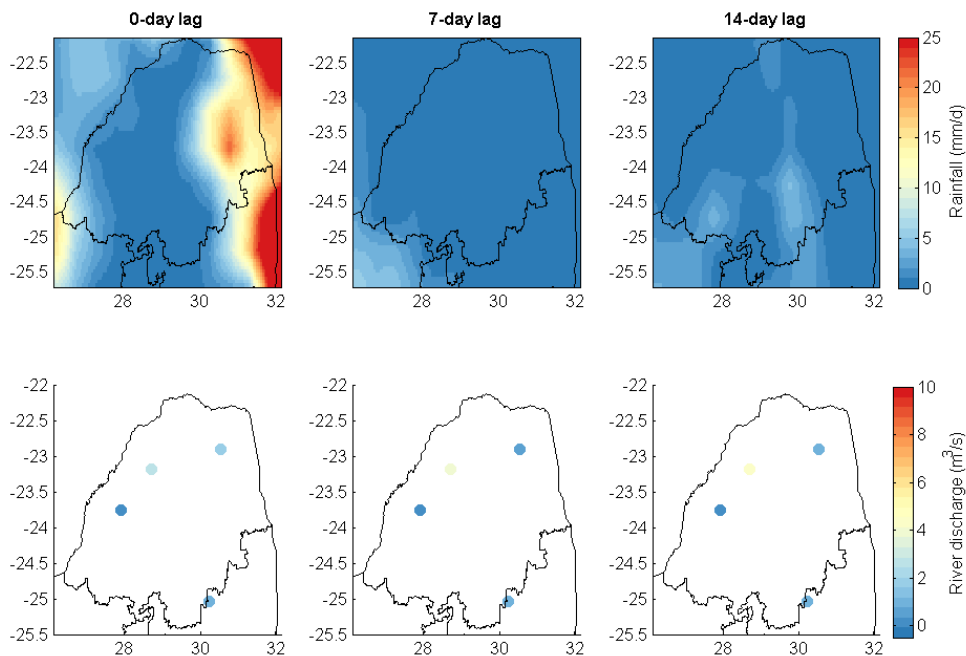
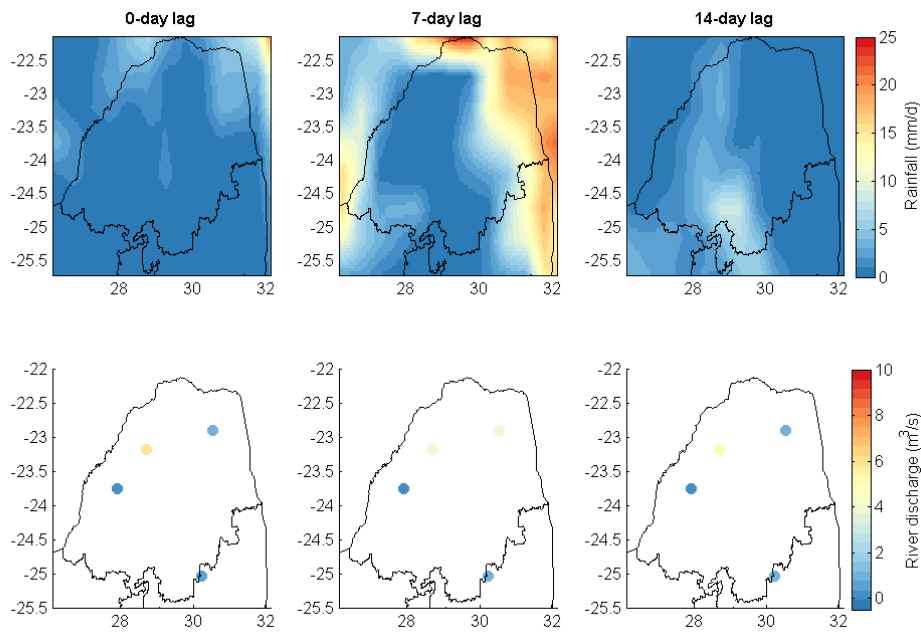


Figure 29: Observed streamflow for the days between 16 and 28 January 2012



16-Jan-2012

Figure 30: CCAM-simulated rainfall (top row) and predicted streamflow of 16 January 2012 at 0-day, 7-day and 14-day lag. The results shown here correspond to stations that displayed a significant relationship between CCAM rainfall and observed streamflow



25-Jan-2012

**Figure 31: CCAM-simulated rainfall (top row) and predicted streamflow of 25 January 2012 at 0-day, 7-day and 14-day lag. The results shown here correspond to stations that displayed a significant relationship between CCAM rainfall and observed streamflow**

### 3.4 Synopsis

This chapter explored the statistically downscaling of CCAM output to streamflows in the north-eastern part of South Africa at seasonal and weather timescales. At a seasonal timescale, a statistical model based on a canonical analysis was used to downscale the 850 hPa geopotential height output of the CCAM to streamflows at lead times up to three months. The streamflow forecasts at lead times from one to three months tended to be positively correlated with naturalised streamflow over more quaternary catchment areas than for the spatial extent of positive correlations between forecasted and naturalised streamflow for the 0-month lead analysis. This pattern is also translated to hit score results: where the highest percentage of statistical forecast model successfully matched the naturalised flow, data tended to correspond with areas of positive correlation values.

At weather timescales, the statistical approach that was taken to downscale CCAM outputs to streamflow over our study areas was different from that employed at a seasonal timescale. For the weather timescale, in order to reduce errors associated with serial correlation in the data set, a random sampling method was applied to extract 100 days for which a linear regression statistical model was built. This model was tested for two case studies, namely, the tropical cyclone Funso and tropical depression Dando. The deterministic flow forecasts (produced by the linear regression model at a few selected stations spread across the north-eastern region of South Africa) were relatively small compared with the observed values during the Funso and Dando events. However, the predicted flows cannot be disregarded as the statistical model applied here does not account for the antecedent condition of the river basin and interbasin water transfers. Perhaps using an ensemble system and incorporating a hydrological model such as ACRU might improve predictability at this particular timescale.

## 4 FORECAST PRODUCTS: DISPLAYS AND TAILOR MADE OUTPUTS

### 4.1 Introduction

Seasonal forecasts of rainfall and temperature in recent years have played a major role in disaster risk management. In the agricultural sector, seasonal forecasts can be useful for estimating crop yields, as well as planning crop selection, planting times and irrigation methods (e.g. Malherbe et al., 2014). In the public health sector, it has been demonstrated that seasonal climate forecasts can be useful to predict the spread of diseases such as malaria and meningitis and thereby preventing and potentially reducing loss of life by supplying vaccines in the anticipated hot spot areas (e.g. Pandya et al., 2015; Tompkins & Giuseppe, 2015). Seasonal and weather forecasts also play a vital role in the management of water resources (Mukheibir, 2008). The examples mentioned above are but a fraction of the diverse application of seasonal forecasts.

In this project, we explored the application of seasonal and weather forecasts in hydrology with the aim of building a functional early flood warning system. Section 4.2 presents the forecast products at seasonal and weather timescales specifically tailored for a hydrological application as developed through the project. Section 4.3 presents measures taken to ensure that the results of this project benefit the community. It is followed by a synopsis in Section 4.4.

### 4.2 Forecast Displays

#### 4.2.1 Seasonal outlook

Figure 32 shows that the fluctuations of SST anomalies between the warm, cold and neutral phases of the El Niño Southern Oscillation (ENSO) – indicated by red, blue and green shaded areas respectively – are highly variable from one year to the other. The first two phases are commonly referred to as El Niño and La Niña respectively, which are often associated with either anomalously dry or wet summer (DJF) seasons over southern Africa. Based on the  $\pm 0.5^{\circ}\text{C}$  threshold of the Ocean Niño Index (ONI), the 2017/2018 summer season was dominated by the neutral phase conditions of ENSO (see Figure 32).

The CSIR's new seasonal ensemble forecasting system was launched in November 2017. This newly developed system (CCAM) was coupled to the CABLE land-surface model and comprised 12 ensemble members built as a function of 12 slightly different NCEP Environmental Modelling Center's GFS atmospheric states and forced with multi-model SSTs (Landman et al., 2014). A comprehensive description of this system was given in Section 3.2.1.

Figure 33 shows the first ever probabilistic seasonal rainfall forecast release of the CCAM CABLE ensemble prediction system (C192 stretched grid with 8 km zoom-in over the southern Africa region). For the 2017/2018 summer season, drier conditions in the area covering the central interior and the east coast region of South Africa were predicted. In the western part of our study area, that is, the area including the Limpopo, Mpumalanga and Gauteng provinces as well as the eastern parts of the North West Province, wetter than normal rainfall condition were anticipated (as seen in Figure 33).

The summer seasons of 2009/2010, 2010/2011 and 2014/2015, which correspond to the warm, cold and neutral phase of ENSO, respectively, were selected to examine the impact of ENSO phases on streamflow in the quaternary catchment areas over the north-eastern region of South Africa. The CCAM's probabilistic forecast of accumulated streamflow for the three selected summer seasons were generated using the statistical downscaling technique described in Chapter 3, and are presented here as a next example of the application products generated by the project.

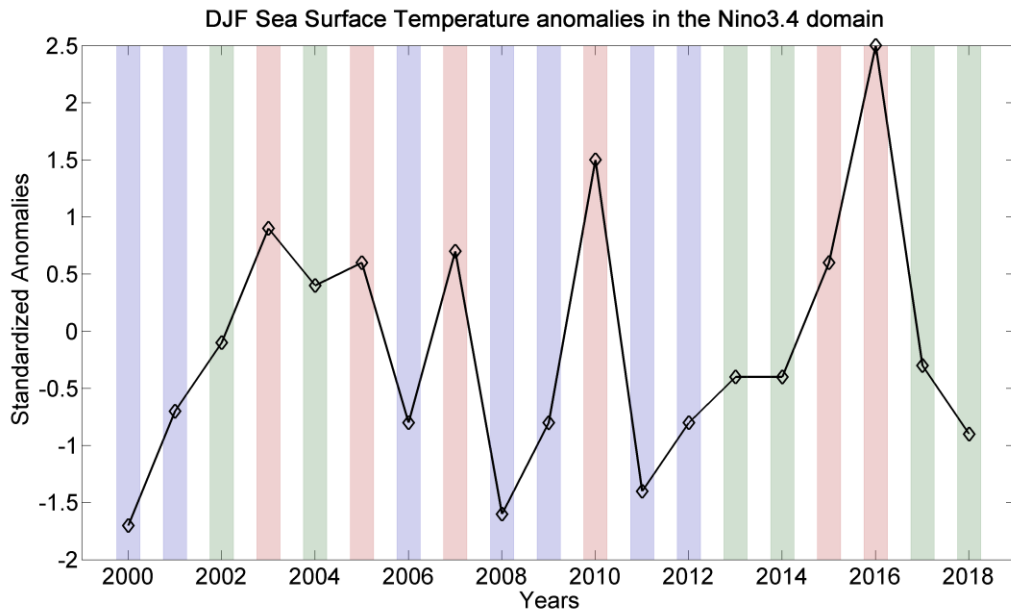


Figure 32: Time series of SST anomalies in the Niño 3.4 region (5° N–5° S, 120–170° W). The shaded areas indicate periods of warm (red), cold (blue) and neutral (green) periods based on  $\pm 0.5^{\circ}\text{C}$  ONI threshold

### CSIR NRE CLIMATE PREDICTION SYSTEM

CCAM-CABLE 8km (Seasonal timescale)

Most likely Category of Rainfall

Forecast Period: Dec 2017 – Feb 2018

No Significance Test Applied

Ensemble size 12

Last Updated 16 Nov 2017

<--- Dry Tendency

Wet Tendency --->

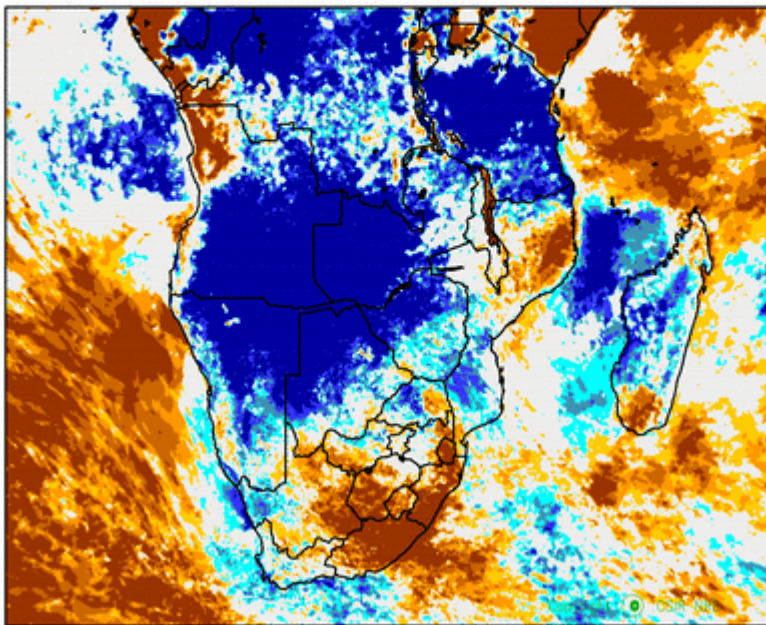
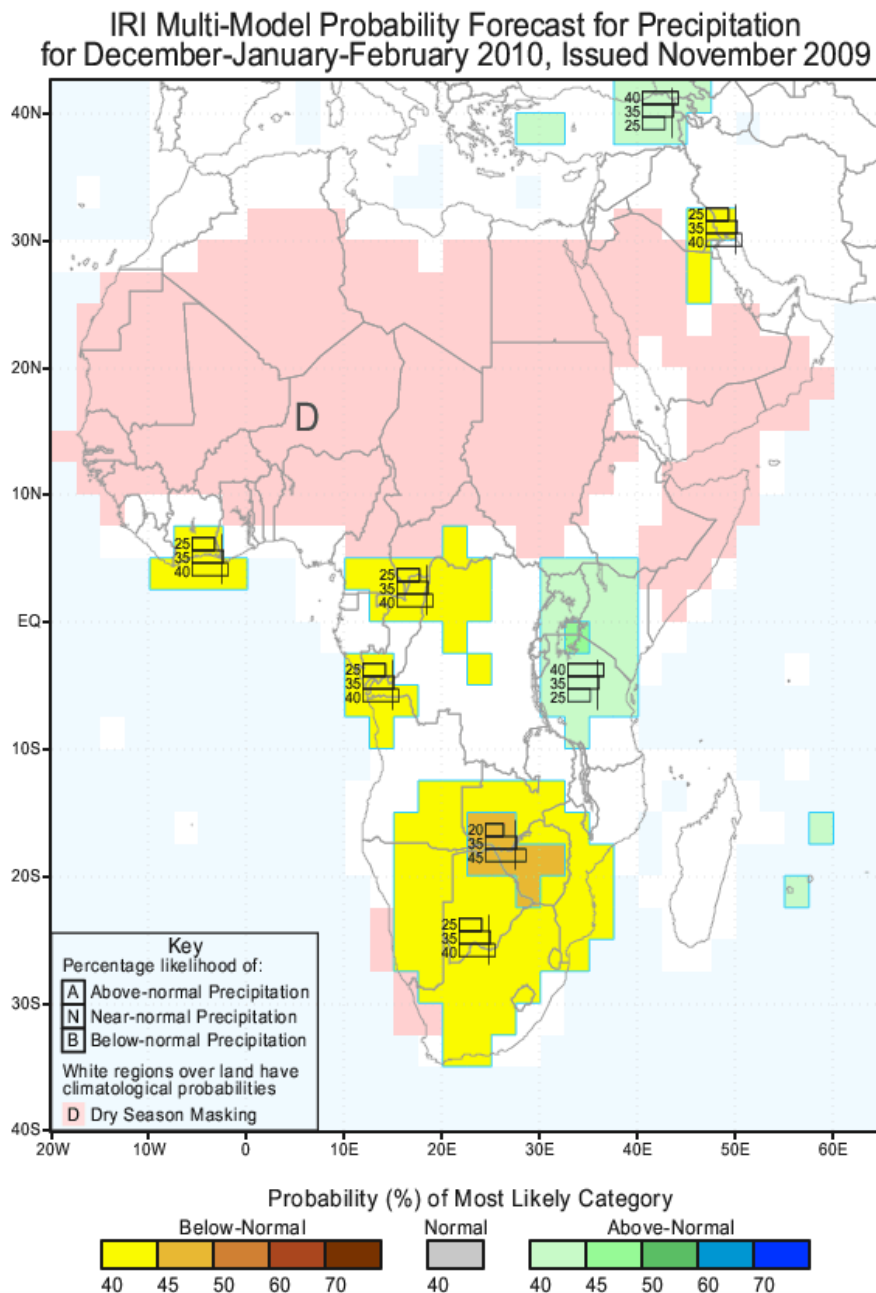


Figure 33: Probabilistic seasonal rainfall forecast release of the CCAM CABLE operation ensemble prediction system (C192 stretched grid with 8 km zoom-in over the southern Africa region)



Figure 34, Figure 37 and Figure 40 show the probabilistic precipitation forecast outputs of the multi-model forecast system of IRI during 2009/2010, 2010/2011 and 2014/2015 respectively. The maps show the tercile probabilities of precipitation, that is, probabilities that the seasonal precipitation will fall into the wettest third of the years (top number), the middle third of the years (middle number), or the driest third of the years (bottom number). The colour shading coincides with the tercile that has the highest forecast probability. These forecast maps are available online (<https://iri.columbia.edu/our-expertise/climate/forecasts/seasonal-climate-forecasts/>).

In most parts of the South Africa during the 2009/2010 summer season, there was a 25% chance that precipitation would be in the wettest third of the years, a 35% chance that precipitation would be in the near-normal third of the years, and a 40% chance that precipitation would be in the driest third of the years (see Figure 34).



**Figure 34: Probabilistic forecast of precipitation for Dec 2009–Feb 2010. Forecast obtained from IRI**

Figure 35 and Figure 36 indicate the predicted probabilities from the CCAM forecast system that the accumulated seasonal streamflow during the 2009/2010 summer would fall into wettest third and the driest third category, respectively. The quaternary catchment area located below (above) the 26° S latitudinal line tend to be dominated by the probabilities of the wettest (driest) third tercile.

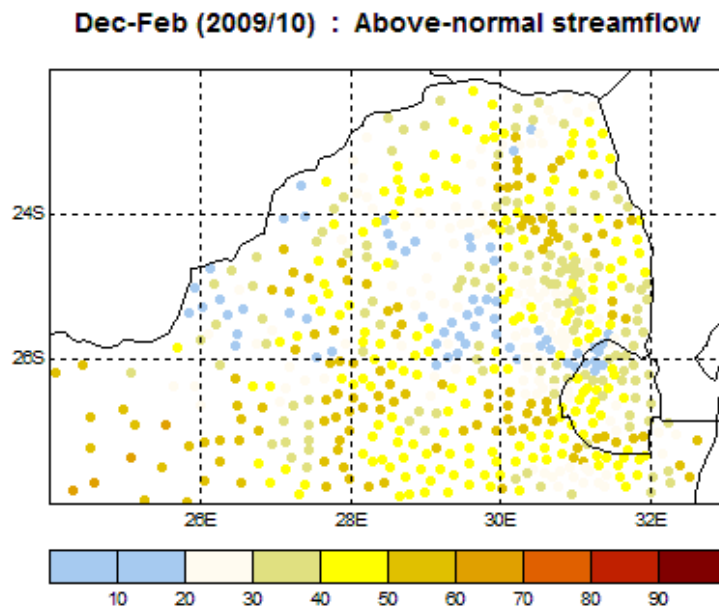


**Figure 35: Probabilities of above-normal accumulated streamflow statistically downscaled in the quaternary catchment areas over the north-eastern region of South Africa for the 2009/2010 summer (Dec-Feb) season**

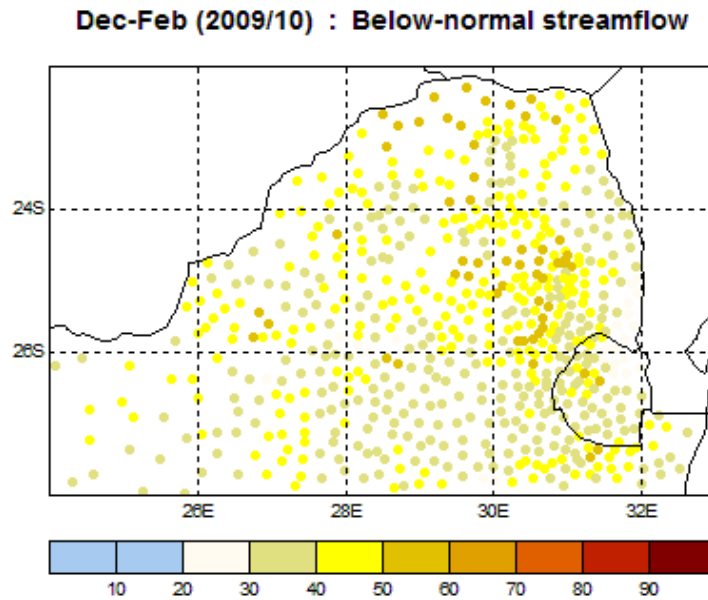


**Figure 36: Probabilities of below-normal accumulated streamflow statistically downscaled in the quaternary catchment areas over the north-eastern region of South Africa for the 2009/2010 summer (Dec-Feb) season**

In the central interior and eastern parts of the South Africa during the summer of 2010/2011 (depicted in Figure 37), the forecast showed about a 50% probability of extreme wet conditions prevailing and only about a 15% chance that extreme dry conditions would occur. In other parts of the country including our study region, a 45% (15%) chance of extreme wet (dry) conditions were predicted. Generally, this

summer season tends to be dominated by extreme wet conditions. This signal seems to have translated to the seasonal accumulation of streamflow in the north-eastern region of the country. The probabilities of seasonal accumulated streamflow to be above-normal ranged from 30% to 80% in most quaternary catchment areas excluding those near the Swaziland–South Africa northern border. There, chances of above-normal conditions occurring were estimated from 10% to 20%. The chances of seasonal accumulated streamflow being below-normal ranged between 10% and 39%.

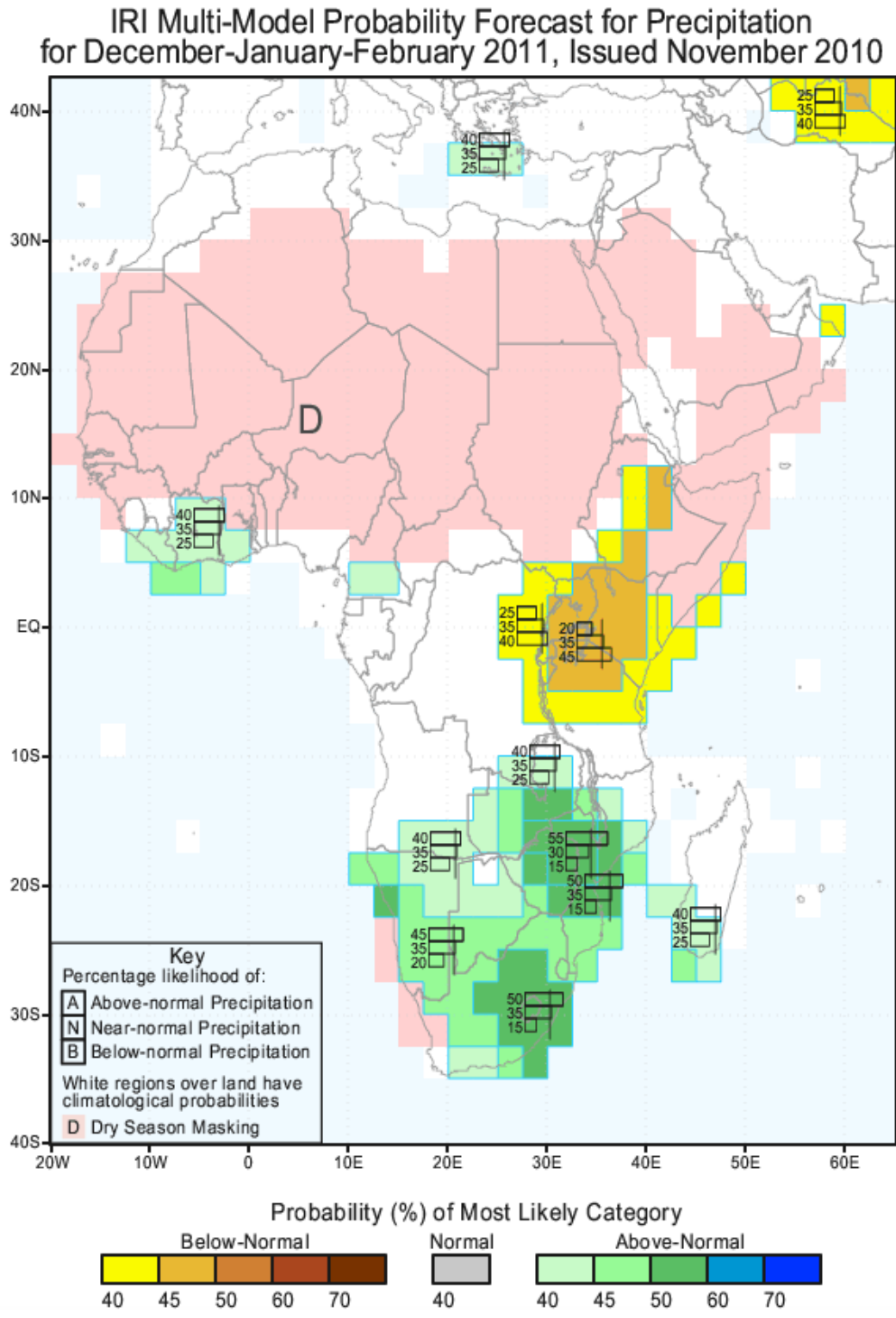


Figure 37: Probabilistic forecast of precipitation for Dec 2010–Feb 2011. Forecast obtained from IRI

**Dec- Feb (2010/11) : Above-normal Streamflow**

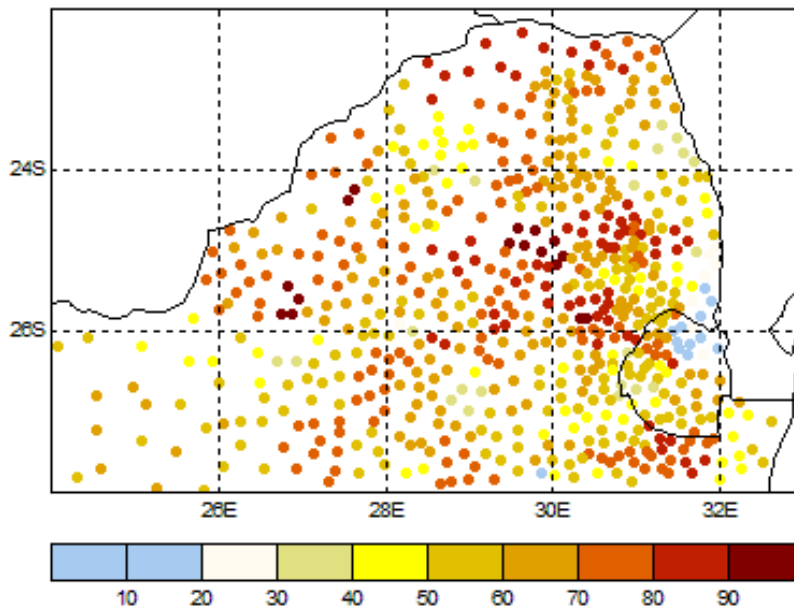


Figure 38: Probabilities of above-normal accumulated streamflow statistically downscaled in the quaternary catchment areas over the north-eastern region of South Africa for the 2010/2011 summer (Dec-Feb) season

**Dec-Feb (2010/11) : Below-normal streamflow**

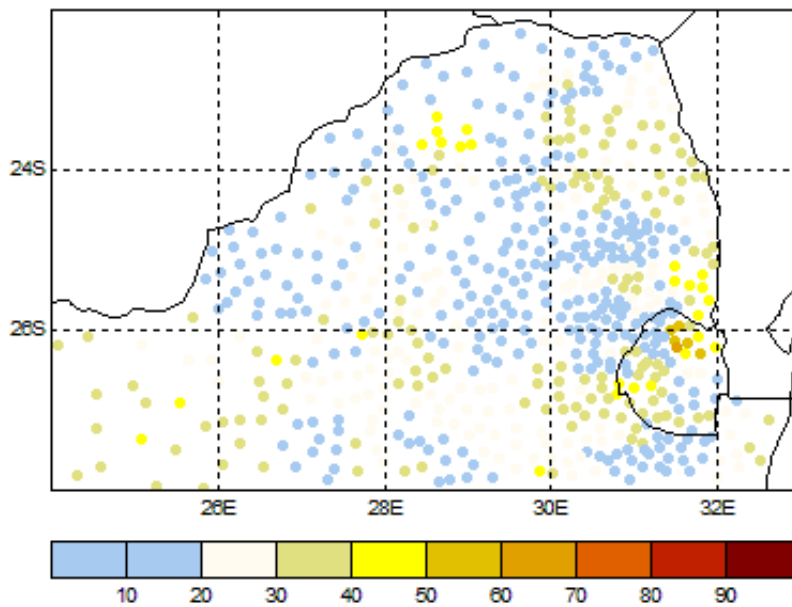
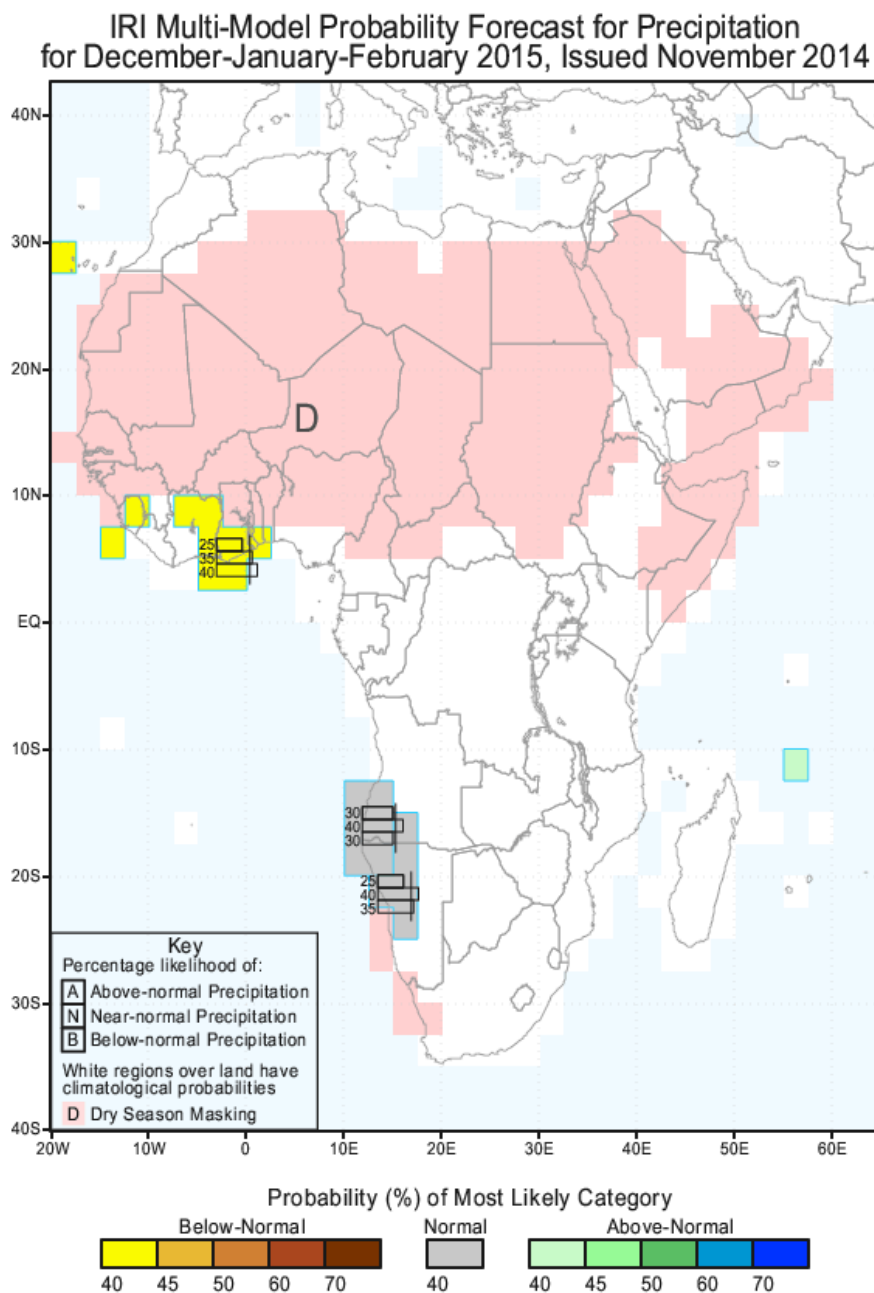
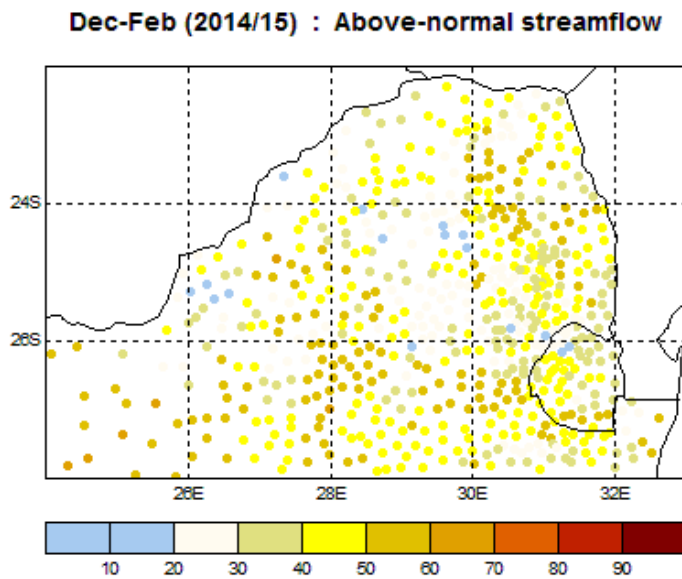


Figure 39: Probabilities of below-normal accumulated streamflow statistically downscaled in the quaternary catchment areas over the north-eastern region of South Africa for the 2010/2011 summer (Dec-Feb) season

The SST anomalies in the equatorial Pacific Ocean manifested as a neutral phase of the ENSO pattern during the 2014/2015 summer season (indicated in Figure 32). The IRI's multi-model precipitation outlook showed a climatological probability; hence, there is no basis for favouring any particular category (see Figure 40). The chances of accumulated streamflow being below-normal were between 20% and 39% throughout the north-eastern region of South Africa (see Figure 42). The probability of above-normal conditions prevailing in most quaternary catchment areas ranged from 30% to 69%. However, as shown in Figure 41, there were a few quaternary catchment areas where the chances of above-normal conditions occurring were relatively low (just under 20% probability recorded). As indicated in Figure 32, although 2014/2015 was classified as a neutral ENSO, the anomalies observed were cooler than normal. Therefore, probabilities of above-normal accumulated streamflow tend to dominate.



**Figure 40: Probabilistic forecast of precipitation for Dec 2014–Feb 2015. Forecast obtained from IRI**



**Figure 41: Probabilities of above-normal accumulated streamflow statistically downscaled in the quaternary catchment areas over the north-eastern region of South Africa for the 2014/2015 summer (Dec-Feb) season**

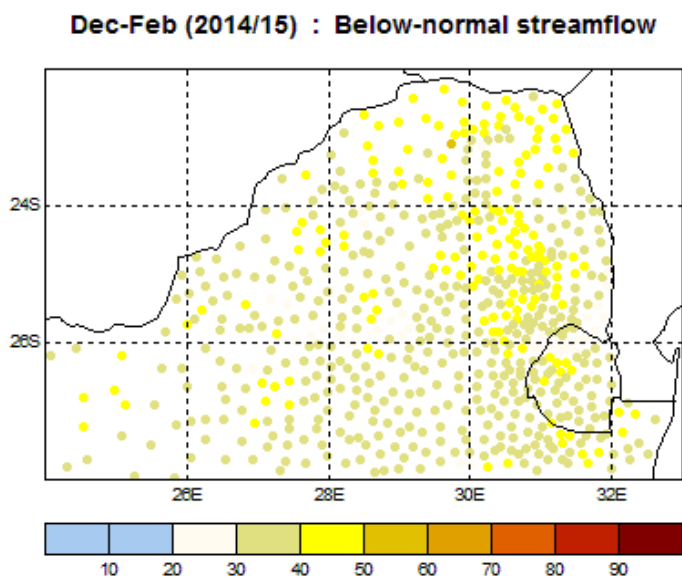


**Figure 42: Probabilities of above-normal accumulated streamflow statistically downscaled in the quaternary catchment areas over the north-eastern region of South Africa for the 2014/2015 summer (Dec-Feb) season**

#### 4.2.2 Medium- to short-range forecast products

The previous WRC project lead by the CSIR (K5/2325) developed a high-resolution ensemble weather forecasting system was developed and launched operationally at the CSIR. The procedure applied to generate forecasts using this system was as follows:

The CCAM was initialised every six hours to produce forecasts of the future state of the atmosphere up to seven days ahead. The model was initialised with atmospheric conditions at 00:00, 06:00, 12:00 and 18:00 UTC downloaded from GFS of the United States of America’s National Oceanic and Atmospheric Administration (NOAA) to produce a global forecast. This forecast applied a stretched-grid approach to obtain a resolution of 50 km over much of the African continent, with the resolution decreasing to about

400 km on the opposite side of the globe [see Engelbrecht et al. (2011) for a discussion of applying CCAM in stretched-grid mode]. Thereafter, the CCAM was dynamically downscaled to produce forecasts at a 15 km resolution over southern Africa. Meteorological variables predicted by the CCAM included daily accumulated rainfall, precipitation rate,  $u$  and  $v$  wind velocity components from 1000 hPa to 200 hPa vertical pressure levels, and minimum and maximum temperatures. Previous forecasts were only prepared for a seven-day lead time, but the forecast time was extended to 14 days. Moreover, the 15 km resolution forecasts are now being nudged within a global forecast of 50 km resolution as opposed to the 50 km resolution covering only part of the African continent, as in the previous forecast system.

Figure 43 shows the four-day outlook based on the initial state of the atmosphere on 19 February 2018 at 00:00 UTC. A few river station points (situated in the focus area) as defined by the DWS were selected to showcase the newly extended medium-range forecast. A detailed description of the selected station is presented in Table 3.

Produced by: The Climate Studies, Modelling and Environmental Health Group of the CSIR.

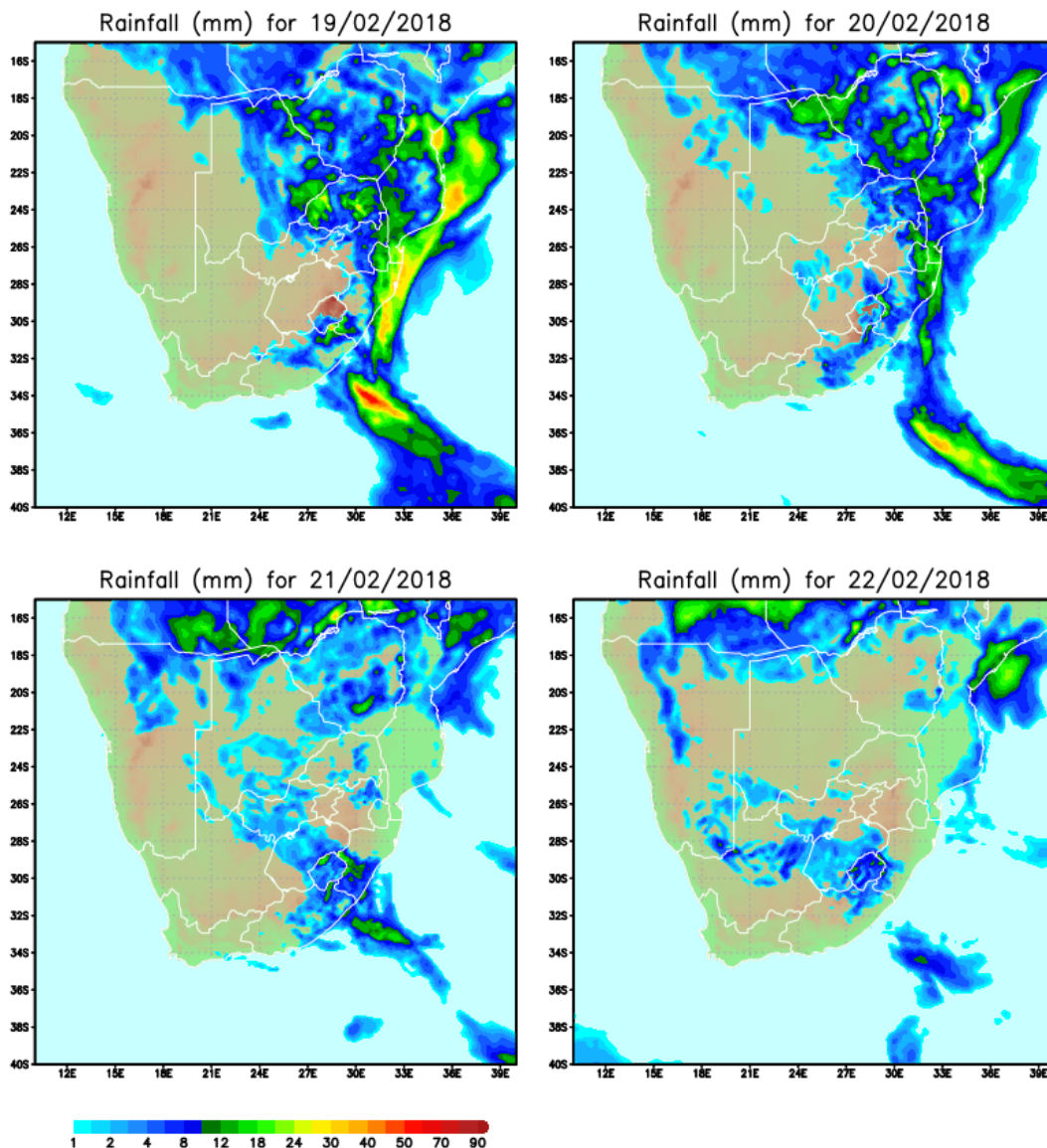
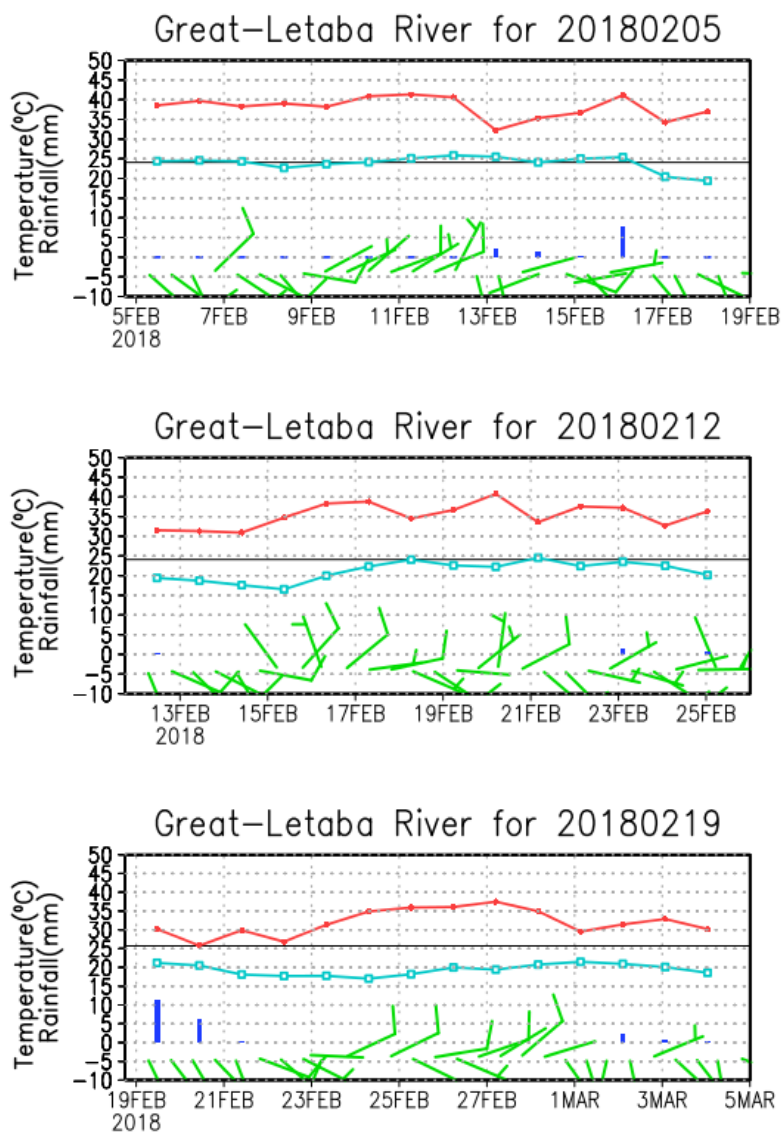


Figure 43: CCAM rainfall (accumulated over 24 hours) four-day forecast. The rainfall forecasts were obtained by initialising CCAM with atmospheric conditions at 02:00 of the 19 February 2018

**Table 3: Location and description of the five selected river stations in the north-eastern region as defined by the DWS**

Station No.	Longitude (° E)	Latitude (° S)	Station Name
B8H008	31.0499	-23.65837	Great Letaba River @ Letaba Ranch
A9H012	30.88925	-22.76851	Luvuvhu River @ Mhinga
A4H005	27.77267	-24.08066	Mokolo River @ Dwaalhoek
X1H017	30.27825	-25.89463	Komati River @ Waterval
A9H003	30.52378	-22.89814	Tshinane River @ Chibase

Figure 44 to Figure 48 show the four-day forecast product at stations located in Great Letaba, Luvuvhu, Mokolo, Komati and Tshinane rivers. In Figure 44 to Figure 48, the top rows present the predicted weather conditions up to 14 days ahead of the rainfall event of the 19 February 2018, the middle rows present the forecast generated 7 days prior to the 19 February 2018 event, and the bottom panels show the forecast generated on the day of the event.



**Figure 44: Fourteen-day forecast produced on 5 February 2018, 12 February 2018 and 19 February 2018 at Great Letaba River at the station point located in Letaba Ranch. Minimum and maximum temperature forecasts are presented by the cyan and red lines respectively. The bars (in blue) indicate the daily rainfall forecast and wind forecast is shown by wind barbs (in green)**



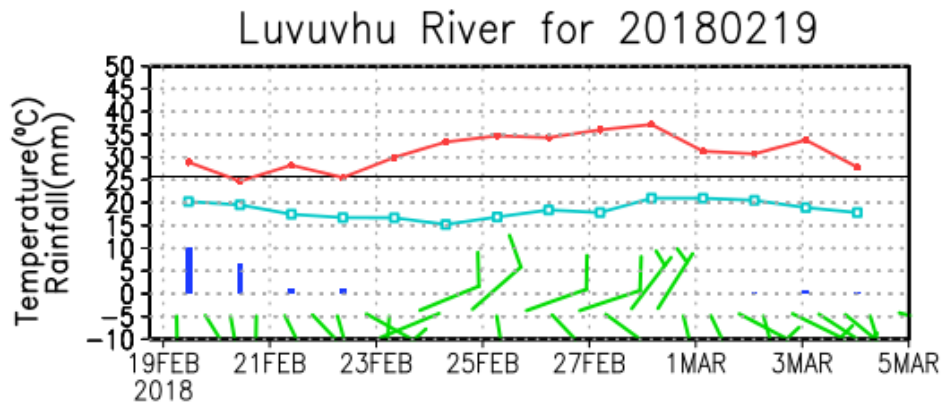
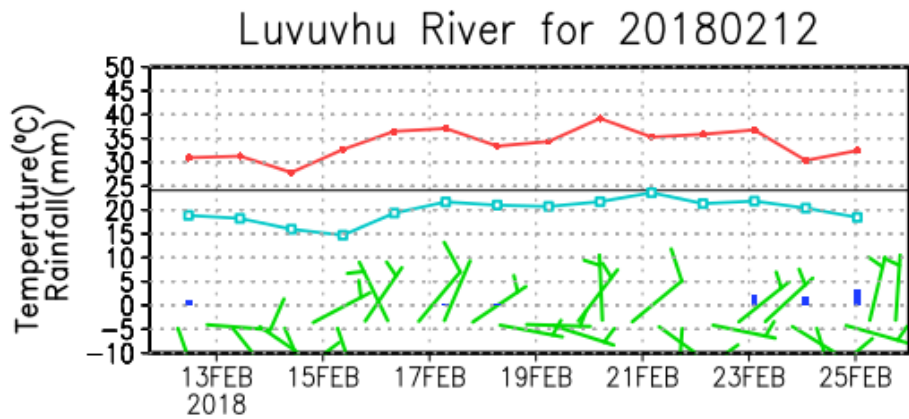
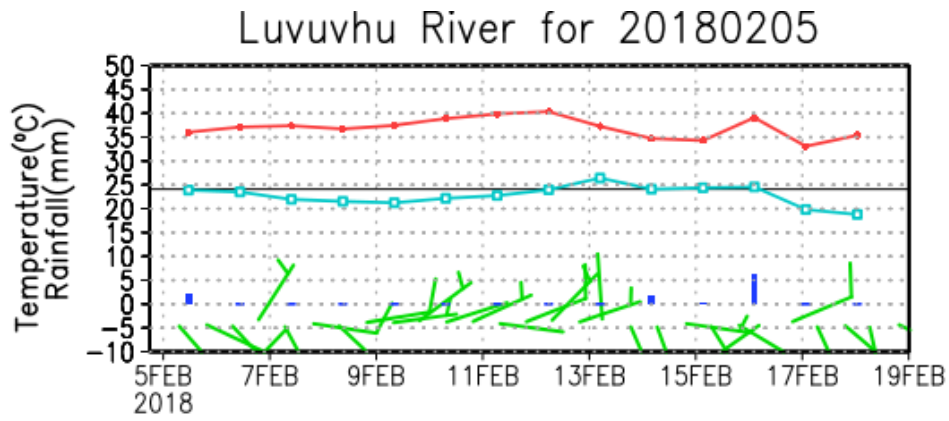


Figure 45: Fourteen-day forecast produced on 5 February 2018, 12 February 2018 and 19 February 2018 at Luvuvhu River at the station point located in Mhinga. Minimum and maximum temperature forecasts are presented by the cyan and red lines respectively. The bars (in blue) indicate the daily rainfall forecast and wind forecast is shown by wind barbs (in green)

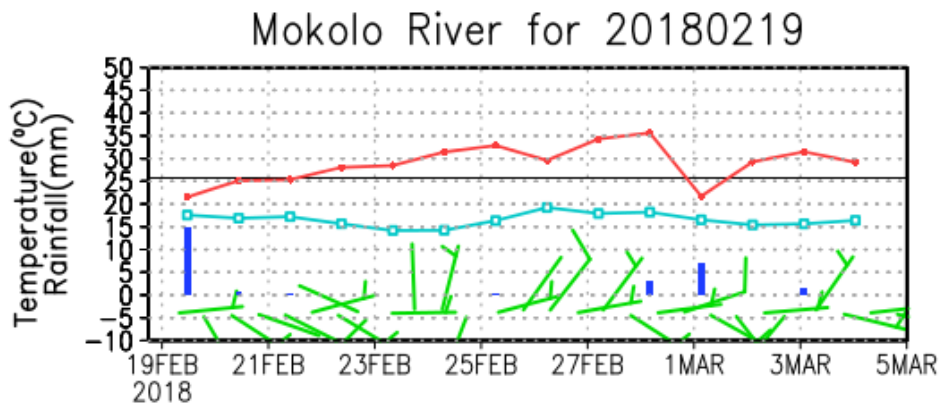
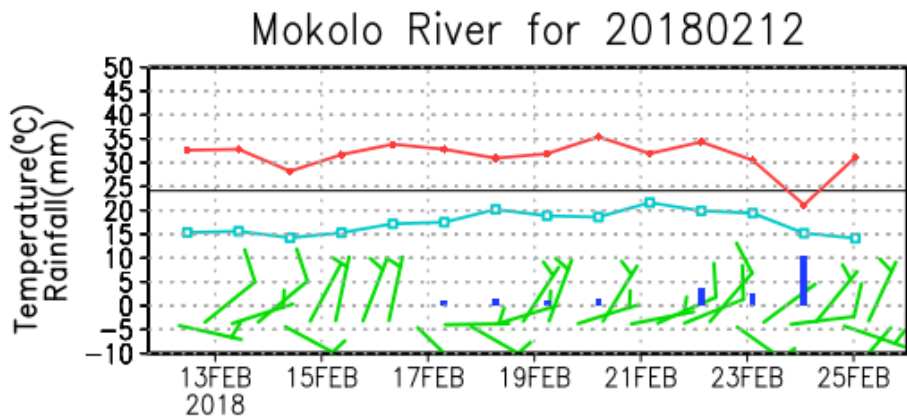
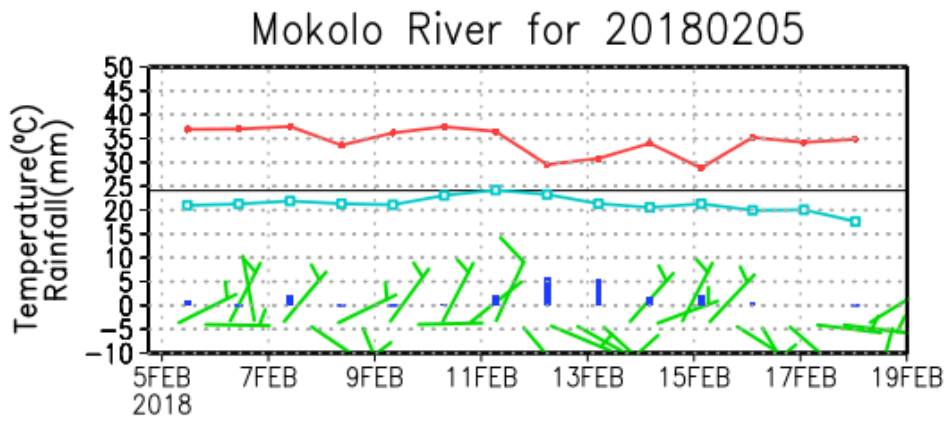


Figure 46: Fourteen-day forecast produced on 5 February 2018, 12 February 2018 and 19 February 2018 at Mokolo River at the station point located in Dwaalhoek. Minimum and maximum temperature forecasts are presented by the cyan and red lines respectively. The bars (in blue) indicate the daily rainfall forecast and wind forecast is shown by wind barbs (in green)

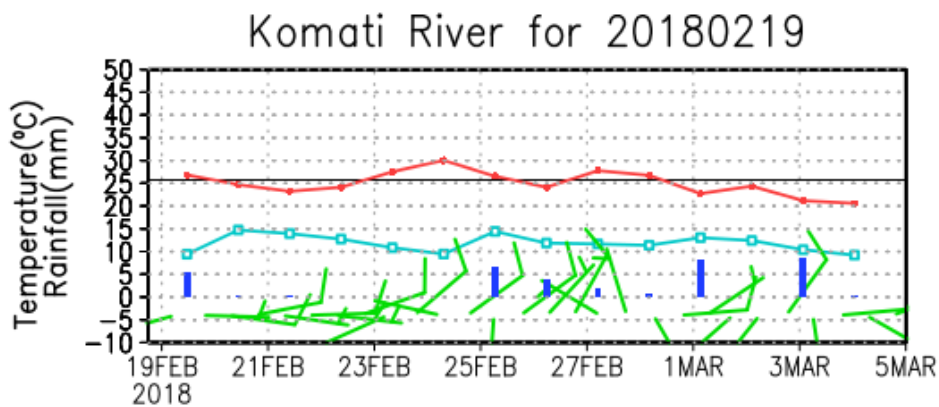
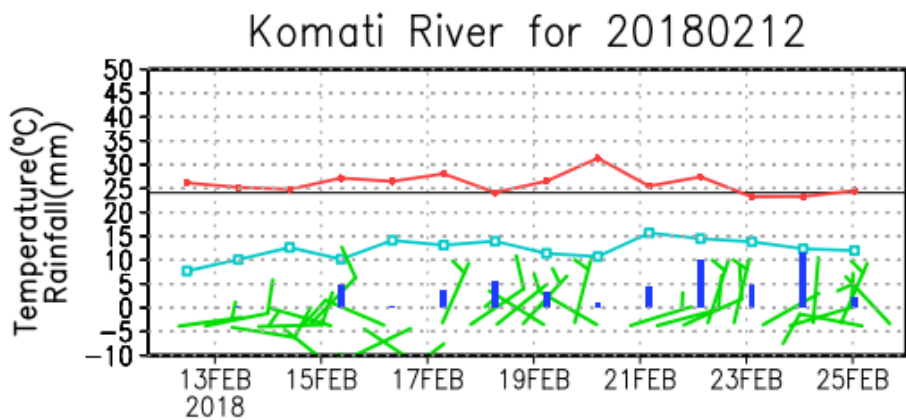
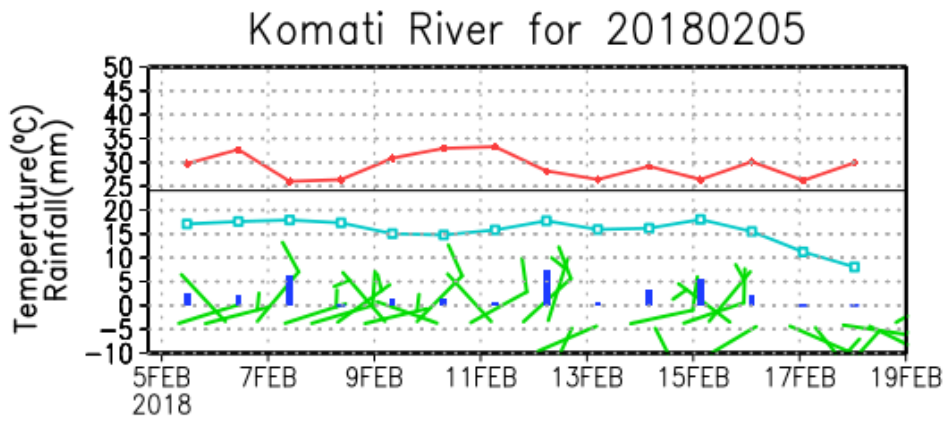


Figure 47: Fourteen-day forecast produced on 5 February 2018, 12 February 2018 and 19 February 2018 at Komati River at the station point located in Waterval. Minimum and maximum temperature forecasts are presented by the cyan and red lines respectively. The bars (in blue) indicate the daily rainfall forecast and wind forecast is shown by wind barbs (in green)

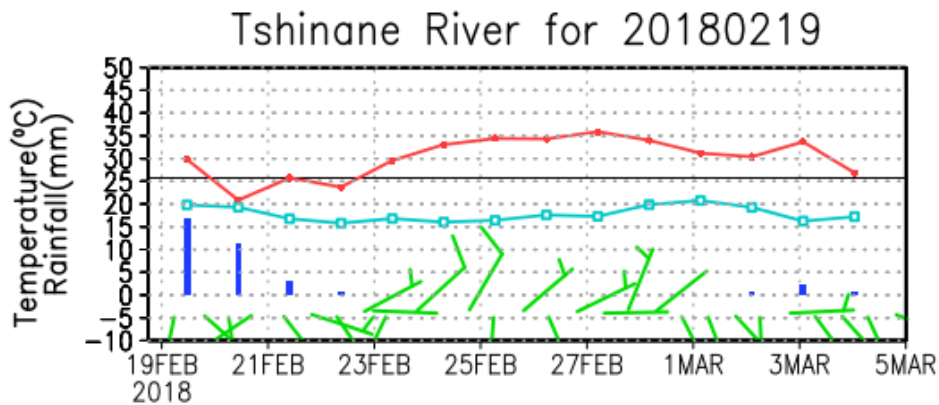
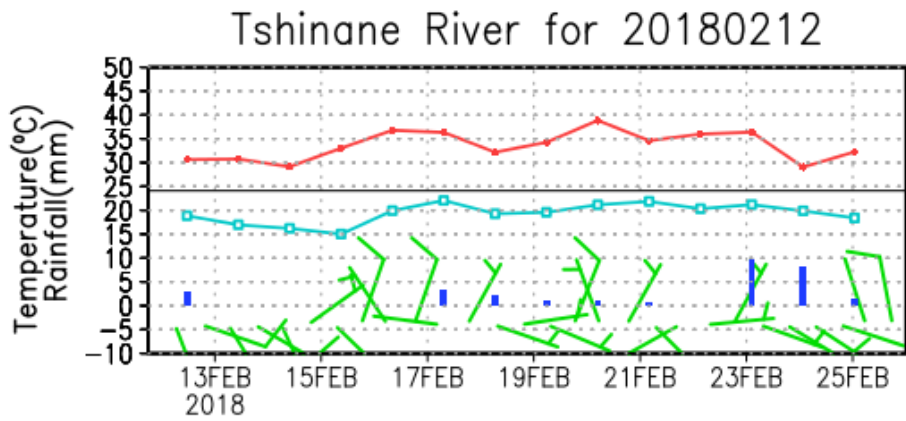
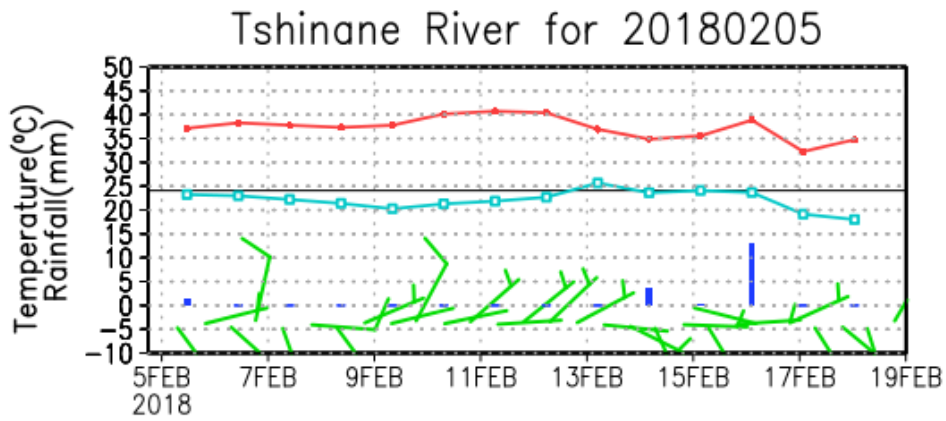


Figure 48: Fourteen-day forecast produced on 5 February 2018, 12 February 2018 and 19 February 2018 at Tshinane River at the station point located in Chibase. Minimum and maximum temperature forecasts are presented by cyan and red lines respectively. The bars (in blue) indicate the daily rainfall forecast and wind forecast is shown by wind barbs (in green)

### **4.3 Community Engagement**

To ensure that the project research found a direct application in Limpopo, the research team participated in the Provincial Climate Change Working Group meeting, which was organised by the Limpopo Department of Economic Development, Environment and Tourism. The meeting was held on 8 March 2018 at Masana Lodge in Polokwane. Representatives from various institutions attended, which included Limpopo district municipalities.

The main purpose of the meeting was for key stakeholders to discuss the implementation of Limpopo Province's climate change action plan and to report on the progress already made in the five district municipalities of Limpopo. The agenda of the meeting and attendance register are given in Appendix 1A and 1B.

The CSIR research team gave presentations on the climate variability of Limpopo, projections of future climate change, and climate predictions on seasonal to short-range forecasts and their potential application in hydrology. This engagement with the key stakeholders allowed the research team to understand the work being done in the province and provided the opportunity to tailor the forecast products to support ongoing project in the district municipalities.

### **4.4 Synopsis**

The aim of this chapter was to present the forecast products from seasonal to weather timescales as well as their application in hydrology. Generally, the climate of South Africa is prone to high interannual variability, which is mainly driven by the teleconnection to the fluctuation of SST anomalies in the tropical Pacific Ocean, also known as ENSO. ENSO tends to fluctuate between three phases, namely: warm (El Niño), cold (La Niña) and neutral. The warm (cold) phase is typically linked to drier and hotter (wetter and cooler) climate conditions.

Three summer periods (2009/2010, 2010/2011 and 2014/2015) coinciding with all three ENSO phases were selected and the probabilistic forecasts during these periods were presented. The results showed that during La Niña events, the tendency of high probabilities of above-normal accumulated streamflow occurring was consistent across the quaternary catchment areas in the north-eastern region of South Africa. In the event of an El Niño, the highest chances of seasonal accumulated streamflow to be below-normal tended to be restricted to catchments areas located north of the 26° S latitudinal line; those positioned south of this line tended to be dominated by probabilities of above-normal conditions prevailing.

The analysis of a neutral ENSO-phased summer showed that this ENSO phase tended to favour the occurrence of above-normal seasonal accumulated streamflow. However, it should be acknowledged that during the considered neutral ENSO event, the SST anomalies were more inclined towards a cold ENSO; hence, probabilities of above-normal accumulated streamflow were predominant. The neutral ENSO event could be inclined towards a warm ENSO phase. The implication of such an event on seasonal accumulated streamflow needs to be explored.

All cases provided here serve as examples of the forecast products generated by the project. More comprehensive work is needed in terms of the linkage between seasonal streamflow and the neutral ENSO phase in particular. Such a study will aid in improving effectiveness of the early flood warning systems. The extended medium-range forecast products tailored for primary rivers in the Limpopo Province were also presented. These products, when monitored daily, can aid in the early detection of possible extreme weather events.

## 5 CONCLUSION AND RECOMMENDATIONS

The interannual rainfall variability prevalent over South Africa's summer rainfall region is mainly due to the teleconnected influence of the SST anomalies in the tropical Pacific Ocean. In an event where anomalously warmer (cooler) SSTs are observed over the domain [5° N–5° S, 120–170° W], which is commonly referred to as a Niño 3.4 region, there tends to be drier (wetter) than normal rainfall conditions. These drier (wetter) conditions can manifest themselves on a daily timescale as a low (high) frequency of rainfall days. Weather systems are also affected, with wetter conditions associated with more rain-producing systems (such as cut-off lows, TTTs, mesoscale complex systems as well as tropical cyclones), which tend to bring heavy rainfall that may lead to flooding.

The main aim of this study was formulated as an early flood warning strategy tool, which was termed *ready-set-go*. The tool involves using seasonal forecasts to prepare for potentially wetter than normal seasonal conditions, which may imply the occurrence of flood events. This component of the strategy is referred to as the *ready* component. Those likely to be affected by floods as well as risk managers can then begin to monitor the medium-range forecast (up to 14 days) (*set* mode) to ensure that contingency plans in risk-prone areas are in place. The *go* part includes short-range weather forecasting for the next 48-hour period, which is the action step. Risk managers can then start evacuating people to lessen the societal impacts of floods.

Against this background, the project explored the following:

- How the CSIR's current weather and seasonal forecast model configurations can be utilised further for hydrological applications.
- The skill of the CCAM weather and hydrological forecasts as short- and medium-range timescales.
- How well the river routing system of the CABLE land-surface model represents real flows over the north-eastern interior of South Africa.
- Whether the CCAM output can be downscaled successfully to seasonal and daily river flows over the north-eastern interior.
- The benefit that the envisaged ready-set-go approach hold for society and disaster management.

The main objective of Chapter 2 was to investigate the ability of the CCAM in combination with the dynamic land-surface model, CABLE, to simulate river flows in the north-eastern region of South Africa when coupled to a dynamic river routing scheme. Two experiments were performed: the one with the CCAM CABLE model at a relatively coarse resolution; the other with the CCAM CABLE model run at a higher resolution (i.e. at 8 km resolution). At a higher resolution model configuration, the CCAM CABLE run with the river routing scheme was able to realistically simulate major rivers, including the Orange, Vaal, Tugela and Limpopo, across South Africa. These experiments represent the first applications of a dynamic river routing scheme in South Africa.

To understand the feasibility of downscaling the CCAM output at daily timescales, a random sampling method was applied to extract 100 days for which a linear regression statistical model was built. This model was tested for two case studies, namely, tropical cyclone Funso and tropical depression Dando. The deterministic forecast values produced by the linear regression model at a few selected stations spread across the north-eastern region of South Africa were relatively small compared with the observed values during the Funso and Dando events. However, the predicted flows' positive correlation to observed flows cannot be disregarded as the statistical model applied here does not account for the antecedent condition of the river basin and the interbasin water transfers. This implies that short-range weather forecasting in combination with statistical downscaling can function as the go component in a ready-set-go early warning flood management tool for north-eastern South Africa. Medium-range

forecasts can be used for the set stage of such a system. Further afield is the application of dynamic river routing or nested mechanistic hydrological models, such as ACRU or Pitman, for short-range streamflow forecasting. Such systems would, however, require that intricate streamflow initialisation methods be developed.

At the seasonal timescale, a statistical model was built using the CPT executed in a canonical correlation mode. The streamflow forecasts at lead times from one to three months tend to be positively correlated with naturalised streamflow over more quaternary catchment areas than for the spatial extent of positive correlations between forecasted and naturalised streamflow for 0-month lead analysis. This pattern is also translated to hit score results. Three summer periods (2009/2010, 2010/2011 and 2014/2015) that coincided with cold, warm and neutral phases of ENSO were analysed to understand the teleconnected impacts of ENSO to streamflows in the north-eastern region of South Africa. The results showed that during La Niña events, the tendency of high probabilities of above-normal accumulated streamflow occurring tends to be consistent across the quaternary catchment areas in the north-eastern region of South Africa. During El Niño events, below-normal accumulated seasonal streamflow can be anticipated; however, the probability of such an event occurring is predicted to be relatively small in comparison to the probability associated with a La Niña event. The analysis of a neutral ENSO phase that is more inclined to La Niña SST properties showed that this ENSO phase tends to favour the occurrence of above-normal seasonal accumulated streamflow. In summary, seasonal forecast skill in predicting wet conditions over north-eastern South Africa during La Niña years do translate into the skill of forecasting anomalously high values of streamflow, implying that numerical seasonal forecast systems can provide the set stage of a ready-set-go early warning approach for managing floods in north-eastern South Africa.

The robustness of any early warning system needs to be tested thoroughly before it can be launched operationally as an inaccurate warning signal would potentially lead to a loss of money (in a case where resources are directed inaccurately) or loss of life where the system completely fails to pick up extreme events. In order to test the robustness of the system, an observed river data set is required. The unavailability of a complete and consistent time series of observed river water levels and river flows at monthly and daily temporal resolution posed a limitation to this research.

The future of early warning systems for streamflow and flood events may well increasingly involve the application of dynamic river routing schemes. When performing CCAM CABLE model runs with the river routing scheme activated, the model needs to be spun up from a dry state. It takes several simulation years for the model to reach a level where river basins contain any water. Since the seasonal forecast model usually ran once a month, the use of a dynamic river routing scheme seems feasible at this timescale, provided that sufficient computational resources are available to spin up the model rivers to suitable states that represent reality. However, on daily timescales it could be a challenge to use the river routing scheme operationally. Also, the river routing scheme within CCAM CABLE essentially computes all flow-related variables based on purely on rainfall-flow relationships and does not include factors such as interbasin transfers and human decision-making around water storage. Until such features are built into dynamic river routing schemes, the incorporation of already existing hydrological models such as ACRU and Pitman in short-range and seasonal early warning systems could potentially improve the effectiveness of early flood warning tools.

## LIST OF REFERENCES

- Asante, K. O., Macuacua, R. D. & Artan, G. A., 2007. Developing a flood monitoring system from remotely sensed data for the Limpopo basin. *IEEE Transactions on Geoscience and Remote Sensing*, 45(5), pp. 1709-1714.
- Bauer, P., Thorpe, A. & Brunet, G., 2015. The quiet revolution of numerical weather prediction. *Nature*, 525, pp. 47-55.
- Behera, S. K., Salvekar, P. S. & Yamagata, T., 2000. Simulation of interannual SST variability in the tropical Indian Ocean. *Journal of Climate*, 13, pp. 3487-3499.
- Beraki, A. F., DeWitt, D., Landman, W. A. & Olivier, C., 2014. Dynamical seasonal climate prediction using an ocean-atmosphere coupled climate model developed in partnership between South Africa and the IRI. *Journal of Climate*, 27, pp. 1819-1741.
- Beraki A.F., Landman, W. A., DeWitt, D. & Olivier, C., 2016. Global dynamical forecasting system conditioned to robust initial and boundary forcings: seasonal context, *International Journal of Climatology*, DOI: 10.1002/joc.4643
- Blamey, R. C. & Reason, C. J. C., 2009. Numerical simulation of a mesoscale convective system over the east coast of South Africa. *Tellus*, 61(1), pp. 17-34.
- Blamey, R. C. & Reason, C. J. C., 2012. Mesoscale convective complexes over Southern Africa. *Journal of Climate*, 25, pp. 753-766.
- Blamey, R. C. & Reason, C. J. C., 2013. The role of mesoscale convective complexes in southern Africa summer rainfall. *Journal of Climate*, 26, pp. 1654-1668.
- Bougeault, P., 2003. The WGNE survey of verification methods for numerical prediction of weather elements and severe weather events, Météo-France, Toulouse. [Online] Available at: [http://www.cawcr.gov.au/projects/verification/Bougeault/Bougeault\\_Verification-methods.htm](http://www.cawcr.gov.au/projects/verification/Bougeault/Bougeault_Verification-methods.htm)
- Braman, L. M. et al., 2013. Climate forecast in disaster management: Red Cross flood operations in West Africa, 2008. *Disasters*, 37, pp. 144-164.
- Cai, W. et al., 2015. Increased frequency of extreme La Niña events under greenhouse warming. *Nature Climate Change*, p. DOI: 10.1038/NCLIMATE2492
- Christensen, J. H. et al., 2007. Regional climate projections. In: S. Solomon, et al. (eds). *Climate Change 2007: The Physical Science Basis. Contribution of Working Group I to the Fourth Assessment Report of the Inter-Governmental Panel on Climate Change*. Cambridge: University Press, pp. 591-648.
- Cloke, H. L. & Pappenberger, F., 2009. Ensemble flood forecasting: A review. *Journal of Hydrology*, 375, pp. 613-625.
- Collischonn, W., Haas, R., Andeolli, I. & Tucci, C. E. M., 2005. Forecasting River Uruguay flow using rainfall forecasts from a regional weather-prediction model. *Journal of Hydrology*, 205, pp. 87-98.
- CSIRO, 2013. CSIRO technical report. [Online] Available at: [http://www.clw.csiro.au/publications/scientific\\_reports.html](http://www.clw.csiro.au/publications/scientific_reports.html)



- De Coning, E., Forbes, G. S. & Poolman, E., 1998. Heavy precipitation and flooding on 12-14 February 1996 over summer rainfall regions of South Africa: Synoptic and insentropic analyses. *National Weather Digest*, 22, pp. 25-36.
- Devia, G. K., Ganasri, B. P. & Dwarakish, G. S., 2015. A review on hydrological models. *Aquatic Procedia*, 4, pp. 1001-1007.
- Dieppois, B., Rouault, M. & New, M., 2015. The impact of ENSO on Southern African rainfall in CMIP5. *Climate Dynamics*, 45, p. 2425–2442.
- Doi, T., et al., 2014. Annual report of the Earth Simulator: April 2014–March 2015. Center for Earth Information Science and Technology Rep., p. 147. [Online] Available at [http://www.jamstec.go.jp/ceist/publication/annual/annual2014/pdf/AnnualReport\\_ES\\_2015.pdf](http://www.jamstec.go.jp/ceist/publication/annual/annual2014/pdf/AnnualReport_ES_2015.pdf)
- Doi, T., Behera, S. K. & Yamagata, T., 2016. Improved seasonal prediction using the SINTEX-F2 coupled model. *Journal of Advances in Modeling Earth Systems*, 8, 1847–1867, DOI: 10.1002/2016MS000744
- Du Plessis, L. A., 2002. A review of effective flood forecasting, warning and response system for application in South Africa. *Water SA*, 28(2), pp. 129-138.
- Duan, Z. et al., 2016. Evaluation of eight high spatial resolution gridded precipitation products in Addige Basin (Italy) at multiple temporal and spatial scales. *Science of the Total Environment*, 573, pp. 1536-1553.
- Dutta, S. C., Ritchie, J. W., Freebairn, D. M. & Abawi, G. Y., 2006. Rainfall and streamflow response to El Niño Southern Oscillation: A case study in semiarid catchment, Australia. *Hydrological Sciences Journal*, 51(6), pp. 1006-1020.
- Engelbrecht, C. J., Engelbrecht, F. A. & Dyson, L. L., 2012. High-resolution model-projected changes in mid-tropospheric closed-lows and extreme rainfall events over southern Africa. *International Journal of Climatology*, DOI: 10/1002/joc.3420
- Engelbrecht, F. & Bopape, M., 2010. Forecasting: The science of crystal ball gazing! ESKOM Convention Centre, Midrand, s.n.
- Engelbrecht, F., McGregor, J. L. & Engelbrecht, C. J., 2009. Dynamics of the Conformal-Cubic Atmospheric Model projected climate-change signal over southern Africa. *International Journal of Climatology*, pp. 1013-1033.
- Engelbrecht, F. A., McGregor, J. L., Katzfey, J. & Thatcher, M., 2011a. High-resolution projections of climate change over Africa using a variable-resolution global atmospheric model. *International Conference on the Coordinated Regional Downscaling Experiment (CORDEX)*. International Centre for Theoretical Physics, Trieste, Italy.
- Engelbrecht, F. A. et al., 2011b. Multi-scale climate modelling over Southern Africa using a variable-resolution global model. *Water SA*, 37(5), pp. 647-658.
- Engelbrecht, F. et al., 2015. Projections of rapidly rising surface temperatures over Africa under low mitigation. *Environmental Research Letters*, 10(8).

- Fox-Rabinovitz, M. et al., 2008. Stretched-grid Model Intercomparison Project: Decadal regional climate simulations with enhanced variable and uniform-resolution GCMs. *Meteorology and Atmospheric Physics*, pp. 159-177.
- Funk, C. et al., 2015. The climate hazards infrared precipitation with stations: A new environmental record for monitoring extremes. *Scientific Data*, DOI: 10.1038/sdata.2015.66
- Hamill, T., Whitaker, J. & Wei, X., 2004. Ensemble reforecasting: Improving medium range forecast skill using retrospective forecasts. *Monthly Weather Review*, 132, pp. 1434-1447.
- Hamill, T. M., 1997. Reliability diagrams for multicategory probabilistic forecasts. *Weather and Forecasting*, 12, pp. 736-741.
- He, Y. et al., 2009. Tracking the uncertainty in flood alerts driven by grand ensemble weather predictions. *Meteorological Applications*, DOI: 10.1002/met.132
- Holtzlag, A.A.M. & Boville, B.A., 1993. Local versus non-local boundary layer diffusion in a global climate model. *Journal of Climate*, 6, pp. 1825-1842.
- Hudson, D. A. & Alves, O., 2009. Dynamical monthly forecasting for Australia: Bridging the gap between weather and seasonal forecasting. *9th International Conference on Southern Hemisphere Meteorology and Oceanography*, 9-13 Feb. Melbourne.
- James, R. & Washington, R., 2013. Changes in African temperature and precipitation associated with degrees of global warming. *Climatic Change*, 117, pp. 859-872.
- Jie, W. et al., 2014. Improvement of 6-15 day precipitation forecast using a time-lagged ensemble method. *Advances in Atmospheric Sciences*, 31, pp. 293-304.
- Johnston, P. A. et al., 2004. Review of seasonal forecasting in South Africa: Producer to end-user. *Climate Research*, 28(1), pp. 67-82.
- Jury, M. R., 2012. An inter-comparison of model-simulated east–west climate gradients over South Africa. *Water SA*, 38(4), pp. 467-477.
- Kalnay, E., 2003. *Atmospheric Modelling, Data Assimilation and Predictability*. New York, NY: Cambridge University Press.
- Kanamitsu, M. et al., 2002. NCEP-DOE AMIP-II reanalysis(R-2). *The Bulletin of the American Meteorological Society*, pp. 1631-1643.
- Katzfey, J., 2012. High-resolution climate projections for Vietnam. [Online] Available at: <http://vnclimate.vn/publications/Reports/Reports-10/> [Accessed 31 March 2015].
- Katzfey, J. J. & McGregor, J. L., 2005. *High-resolution Weather Predictions for the America's Cup in Auckland: A Blend of Model Forecast, Observations and Interpretation*. Aspendale: CSIRO Atmospheric Research.
- Katzfey, K. K., McGregor, J. M., Nguyen, K. & Thatcher, M., 2009. Dynamical downscaling techniques: Impacts on regional climate change signals. *18th World IMACS/MODSIM Congress*, Cairns, Australia.

- Kowalczyk, E. A., Garratt, J. R. & Krummel, P. B., 1994. Implementation of a soil-canopy scheme into the CSIRO GCM -regional aspects of the model response. *CSIRO Division of Atmospheric Research Technical Papers*, 32, p. 59.
- Kowalczyk, E. A. et al., 2006. *The CSIRO Atmosphere Biosphere Land Exchange (CABLE) Model for Use in Climate Models and as an Offline Model*. Aspendale: CSIRO Marine and Atmosphere Research.
- Krishnamurti, T. N. et al., 2000. Multimodel ensemble forecasts for weather and seasonal climate. *Journal of Climate*, pp. 4196-4216.
- Landman, S. et al., 2012a. A short-range weather prediction system for South Africa based on a multi-model approach. *Water SA*, pp. 756-773.
- Landman, W. A., Mason, S. J., Tyson, P. D. & Tennant, W. J., 2001. Statistical downscaling of GCM simulations to streamflows. *Journal of Hydrology*, 252, pp. 221-236.
- Landman, W. A. et al., 2009. Model output statistics applied to multi-model ensemble long-range forecasts over South Africa, Water Research Commission, Pretoria. WRC Report No. 1492/1/08.
- Landman, W. et al., 2010. Atmospheric modelling and prediction at time scales from days to seasons, Council for Scientific and Industrial Research, Pretoria.
- Landman, W. A. & Beraki, A., 2012. Multi-model forecast skill for midsummer rainfall over southern Africa. *International Journal of Climatology*, 32, pp. 303-314.
- Landman, W. A. et al., 2012b. Seasonal rainfall prediction skill over South Africa: 1- vs. 2-tiered forecasting systems. *Weather and Forecasting*, 27, pp. 489-501.
- Landman, W. A., 2014a. How the International Research Institute for Climate and Society has contributed towards seasonal climate forecast modelling and operations in South Africa. *Earth Perspectives*, 1(22).
- Landman, W. A., Beraki, A., DeWitt, D. & Lötter, D., 2014b. SST prediction methodologies and verification considerations for dynamical mid-summer rainfall forecasts for South Africa. *Water SA*, 40(4), pp. 615-622.
- Landman, W. A. et al., 2015. Unifying weather and climate variability predictions: An operational seamless forecasting system for southern Africa at time scales from days to seasons, Water Research Commission, Pretoria. WRC Report No. 2050/1/14.
- Lazenby, M., Landman, W. A., Garland, R. & DeWitt, D., 2014. Seasonal temperature prediction skill over southern Africa and human health. *Meteorological Applications*, 21, pp. 963-974.
- Leutbecher, M. & Palmer, T. N., 2008. Ensemble forecasting. *Journal of Computational Physics*, pp. 3515-3539.
- Lindesay, J. A., 1988. Southern African rainfall, southern oscillation and southern hemisphere semi-annual cycle. *Journal of Climatology*, 8, pp. 17-30.
- Lindesay, J. A. & Vogel, C. H., 1990. Historical evidence for southern oscillation-southern African rainfall relationships. *International Journal of Climatology*, 10, pp. 679-689.

- Lu, C., Yuan, H., Schwartz, B. E. & Benjamin, S. G., 2007. Short-range numerical weather prediction using time-lagged ensembles. *American Meteorological Society*, pp. 580-595.
- Madec, G., 2006. NEMO ocean engine. Note du Pôle de Modélisation IPSL Rep., p. 110.
- Magnusson, L. & Kallen, E., 2013. Factors influencing skill improvements in the ECMWF forecasting system. *Monthly Weather Review*, 141, pp. 3142-3153.
- Malherbe, J., Engelbrecht, F. A. & Landman, W. A., 2013. Projected changes in tropical cyclone climatology and landfall in the Southwest Indian Ocean region under enhanced anthropogenic forcing. *Climate Dynamics*, 40, pp. 2867-2886.
- Malherbe, J. et al., 2014. Seasonal forecasts of the SINTEX-F coupled model applied to maize yield and streamflow estimates over north-eastern South Africa. *Meteorological Applications*, 21, pp. 733-742.
- Manhique, A. J., Reason, C. J. C., Rydberg, L. & Fauchereau, N., 2011. ENSO and Indian Ocean sea surface temperatures and their relationships with tropical temperate troughs over Mozambique and the Southwest Indian Ocean. *International Journal of Climatology*, 31(1), pp. 1-13.
- Mason, I., 1982. A model for assessment of weather forecasts. *Australian Meteorological Magazine*, 30, pp. 291-303.
- Mass, C. F., Ovens, D., Westrick, K. & Colle, B. A., 2002. Does increasing horizontal resolution produce more skilful forecasts? The results of two years real-time numerical weather prediction over the Pacific Northwest. *Bulletin of American Meteorological Society*, pp. 407-429.
- McGregor, J. L., 2003. A new convection scheme using simple closure. Melbourne, BMRC, pp. 33-36.
- McGregor, J. L., 2005a. C-CAM: Geometric aspects and dynamical formulation. CSIRO Atmospheric research Tech. Paper No. 70, p. 43.
- McGregor, J. L., 2005b. Geostrophic adjustment for reversibly staggered grids. *Monthly Weather Review*, 133, pp. 1119-1128.
- McGregor, J. L. & Dix, M., 2005. The Conformal-Cubic Atmospheric Model: Progress and plans. s.l., CSIRO Atmospheric Research.
- McGregor, J. L. & Dix, M. R., 2001. The CSIRO conformal-cubic atmospheric GCM. In: P. F. Hodnett (ed.). *Proceedings of the IUTAM Symposium on Advances in Mathematical Modelling of Atmosphere and Ocean Dynamics*. Dordrecht: Kluwer, pp. 197-202.
- McGregor, J. L. & Dix, M. R., 2008. An updated description of the Conformal-Cubic Atmospheric Model. In: K. Hamilton & W. Ohfuchi (eds). *High Resolution Simulation of the Atmosphere and Ocean*. s.l.: Springer Verlag, pp. 51-76.
- McGregor, J. L., Gordon, H. B., Watterson, I. G., Dix, M. R. & Rotstayn, L. D., 1993. The CSIRO 9-level atmospheric general circulation model. CSIRO Div. Atmospheric Research Tech. Paper No. 26, p. 89.
- Miller, J. R., Russell, G. L. & Caliri, G., 1994. Continental-scale river flow in climate models. *Journal of Climate*, 7, pp. 914-928.

- Mitchell, T. D. & Jones, P. D., 2005. An improved method of constructing a database of monthly climate observations and associated high-resolution grids. *International Journal of Climatology*, 25, pp. 693-712.
- Mpheshea, L., 2014. *An Investigation into the Relative Contributions of ENSO, Benguela Nino and the Sub-tropical Indian Ocean Dipole on Summer Rainfall Over Southern Africa*. Cape Town: University of Cape Town.
- Mpheshea, L. E. & Landman, W. A., 2015. Predicting the extreme 2015/2016 El Nino event. Hennops River Valley, South Africa. South African Society for Atmospheric Sciences: 31 Annual Conference.
- Muchuru, S., Landman, W. A. & DeWitt, D., 2015. Prediction of inflows into Lake Kariba using a combination of physical and empirical models. *International Journal of Climatology*, In Press.
- Muchuru, S., Landman, W. A., DeWitt, D. & Lötter, D., 2014. Seasonal rainfall predictability over the Lake Kariba catchment area. *Water SA*, 40(3), pp. 461-469.
- Mukheibir, P., 2008. Water resources management strategies for adaptation to climate-induced impacts in South Africa. *Water Resources Management*, 22(9), pp. 1259-1276.
- Mulenga, H. M., Rouault, M. & Reason, C. J. C., 2003. Dry summers over northeastern South Africa and associated circulation anomalies. *Climate Research*, 25, pp. 29-41.
- Muller, H., Peters, C., Shu, Y. & Terhorst, A., 2013. Provenance in streamflow forecasting. Genoa, Italy, EDBT/ICDT 2013 Joint Conference.
- Niang, I. et al., 2014. Chapter 22. In: V. R. Barros et al. (eds). *Climate Change 2014: Impacts, Adaptation, and Vulnerability. Part B: Regional Aspects. Contribution of Working Group II to the Fifth Assessment Report of the Intergovernmental Panel on Climate Change*. Cambridge, United Kingdom and New York, USA: Cambridge University Press, pp. 1-115.
- Palmer, T. N. et al., 2004. Development of a European multimodel ensemble system for seasonal-to-interannual prediction (DEMETER). *Bulletin of the American Meteorological Society*, DOI: 10.1175/BAMS-85-6-853
- Palmer, T. N., Doblus-Reyes, F. J., Weisheimer, A. & Rodwell, M. J., 2008. Toward seamless prediction: Calibration of climate change projections using seasonal forecasts. *Bulletin of the American Meteorological Society*, pp. 459-470.
- Pandya, R. et al., 2015. Using weather forecasts to help manage meningitis in the west African Sahel. *American Meteorological Society*, pp. 103-115.
- Pappenberger, F., Scipal, K. & Buizza, R., 2008. Hydrological aspects of meteorological verification. *Atmospheric Science Letters*, 9, pp. 43-52.
- Pappenberger, F., Thielen, J. & Medico, M. D., 2011. The impact of weather forecast improvements on large scale hydrology: Analysing a decade of forecast of the European Flood Alert System. *Hydrological Processes*, 25, pp. 1091-1113.
- Pappenberger, F. et al., 2015a. How do I know if my forecasts are better? Using benchmarks in hydrological ensemble prediction. *Journal of Hydrology*, 522, pp. 697-713.

- Pappenberger, F. et al., 2015b. The monetary benefit of early flood warnings in Europe. *Environmental Science & Policy*, 51, pp. 278-291.
- Philippon, N., Rouault, M., Richard, Y. & Favre, A., 2012. The influence of ENSO on winter rainfall in South Africa. *International Journal of Climatology*, 32(15), p. 2333–2347.
- Pitman, A. J., 2003. Review: The evolution and revolution in land surface schemes designed for climate model. *International Journal of Climatology*, 23, pp. 479-510.
- Potgieter, C. J., 2007. Short-range weather forecasting over southern Africa with the conformal-cubic atmospheric model. Unpublished MSc dissertation, University of Pretoria, South Africa.
- Ran, Q. et al., 2018. Evaluation of quantitative precipitation predictions by ECMWF, CMA and UKMO for flood forecasting: Application to two Basins in China. *Natural Hazards Review*, 19(2), DOI: 10.1061/(ASCE)NH.1527-6996.0000282
- Ratnam, J. V., Behera, S. K., Doi, T., Ratna, S. B. & Landman, W. A., 2017. Improvements to the WRF seasonal hindcasts over South Africa by bias correcting the driving SINTEX-F2v CGCM fields. *Journal of Climate*, 29, 2815–2829, DOI: 10.1175/JCLI-D-15-0435.1
- Reason, C. & Keibel, A., 2004. Tropical cyclone Eline and its unusual penetration and impacts over the southern African mainland. *Weather and Forecasting*, 19, pp. 789-805.
- Reason, C. J. C., Landman, W. & Tennant, W., 2006. Seasonal to decadal prediction of Southern African climate and its links with the variability of the Atlantic Ocean. *American Meteorological Society*, pp. 941-955.
- Roeckner, E. et al., 2003. The atmospheric general circulation model ECHAM5. Part I: Model description. Max-Planck-Institut für Meteorologie Rep. 349, p. 127. [Online] Available at [https://www.mpimet.mpg.de/fileadmin/publikationen/Reports/max\\_scirep\\_349.pdf](https://www.mpimet.mpg.de/fileadmin/publikationen/Reports/max_scirep_349.pdf)
- Rojas, O., Li, Y. & Cumani, R., 2014. The influence of El Niño on the global agricultural areas. In: *Understanding the Drought Impact of El Niño on the Global Agricultural Areas: An Assessment Using FAO's Agricultural Stress Index (ASI)*. Rome: Food and Agriculture Organization of the United Nations, pp. 9-13.
- Ropelewski, C. F. & Halpert, M. S., 1989. Precipitation patterns associated with high index phase of the southern oscillation. *Journal of Climate*, 2, pp. 268-284.
- Rotstayn, L. D., 1997. A physically based scheme for the treatment of stratiform clouds and precipitation in large-scale models. I: Description and evaluation of the microphysical processes. *Quarterly Journal of the Royal Meteorological Society*, 123, pp. 1227-1287.
- Rouault, M. & Richard, Y., 2003. Intensity and spatial extension of drought in South Africa at different time scales. *Water SA*, 29(4), pp. 489-500.
- Sasaki, W., Doi, T., Richards, K. J. & Masumoto, Y., 2014. Impact of the equatorial Atlantic sea surface temperature on the tropical Pacific in a CGCM. *Climate Dynamics*, 43, 2539-2552, DOI: 10.1007/s00382-014-2072-1


- Sasaki, W., Doi, T., Richards, K. J. & Masumoto, Y., 2015. The influence of ENSO on the equatorial Atlantic precipitation through the Walker circulation in a CGCM. *Climate Dynamics*, 44, 191-202, DOI: 10.1007/s00382-014-2133-5
- Sasaki, W., Richards, K. J. & Luo, J. J., 2012. Role of vertical mixing originating from small vertical scale structures above and within the equatorial thermocline in an OGCM. *Ocean Modelling*, 57-58, 29-42, DOI: 10.1016/j.ocemod.2012.09.002
- Sasaki, W., Richards, K. J. & Luo, J. J., 2013. Impact of vertical mixing induced by small vertical scale structures above and within the equatorial thermocline on the tropical Pacific in a CGCM. *Climate Dynamics*, 41, 443-453, DOI: 10.1007/s00382-012-1593-8
- Schulze, R. E., 1997. Impacts of global climate change in a hydrological vulnerable region: Challenges to South African hydrologists. *Progress in Physical Geography*, 21, pp. 113-136.
- Schuman, F. G., 1989. History of Numerical Weather Prediction at the National Meteorological Center, *American Meteorological Society*, 4, p. 286.
- Schwanenberg, D. et al., 2015. Short-term reservoir optimization for flood mitigation under meteorological and hydrological forecast uncertainty. *Water Resource Management*, 29(5), pp. 1635-1651.
- Schwartz, G. S. et al., 2017. Toward 1-km ensemble forecasts over large domains. *Monthly Weather Review*, 145(8), pp. 2943-2969.
- Sene, K., 2010. *Hydrometeorology: Forecasting and Applications*. United Kingdom: Springer.
- Simmons, A. J. & Hollingsworth, A., 2002. Some aspects of the improvement in skill of numerical weather prediction. *Quarterly Journal of Royal Meteorological Society*, 128, pp. 647-677.
- Singleton, A. T. & Reason, C. J., 2007. A numerical model study of a severe cut-off low pressure system over South Africa. *Monthly Weather Review*, 135, p. 1128-1150.
- Slingo, J. & Palmer, T., 2011. Uncertainty in weather and climate prediction. *Philosophical Transactions of the Royal Society*, 369, p. 4751-4767.
- Smakhtin, V. Y., Watkins, D. A., Hughes, D. A. S. K. & Smakhtina, O. Y., 1998. Methods of catchment-wide assessment of daily low-flow regimes in South Africa. *Water SA*, 24(3), pp. 173-186.
- Steiner, A. L. et al., 2009. Land surface coupling in regional climate simulations of the West African monsoon. *Climate Dynamics*, 33, pp. 869-892.
- Tennant, W. J., Toth, Z. & Rae, K. J., 2007. Application of the NCEP Ensemble Prediction System to medium-range forecasting in South Africa: New products, benefits, and challenges. *American Meteorological Society*, pp. 18-35.
- Thatcher, M. & McGregor, J. L., 2009. Using a scale-selective filter for dynamical downscaling with the Conformal-Cubic Atmospheric model. *Monthly Weather Review*, 137, pp. 1742-1752.
- Thatcher, M. & McGregor, J. L., 2010. A technique for dynamically downscaling daily-averaged GCM datasets over Australia using the conformal Cubic atmospheric model. *Monthly Weather Review*, 139, pp. 79-95.

- Tompkins, A. M. & Giuseppe, F. D., 2015. Potential predictability of malaria in Africa using ECMWF monthly and seasonal climate forecasts. *Journal of Applied Meteorology and Climatology*, 54, pp. 521-540.
- Valcke, S., A. Caubel, R. Vogelsang & D. Declat, 2004. OASIS3 ocean atmosphere sea ice soil user's guide. CERFACS Tech. Rep. TR/CMGC/04/68, p. 73.
- Vitart, F., Anderson, D. & Stockdale, T., 2003. Seasonal forecasting of tropical cyclone landfall over Mozambique. *Journal of Climate*, 16, pp. 3932-3945.
- Vitart, F. et al., 2008. The new VarEPS-monthly forecasting system: A first step towards seamless prediction. *Quarterly Journal of the Royal Meteorological Society*, pp. 1789-1799.
- Wetterhall, F., Halldin, S. & Xu, C., 2005. Statistical precipitation downscaling in central Sweden with the analog method. *Journal of Hydrology*, 306, pp. 174-190.
- Wilks, D. S., 2011. Forecast verification. In: R. Dmowska, D. Hartmann & H. T. Rossby (eds). *Statistical Methods in Atmospheric Science*. s.l.: Academic Press, pp. 301-394.
- Wilks, D. S., 2011. Statistical forecasting. In: *Statistical Methods in the Atmospheric Sciences*. San Diego, CA: Academic Press, p. 271.
- Winsemius, H. C. et al., 2014. The potential value of seasonal forecasts in a changing climate in southern Africa. *Hydrology and Earth System Sciences*, 18, pp. 1525-1538.
- WMO, 2013. Subseasonal to seasonal prediction project. [Online] Available at: [http://www.s2sprediction.net/file/documents\\_reports/S2S\\_Implem\\_plan\\_en.pdf](http://www.s2sprediction.net/file/documents_reports/S2S_Implem_plan_en.pdf) [Accessed 31 March 2015].
- Yuan, C., Tozuka, T., Landman, W. A. & Yamagata, T., 2014. Dynamical seasonal prediction of southern African summer precipitation. *Climate Dynamics*, 42, pp. 3357-3374.
- Zorita, E. & Von Storch, H., 1999. The analog method as a simple statistical downscaling technique: Comparison with more complicated methods. *Journal of Climate*, 12, pp. 2474-2489.



## APPENDIX

### 1A. Community engagement: The Agenda of the Limpopo Provincial Climate Change Working Group Meeting



**LIMPOPO**  
PROVINCIAL GOVERNMENT  
REPUBLIC OF SOUTH AFRICA

DEPARTMENT OF  
ECONOMIC DEVELOPMENT, ENVIRONMENT & TOURISM

Draft Agenda  
Limpopo Provincial Climate Change Working Group Meeting

**Date:** 08 March 2018  
**Venue:** Masana Lodge (Polokwane)  
**Time:** 08h30 - 15h30

**Meeting objectives:**

- Discussion on implementing climate change action
- Facilitate engagements on enablers of action on climate change
- Consolidate inputs into the Provincial Climate Change Action Plan

Activity	Description	From	To	Time
Registration and Tea	Members arrive	8:30	9:00	0:30
Welcoming & Introduction	Members introduce themselves	9:00	9:10	0:10
Minutes of previous meeting	Minutes of previous meeting discussed and adopted	9:10	09:20	0:10
Climate Variability and projections (CSIR)	Limpopo climate variability	09:20	09:40	0:20
	Climate change projections over southern Africa	09:40	10:00	0:20
	Seasonal forecasting	10:00	10:20	0:20
	Short-range weather forecasting & hydrological forecasts	10:20	10:40	0:20
	Q&A	10:40	10:50	0:10
<b>Tea Break</b>				
Climate Change Action/ Implementation	Presentation of the Draft Provincial Action Plan	11:10	11:30	0:20
	Update on Implementation Projects and comments on the Draft Provincial Plan (Members)	11:30	11:50	0:20
	Options for small scale to large scale biogas production (Ibert Biogas Technology)	11:50	12:30	0:40
	Discussion on the presentations (All)	12:30	13:00	0:30
Lunch	Members Break for Lunch	13:00	14:00	0:30
SANBI Presentations and Discussion	Green Climate Fund Opportunities (SANBI)	14:00	14:30	0:30
DEA Presentation and Discussion	Monitoring and evaluation of Climate Change Adaptation Strategies	14:30	15:00	0:30
Discussion	Next Meeting and Key Items for Discussion	15:00	15:10	0:10
Closure	Wrap-up and Meeting Closure	15:10	15:15	0:05

## 1B. Attendance register

<b>Surname and Initials</b>	<b>Institution/Organisation</b>
Modungwane RM	Limpopo Department of Economic Development, Environment and Tourism (LEDET)
Mphahlele MC	LEDET
Maebaneng MS	LEDET
Sithole TP	QEMS
Makholela T	DEA (National)
Nkwashu LF	LEDET
De Villiers AC	AWARD
Selemela MR	LDARD
Moloto RA	LEDET
Mangena TM	LEDET
Moroatshehla MS	Greater-Letaba Municipality
Maisha TR	CSIR
Lekoana MA	LDARD
Mpheshea LE	CSIR
Beraki AF	CSIR
Phasha K	LEDET
Munjonji L	University of Limpopo
Tshindane M	SANBI
Maleka M	SANBI
Murambadoro M	CSIR
Mwenge Kahinda J	CSIR
Ngoasheng TJ	LEDET
Mphahlele TM	LEDET
Magagane LL	Cog HSTA
Rankapole KJ	OTP
Mudau NR	Mopani District municipality
Dinala IN	LEDET
Makgata RJ	LEDET
Hove F	Choice Trust
Koma C	LEDET
Maleswena MA	LEDET
Ledwaba SS	DEA – LGS
Mokwala M	LEDET
Pilusa MB	Sekhukhune district municipality
Maile H	LEDET
Moloto D	LEDET
Malherbe J	CSIR
Mailula NK	LEDET
Makakula MC	LEDET
Leshabane PS	LEDET
Modipi TJ	LEDET
Maboko T	LEDET
Malesa F	LEDET